Fatty acid transport proteins mediate fatty acid uptake in vivo and play a role in the development of metabolic diseases

by

Brittney Nicole Dietz

A dissertation submitted in partial satisfaction

of the requirements for the degree of

Doctor of Philosophy

in

Metabolic Biology

in the

Graduate Division

of the

University of California, Berkeley

Committee in charge:

Professor Andreas Stahl, Chair
Associate Professor Jen-Chywan (Wally) Wang
Professor George Brooks

Fall 2016

Abstract

Fatty acid transport proteins mediate fatty acid uptake in vivo and play a role in the development of metabolic diseases

by

Brittney Nicole Dietz

Doctor of Philosophy in Metabolic Biology

University of California, Berkeley

Professor Andreas Stahl, Chair

The prevalence of obesity and diet-related diseases is widespread and increasing. Fatty acids have vital biological functions in the body, but can become pathophysiological in many contexts. It is well established that fatty acid uptake into cells is a regulated process mediated by membrane-bound fatty acid transporters. Gain- and loss-of-function studies of fatty acid transport proteins (FATPs) have demonstrated the essential role of fatty acid transporters in maintaining normal fatty acid metabolism and have also indicated that these proteins are involved in the development of diet-related diseases. We do not fully understand the physiological roles of each FATP in every metabolic context. The work presented here focuses on FATP1 and FATP6 activity in the heart and endocrine pancreas, particularly in the context of diabetes.

In Chapter 1, the creation of a FATP6 knockout mouse model that we utilized to study FATP6 activity and function is reported. We found that FATP6 mediated fatty acid uptake in vivo and was specifically responsible for fatty acid availability in the heart. Deletion of FATP6 resulted in reduced cardiac lipid levels, cardiac dilation, reduced systolic function, and elevated rates of apoptosis in cardiomyocytes. This phenotype was rescued by high-fat diet feeding. While the location and mechanism of FATP6 activity have not been fully defined, we hypothesize that lack of FATP6 expression leads to reduced cardiac fatty acid utilization, which in turn leads to reduced cardiac function.

In Chapter 2, our efforts to determine the role of FATP1 and FATP6 in the development of diabetic cardiomyopathy are described. Diabetic cardiomyopathy is a heart condition characterized by enhanced fatty acid utilization. We induced diabetes in wild-type and FATP1 and FATP6 knockout mice by feeding them a high-fat diet and injecting them with two low-doses of streptozotocin. This protocol produced hyperglycemia but did not result in a robust model of diabetic

cardiomyopathy. Due to the lack of a strong phenotype in the heart, we did not detect significant differences in cardiac metabolism or function with deletion of FATP1 or FATP6.

In Chapter 3, a novel role for FATPs in the endocrine pancreas is presented. FATPs are differentially expressed in pancreatic islets, with FATP1 localizing to beta cells. We used islets from FATP1 knockout mice to analyze how FATP1 expression affected the susceptibility of beta cells to lipotoxicity. Deletion of FATP1 protected beta cells from palmitate-induced apoptosis, despite normal levels of fatty acid uptake and palmitate-induced ER stress in FATP1 knockout islets. Although the mechanism explaining this outcome is not clear, beta cells from FATP1 knockout mice may differentially store neutral lipid and this may make the cells less susceptible to palmitate-induced cell death.

In Chapter 4, our attempts to characterize small molecule inhibitors of FATPs are portrayed. We tested the ability of two classes of potential FATP inhibitors to reduce FATP activity in FATP-overexpressing cells and in cells that endogenously express FATPs. Phospholipid-based inhibitors did not reduce FATP-mediated fatty acid uptake at feasible concentrations. A dihydropyrimidone-based inhibitor effectively reduced FATP1- and FATP4-mediated fatty acid uptake in cell models overexpressing these proteins but did not affect endogenous FATP1 or FATP4 activity in other cell models.

Taken together, these results contribute to the growing body of evidence that establishes a role for FATPs in fatty acid transport in the body as well as in the development of diet-related diseases. Specifically, this work shows novel roles for FATP6 in cardiac metabolism and function and FATP1 in pancreatic beta cell metabolism and function. Clearly, FATPs are important regulators of metabolism, are implicated in metabolic disorders, and should be extensively studied as potential therapeutic targets.

To my parents

Table of Contents

Acknowledgements

Many people contributed to this work. First, I would like to thank my advisor, Andreas Stahl, who is an expert in the field of fatty acid metabolism and provided me with countless feedback while collecting and analyzing this data. Aside from being an intellectual resource, Andreas was an excellent scientist to look up to while I completed graduate school. He works tirelessly, yet with integrity and enthusiasm. I would also like to thank Wally Wang and George Brooks for being on my dissertation committee and facilitating my graduate career.

In addition, I must give credit to the hands that actually composed the data. Angelica Zabronsky, Kevin Dales, Bianca Vora, and Jami Wang deserve special mention for their hours spent in the lab, their dedication to the work, and their invaluable friendship. Other students who helped me at the bench include Spencer Pace, Allison McQueen, Diego Britto, Paulo Olivie, Heather Tran, and Brenda Cheah.

I worked among and with a fantastic group of lab members. I am grateful to Courtney Anderson for teaching me most of what I know about scientific technique, as well as Lacey Andrews, Ching-Fang Chang, Rost Chudnovskiy, Judith Kraiczy, Jiehan Li, Biao Nie, Hyo Min Park, Kevin Tharp, Diyala Shihadih, and Pete Zushin for lending me a hand and providing advice when I needed it and chatting with me whether I needed it or not.

Steve Ruzin and Denise Schichnes of the Biological Imaging Facility were like second mentors to me and are incredibly helpful people. I would also like to thank the technicians, veterinarians, and other staff members at the Northwest Animal Facility that kept my mice healthy and safe throughout my experiments. Vinh Nguyen, Emily Wilson, and Mike Wendland provided me with technical assistance.

The Nutritional Sciences and Toxicology department at the University of California, Berkeley, provided an environment conducive for collaboration. Each lab contributed in one way or another to the work presented here. The dietetics program in our department supplied me with a framework of human nutrition and disease that gave a broader meaning to my work. I also need to thank Olga O'Connor for going above and beyond to get me enrolled in my graduate program.

Kristin Obrochta was my first scientific mentor at Berkeley and was a valuable resource in research, but was an even more valuable friend. Marta Vuckovic spent many hours discussing my work as well as enjoying life in the Bay Area with me. Kristin and Marta encouraged me to finish graduate school more than anyone else and are amazing examples of how to balance being a scientist, a wife, and a mother.

Finally, I'd like to acknowledge my cheerleaders outside of the lab. First, I am grateful to my parents and my brother, who never stopped believing in me, even when I did not believe in myself. From the day I was born, my mom and dad taught me how to work hard and not take anything in life for granted. I have also received immeasurable support from my husband, Timothy, and am thankful for the final seed of motivation he gave me to complete this dissertation. Most importantly, I am grateful for the peace that passes all understanding and the ultimate inspiration to make our world a better place that I receive from my Savior.

Introduction

According to the National Institutes of Health, the majority of Americans are considered to be overweight[1]. Over one-third of the population is obese or extremely obese, with body mass indexes over 30. The prevalence of overweight and obesity has increased each year over the last 50 years and one-third of adolescents in the United States are overweight or obese. The long-term consequences of the obesity epidemic have yet to be fully realized, but our society is already faced with an increasing burden of diet-related diseases like cardiovascular disease and diabetes. Heart disease is the leading cause of death in the United States[2] and 21.3 million people in the United States have diabetes[3]. The diabetes incidence rate has increased so drastically that if trends continue, by 2050, one in three people will have the disorder. The estimated cost to society for these two conditions alone is over $300 billion a year in the United States. Obesity is also associated with many other chronic diseases, including cancer, hypertension, non-alcoholic fatty liver disease, and osteoporosis. Given the extreme prevalence of obesity and diet-related diseases in the United States, it is imperative that we strive to better understand the link between nutrition, metabolism, and health as well as discover and advance therapeutic strategies to treat these diseases.

Fatty acids are important molecules that are involved in a variety of biological processes. Besides being a major fuel source, they also activate intracellular signal transduction cascades, regulate metabolic enzymes, bind transcription factors, provide substrates for posttranslational protein modification, and serve as precursors to components of the cell membrane and mediators of the immune response[4,5]. While adequate fatty acid levels are essential to maintain normal biological function, excess fatty acids in circulation and in peripheral tissues can become pathophysiological. Ectopic lipid accumulation in tissues like skeletal muscle, liver, heart, and pancreatic beta cells can lead to insulin resistance and lipotoxicity[4,6–8].

Because of the association between obesity and metabolic diseases, much effort has been made to understand how exogenous fatty acids enter peripheral tissues. We now know that while some fatty acids can diffuse across the plasma membrane, the majority of fatty acid uptake into cells is protein-mediated[4,9,10]. Fatty acid transport proteins (FATPs)[4], fatty acid translocase (CD36)[11], and plasma membrane fatty acid binding protein (FABPpm)[12] have been shown to facilitate fatty acid uptake into cells in vitro and in vivo. The focus of this work will be on fatty acid transport proteins.

The FATP family is an evolutionarily conserved family of proteins made up of six members (SLC27A1-6). All FATPs have a signature 311-amino acid FATP sequence, an AMP-binding domain[4], and at least one transmembrane domain[13,14]. Gain- and loss-of-function studies of FATPs in vitro and in vivo have provided extensive evidence that these proteins facilitate fatty acid uptake[4,15]. In mice, FATP1 contributes to insulin-induced fatty acid uptake in skeletal muscle and adipose tissue[16,17] and FATP2 and FATP5 mediate fatty acid uptake in the liver[18,19].

FATPs were first localized to the plasma membrane[13], although they have also been found on the endoplasmic reticulum, especially in cell models in which FATPs are overexpressed[20]. In peripheral tissues, FATP1 actually translocates from an intracellular compartment to the plasma membrane in response to insulin stimulation[21] or muscle contraction[22]. FATPs have also been shown to be transcriptionally regulated by insulin[23,24] and the peroxisome proliferator-activated receptor family[25].

The mechanism of FATP-mediated fatty acid uptake is not clear. FATPs exhibit acyl-CoA synthetase activity[26] and it has been proposed that this enzymatic activity contributes to their ability to facilitate fatty acid entry into cells through a process called vectorial acylation[10]. While some contend that this metabolic trapping of fatty acids inside the cell is the primarily mechanism explaining FATP-mediated fatty acid uptake[27], biochemical studies in yeast have shown that mutating various regions of these proteins results in differential changes in fatty acid uptake and acyl-CoA activity, suggesting that the two activities are distinct[28]. It has also been proposed that FATPs work with other transport proteins or acyl-CoA synthetases to promote fatty acid uptake into cells[29,30]. Regardless of the exact mechanism, it is clear that FATPs facilitate fatty acid uptake, and this work focuses on the physiological impact of this activity.

FATPs are differentially expressed throughout the body. FATP1 is widely expressed in metabolic tissues, including white adipose tissue, brown adipose tissue, skeletal muscle, and the heart[13]. FATP2 and FATP5 are primarily expressed in the liver[31,32]. FATP3 is expressed in the lung and brain[33], FATP4 in the small intestine and in white adipose tissue[34], and FATP6 in the heart[35]. Knockout mouse models have been developed for a subset of FATPs and have shown that FATP expression is important in preserving normal fatty acid metabolism. FATP1 knockout mice are not able to maintain thermogenesis in response to cold exposure[36] and FATP4 knockout mice die within days of birth due to a skin condition[37]. Studies in knockout mice have also implicated FATPs as therapeutic targets for the treatment of metabolic diseases. FATP1 knockout mice are protected from diet-induced obesity[17] and FATP5 knockout mice are protected from the development of non-alcoholic fatty liver disease[19].

Because of the pressing diet-related health concerns in our country and the body of evidence suggesting therapeutic potentials for FATPs, we are particularly interested in FATP activity in metabolic tissues and the impact these proteins have on tissue function. Previous studies have focused on the biochemical activity of FATPs or on a specific FATP in a particular tissue, so we do not fully understand the physiological role of each FATP in every metabolic context.

The work described here focuses on FATP1 and FATP6 activity in the heart and in the endocrine pancreas. This is the first report of a FATP6 knockout mouse model, and in Chapter 1, it is shown that FATP6 mediates fatty acid uptake in the heart and that loss-of-function of FATP6 in mice results in dilated cardiomyopathy. In Chapter 2, FATP1 and FATP6 activity is evaluated in the context of diabetic cardiomyopathy, a heart condition that affects diabetic patients and is thought to be dependent on excess fatty acid utilization in the heart[38,39]. This work is also the first to describe the expression of FATPs in the endocrine pancreas, and in Chapter 3 it is

shown that deleting FATP1 protects beta cells from palmitate-induced apoptosis. In the final chapter, our efforts to find a small molecule inhibitor for FATPs are presented. Overall, our findings validate the essential role of FATPs in maintaining normal fatty acid metabolism and confirm the implication of FATPs in the development of metabolic diseases.

Chapter 1: Deletion of fatty acid transport protein 6 results in reduced cardiac lipid levels and dilated cardiomyopathy

Rationale

Fatty acid transport proteins (FATPs) mediate fatty acid uptake in vivo and are important contributors to metabolic homeostasis[4]. Altered expression of FATPs results in increased susceptibility to or protection from metabolic diseases like insulin resistance[21], non-alcoholic fatty liver disease[40], and cardiomyopathy[41]. Fatty acid transport protein 6 (FATP6) is a member of the FATP family. Like other FATPs, it enhances fatty acid uptake when overexpressed in cells[35]. It is primarily expressed in the heart, localizing to the sarcolemma adjacent to cardiac microvasculature[35]. In a study of a single nucleotide polymorphism in the FATP6 gene in humans, researchers found that subjects with the FATP6 variant had altered blood lipid levels, decreased blood pressure, and increased left ventricular mass[42].

The heart utilizes fatty acids for 70% of its energy production[43–45] and alterations in cardiac substrate utilization are maladaptive[8,46,47]. Enhanced cardiac fatty acid oxidation, which occurs in obesity and diabetic cardiomyopathy[48,49], leads to a reduction in overall cardiac efficiency[47,50]. Reduced fatty acid oxidation, as observed in cases of hypertrophic[51,52] and dilated cardiomyopathy[53], ischemia[54,55], and hypertension[56,57] also leads to reduced cardiac inefficiency and eventually heart failure[47,52,58]. Genetic mouse models have unequivocally shown that alterations in fatty acid metabolism directly cause cardiac dysfunction[59–65].

Due to the vital importance of maintaining normal rates of fatty acid utilization in the heart, cardiac fatty acid transport is a regulated process[45,47]. Besides FATP6, fatty acid transport protein 1 (FATP1), fatty acid translocase (CD36), and plasma membrane fatty acid binding protein (FABPpm) are fatty acid transporters that are expressed in the heart[66]. These transporters are regulated by fatty acid supply and demand through insulin action, muscle contraction, oxygen deprivation, and gene transcription[66].

Fatty acid transport in the heart is a multi-step process. Circulating albumin-bound fatty acids or fatty acids hydrolyzed from lipoprotein triglycerides must first cross the cardiac endothelium as free fatty acids[8,45]. Fatty acids then bind to albumin and traverse the interstitial space. Finally, free fatty acids are taken up through the sarcolemma membrane. While we do not fully understand the mechanism by which each fatty acid transporter contributes to the individual steps in this process, it is clear that the amount of fatty acid taken up by cardiac tissue is a protein-mediated process. Fatty acid uptake by the heart is saturable, is reduced by membrane-bound protein digestion, and can be inhibited with small molecule inhibitors against fatty acid transporters[66–70]. Other groups have shown that manipulating the expression of fatty acid transporters results in changes in cardiac metabolism[11,41,60,71] and in some cases, cardiac function[41].

Most of the work on fatty acid transport in the heart has centered on CD36 expression and function[66]. While one study evaluated the impact of overexpression of FATP1[41], no one has investigated the impact of loss-of-function of FATPs in the

heart or has evaluated the role of FATP6 in vivo. We hypothesized that like other FATPs, FATP6 would mediate fatty acid uptake in vivo. Specifically, we were interested in whether FATP6 expression affected cardiac metabolism and function. Through generation of a lacZ-tagged FATP6 whole-body knockout mouse, we found that FATP6 has a different expression pattern in mice than in humans and that FATP6 mediates fatty acid availability in the heart. After investigating the effects of FATP6 expression on cardiac metabolism and function in the context of a chow and high-fat diet, we found a novel role for FATP6 in maintaining cardiac lipid levels and normal systolic function.

Results

Human FATP6 facilitates fatty acid uptake in vitro

We overexpressed the human FATP6 gene in HEK293 cells in order to investigate the biochemical activity of FATP6 in vitro. Stable transfection of FATP6 resulted in increased FATP6 gene expression compared to cells transfected with empty vector (**Fig. 1A**). We made multiple clonal cell lines from these stably transfected cells, screened them for expression of FATP6, and used the clone with the most robust expression of FATP6 in subsequent studies.

We assessed the fatty acid uptake capabilities of the FATP6-overexpressing cells with a real-time fatty acid uptake assay. We incubated the cells with BODIPY-fatty acid bound to bovine serum albumin and measured the fluorescence of the cells over time. We then compared the rate of fatty acid uptake of cells expressing FATP6 to cells expressing empty vector or FATP5. We have previously shown that FATP5-expressing cells have significantly enhanced fatty acid uptake[40]. While we see an increased rate of BODIPY-fatty acid uptake in the FATP5-expressing cells, the FATP6-expressing cells had the same rate of uptake as cells expressing empty vector (**Fig. 1B**).

We used C1-BODIPY-C12 (Molecular Probes #D3283), a fluorescent fatty acid analog that mimics the size and structure of a 16-carbon saturated fatty acid, in our real-time fatty acid uptake assay. We also tested FATP6 activity on C^{14}-oleate, an unsaturated fatty acid without a fluorescent tag. For this assay, we incubated FATP6-expressing cells and control cells with C^{14}-oleate for ten minutes and measured the accumulation of radioactivity in the cell lysates. We found that like FATP5-expressing cells, FATP6-expressing cells accumulated significantly more radioactive oleate than cells expressing empty vector, suggesting that FATP6 expression enhanced cellular uptake of oleate (**Fig. 1C**).

Human FATP6 has acyl-CoA synthetase activity in vitro

Other members of the FATP family have been shown to have acyl-CoA synthetase activity[4]. These proteins not only enhance cellular uptake of fatty acids, but also help "trap" the fatty acids inside the cell and activate them for downstream metabolic functions through a process termed vectorial acylation[10]. To test the acyl-CoA synthetase activity of human FATP6, we performed an acyl-CoA synthetase

activity assay with BODIPY-fatty acid on cells expressing FATP6, empty vector, or acyl-CoA synthetase 4 (ACSL4), a known acyl-CoA synthetase. We incubated the cell lysates with BODIPY-fatty acid for 20 minutes and then performed a lipid extraction with Dole's reagent to separate the intracellular hydrophobic fatty acids from the aqueous fatty acyl-CoAs. We then measured the fluorescence in the aqueous phase. Like ACSL4-expressing cells, FATP6-expressing cells had significantly more fluorescence in the aqueous phase than cells expressing empty vector, indicating that human FATP6 has acyl-CoA sythetase activity (**Fig. 1D**).

Generation of FATP6 whole-body knockout mice

Cumulatively, our biochemical assays show that FATP6 facilitates fatty acid uptake in vitro. Our lab and others have also demonstrated important physiological roles of FATPs in vivo[4]. FATPs are differentially expressed throughout the body, mediate tissue fatty acid availability, and therefore impact the development of metabolic disorders like insulin resistance and hepatic steatosis in mammals. To investigate the physiological importance of FATP6, we generated whole-body FATP6 knockout mice.

To make whole-body knockout mice, we utilized a knockout-first, promoter-driven allele designed by the Knockout Mouse Project (**Fig. 2A**). When expressed, this transgene results in a truncated, nonfunctional FATP6 gene and expression of β-galactosidase driven by the FATP6 promoter. This allele can also be modified by homologous recombination with Flippase to produce a conditional knockout allele, which can then be further modified with Cre recombinase to remove the third exon of the gene in a time- or tissue-specific manner.

Researchers at the Mouse Biology Program at the University of California, Davis, created chimeric mice using two clones of the knockout-first, promoter-driven allele. We bred these chimeric mice to produce heterozygous ($FATP6^{-/+}$) and homozygous ($FATP6^{-/-}$) transgenic mice. We verified the transgene location at the FATP6 locus with long-range PCR. The PCR primers were designed to create products that span the endogenous FATP6 allele and the transgene (**Fig. 2A** and **Table S1**). We confirmed the position of both the 3' and 5' arm of the gene (**Fig. 2B**). We also used quantitative PCR to confirm partial and full deletion of the FATP6 gene in multiple tissues in heterozygous and homozygous transgenic mice, respectively (**Fig. 2C**).

Whole-body FATP6 knockout mice are viable and breed normally

We used both colonies of mice generated by the two distinct transgene vector clones in subsequent studies. Both colonies appeared to have normal breeding patterns and produce litters of average size and gender distribution (**Table S3**). Heterozygous breeding pairs produced pups in normal Mendelian ratios. The resulting phenotypes that we describe did not differ between the two colonies, suggesting that the observed phenotypes were driven by loss-of-function of FATP6 and not by off-target effects.

FATP6 is highly expressed in the testes, placenta, and lung in the mouse

We screened wild-type C57BL/6J mice for expression of FATP6 by performing quantitative PCR on a panel of tissues. We found the highest expression of FATP6 in the testes and lower expression of FATP6 in the placenta and the lung (**Fig. 3A**). This expression pattern differs from that observed in humans[35]. Similar patterns and levels of FATP6 expression were observed in both male and female mice, mice of various ages, mice of various strains, and in rats (data not shown).

We utilized the transgene in our knockout mice to further investigate FATP6 expression in mice. The unaltered transgene results in expression of β-galactosidase driven by the endogenous FATP6 promoter, so we can test for FATP6 expression by measuring β-galactosidase activity. We measured β-galactosidase activity in tissue lysate from a panel of tissues from both wild-type and FATP6$^{-/-}$ mice with an assay utilizing a luminescent β-galactosidase substrate. We observed β-galactosidase activity above endogenous β-galactosidase activity in the testes, placenta and lung (**Fig. 3B**). The pattern and magnitude of this activity corresponded to the results obtained from our quantitative PCR screen.

To pinpoint where FATP6 is expressed within the testes, lung, and placenta, we performed a stain for β-galactosidase activity on tissue sections. By incubating tissue sections with 5-bromo-4-chloro-3-indolyl β-D-galactopyranoside (X-gal), a substrate for β-galactosidase that produces a blue dye when cleaved, we can determine which cell types express FATP6. We stained wild-type tissue in addition to FATP6$^{-/-}$ tissue in order to control for background staining from endogenous β-galactosidase activity. Although we detect background staining in wild-type mouse testes, the staining in FATP6$^{-/-}$ testes was more intense and specifically localized to the spermatocytes (**Fig. 3C**). In the lung, we localized FATP6 expression to the columnar lung epithelial cells. We observed robust staining in the decidua of e12.5 FATP6$^{-/-}$ placenta, but this staining pattern was also observed in wild-type placenta. The endogenous staining pattern masked any FATP6 promoter-driven activity in the placenta.

FATP6$^{-/-}$ mice weigh more than wild-type mice on a chow diet

To evaluate the metabolic phenotype of the whole-body FATP6 knockout mice, we compared general metabolic parameters of FATP6$^{-/-}$ mice to those of wild-type mice on a standard chow diet or a high-fat diet. On a chow diet, FATP6$^{-/-}$ mice have significantly greater body weights and higher circulating insulin levels than wild-type mice (**Table 1**). Wild-type mice fed a high-fat diet for 16 weeks have increased body weight and serum insulin levels compared to chow-fed mice (**Table 1**). FATP6$^{-/-}$ mice also gain body weight and have increased levels of serum insulin after 16 weeks of a high-fat diet. High-fat feeding abolished differences in body weight and insulin levels between wild-type and knockout mice.

FATP6$^{-/-}$ mice have reduced fatty acid uptake in the heart

To investigate whether FATP6 expression affected fatty acid uptake in vivo, we performed a BODIPY-fatty acid uptake assay in live mice. We injected mice with BODIPY-fatty acid bound to bovine serum albumin, waited 15 minutes, then harvested various tissues and measured fluorescence in the tissue lysates. Compared to wild-type mice, FATP6$^{-/-}$ mice showed a trend towards reduced uptake of BODIPY-fatty acid in the lung and white adipose tissue and a significant reduction in BODIPY-fatty acid uptake in the heart (**Fig. 4A**). No change in BODIPY-fatty acid uptake was observed in the liver.

Wild-type mice fed a high-fat diet have increased expression of FATP6 in the heart

FATP6 is highly expressed in human heart[35], and although we do not observe significant levels of FATP6 in mouse heart relative to other tissues, we can detect FATP6 expression in the heart (**Fig. 2C** and **3A**). Using quantitative PCR, we found that wild-type mice fed a high-fat diet have increased expression of FATP6 in cardiac tissue (**Fig. 4B**).

Isolated cardiomyocytes from FATP6$^{-/-}$ mice take up BODIPY-fatty acid at the same rate as cardiomyocytes from wild-type mice

We also evaluated fatty acid uptake in cardiomyocytes isolated from FATP6$^{-/-}$ and wild-type mice. Isolation and tissue culture of neonatal cardiomyocytes from both wild-type and FATP6$^{-/-}$ mice resulted in viable, beating cardiomyocytes within 24 hours of plating cells (**Supplemental Video 1**).

We developed a fatty acid uptake assay utilizing live-cell microscopy to visualize fatty acid uptake in beating cardiomyocytes in real-time. We incubated the cells with BODIPY-fatty acid bound to bovine serum albumin and captured images of the cells every 30 seconds for 30 minutes using an inverted microscope at 20x objective. We saw an increase in cell fluorescence over time, and within 15 minutes, we observed the formation of fluorescent lipid droplets within the cardiomyocytes (**Supplemental Video 2**). We measured the change in cell fluorescence over time using imaging software that quantified individual cell fluorescence. Using this method, we found that cardiomyocytes isolated from FATP6$^{-/-}$ mice had the same rate of fatty acid uptake as cardiomyocytes from wild-type mice (**Fig. 4C**). This data suggests that the reduction in cardiac fatty acid uptake in FATP6$^{-/-}$ mice may be due to global loss-of-function of FATP6 rather than to loss of FATP6 activity in cardiomyocytes, that there are developmental differences in cardiac fatty acid uptake in neonatal and adult mice, or that FATP6 activity in the heart requires factors that we did not recapitulate ex vivo.

FATP6$^{-/-}$ mice have reduced cardiac triglyceride and free fatty acid levels

To further characterize the effects of FATP6 expression on cardiac lipid uptake in vivo, we compared the relative weight of the heart in wild-type and knockout mice fed a chow and high-fat diet. While high-fat diet feeding decreased the relative

weight of the heart in both wild-type and FATP6$^{-/-}$ mice, FATP6 expression itself did not affect heart weight (**Fig. 4D**).

We measured triglyceride content in heart lysate from wild-type and FATP6$^{-/-}$ mice on a chow and high-fat diet. We found that on a chow diet, FATP6$^{-/-}$ mice had significantly lower heart triglyceride levels than wild-type mice (**Fig. 4E**). Feeding mice a high-fat diet ameliorated the effect of FATP6 expression on heart triglyceride levels. We also measured free fatty acid levels and found that on a chow diet, FATP6$^{-/-}$ mice had significantly lower heart free fatty acid levels than wild-type mice, and that this effect was eliminated by high-fat diet feeding (**Fig. 4F**). Taken together, our data indicate that despite low expression of FATP6 in mouse heart, whole-body deletion of FATP6 results in reduced lipid accumulation in the heart.

FATP6$^{-/-}$ mice do not have altered expression of other nutrient transporters in the heart but do have increased expression of PPARα

We tested whether deleting FATP6 affected expression of other fatty acid transporters or glucose transporters in the heart. Using quantitative PCR, we found that feeding mice a high-fat diet increased cardiac expression of FATP1 and CD36 in wild-type mice. However, we saw no compensatory increase in FATP1 or CD36 expression in hearts from FATP6$^{-/-}$ mice (**Fig. 5A** and **B**). In fact, expression of CD36 did not increase in FATP6$^{-/-}$ mice on a high-fat diet like it did in wild-type mice (**Fig. 5B**). Although not significant, we found a trend towards increased expression of glucose transporter 1 (GLUT1) and glucose transporter 4 (GLUT4) in FATP6$^{-/-}$ hearts (**Fig. 5C** and **D**). Feeding both wild-type and FATP6$^{-/-}$ mice a high-fat diet decreased expression of glucose transporter 1 (**Fig. 5C**).

Peroxisome proliferator-activated receptor α (PPARα) transcriptionally regulates many genes involved in fatty acid metabolism, including fatty acid transport, and its expression in the heart affects cardiac metabolism and function[72,73]. We found that PPARα expression significantly increased in FATP6$^{-/-}$ mice fed a chow diet (**Fig. 5E**), while this effect was eliminated in mice fed a high-fat diet.

FATP6$^{-/-}$ mice have reduced systolic function

To investigate whether FATP6 expression affected cardiac function, we performed echocardiography. Echocardiography is the standard technique used to measure cardiac function in vivo and is now routinely and reliably performed in small rodents[74–77]. We evaluated cardiac function in wild-type and FATP6$^{-/-}$ mice on a chow and high-fat diet with B-mode measurements in the parasternal long-axis view of the left ventricle and with M-mode measurements in the short-axis view of the middle of the left ventricle. Using these measurements and the software accompanying our ultrasound, we calculated multiple cardiac parameters that are indicative of cardiac function.

Although not significant, we found a trend towards decreased intraventicular septum length and left ventricular posterior wall thickness at both systole and

diastole in FATP6$^{-/-}$ mice on a chow diet compared to wild-type mice (**Table 2** and **Fig. 6A**). We found a significant increase in left ventricle internal diameter at both systole and diastole in FATP6$^{-/-}$ mice compared to wild-type mice on a chow diet (**Table 2** and **Fig. 6B**). Feeding mice a high-fat diet diminished these changes in left ventricular wall thickness and left ventricle diameter (**Table 2** and **Fig. 6A** and **B**). Left ventricular dilation in FATP6$^{-/-}$ mice resulted in a trend towards reduced fractional shortening, which is the change in left ventricle diameter during a cardiac cycle, and in a significant decrease in ejection fraction, or the fraction of blood ejected per heartbeat (**Table 2** and **Fig. 6C**). We also found a significant increase in stroke volume, or the volume of blood ejected per heartbeat, in FATP6$^{-/-}$ mice, while body weight-adjusted cardiac output was maintained (**Table 2** and **Fig. 6D** and **E**). Feeding mice a high-fat diet diminished the effects of loss-of-function of FATP6 on systolic cardiac function (**Table 2** and **Fig. 6C** and **D**). FATP6$^{-/-}$ mice did not have a reduction in weight-adjusted cardiac output as observed in wild-type mice on a high-fat diet (**Table 2** and **Fig. 6E**).

FATP6$^{-/-}$ mice have increased levels of apoptosis in the heart

Alterations in fatty acid metabolism and utilization can lead to an accumulation of fatty acids in cardiomyocytes and to lipotoxicity[8]. To investigate whether FATP6$^{-/-}$ mice had altered levels of apoptosis in the heart, we performed a TUNEL stain on heart sections. Surprisingly, we found significantly increased levels of apoptosis in FATP6$^{-/-}$ hearts from mice fed a chow diet (**Fig. 6F**), although in mice fed a high-fat diet, we did not see a significant difference in rates of apoptosis in the heart between wild-type and FATP6$^{-/-}$ mice.

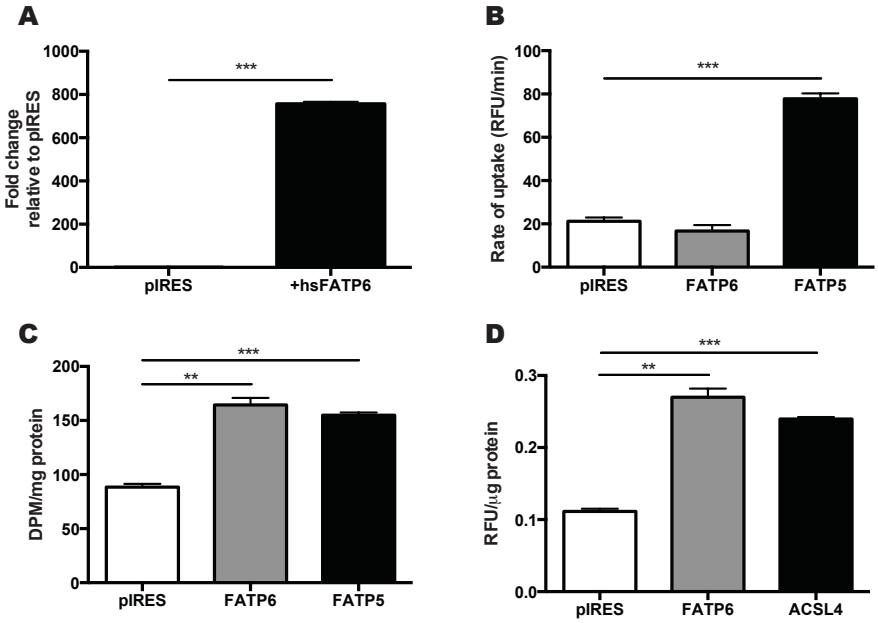

Figure 1. Human FATP6 has fatty acid uptake and acyl-CoA synthetase activity.
A HEK293 cells stably transfected with the human FATP6 gene express significantly more FATP6 transcript than HEK293 cells transfected with an empty vector (n=3). **B** HEK293 cells stably overexpressing FATP6 have the same BOIDPY-fatty acid uptake rate as cells expressing empty vector (n=9). **C** FATP6-overexpressing cells accumulate more C^{14}-oleate than cells expressing empty vector (n=3). **D** FATP6-overexpressing cells have higher acyl-CoA synthetase activity than cells expressing empty vector (n=3). RFU = relative fluorescent units, DPM = disintegrations per minute. *p < 0.05, **p < 0.005, ***p < 0.001. Error bars represent SEM.

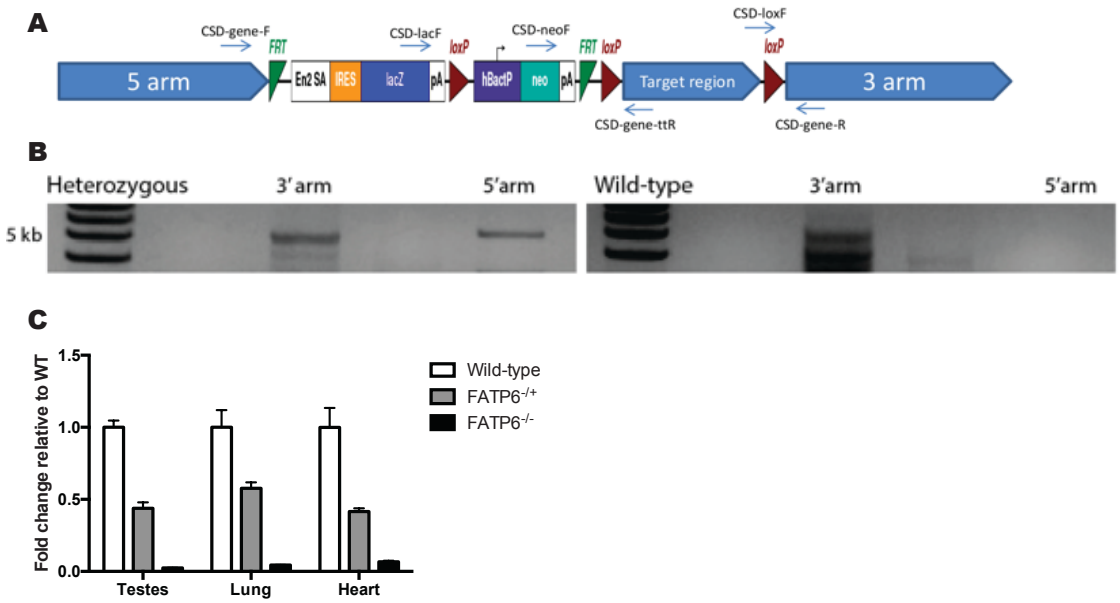

Figure 2. Generation of FATP6 whole-body knockout mice.
A A knockout-first, promoter-driven allele designed by the Knockout Mouse Project targeted exon 3 of the murine FATP6 gene and is shown with the genotyping strategy developed by the Mouse Biology Program at the University of California, Davis. **B** Long-range PCR verification of the correct location of the targeting cassette in the mouse genome and of germline transmission of the transgene. **C** Quantitative PCR verification of the deletion of the FATP6 gene in various mouse tissues in mice heterozygous and homozygous for the transgene.

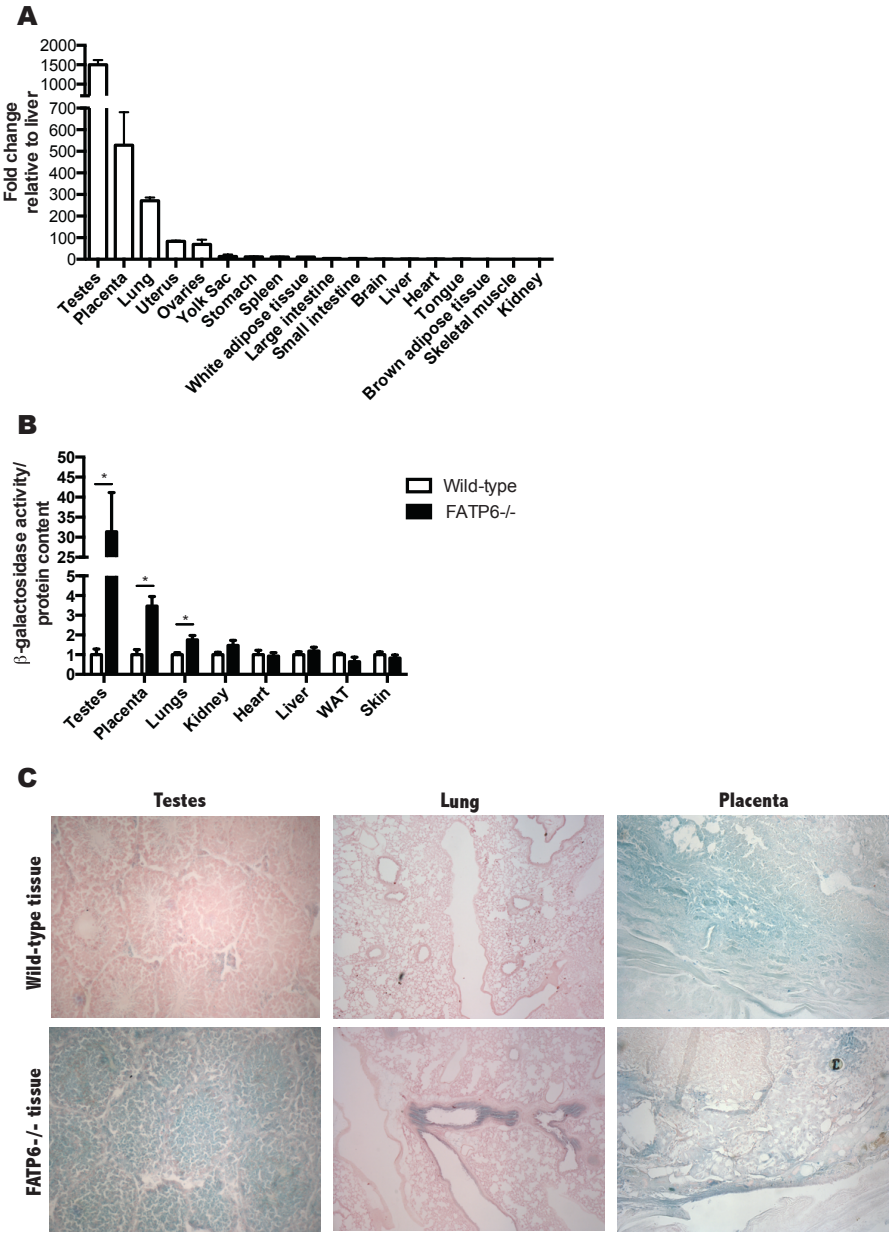

Figure 3. FATP6 is highly expressed in spermatocytes and in lung epithelial cells in the mouse.

A FATP6 mRNA is most highly expressed in the testes, placenta, and lung in C57BL/6J mice (n=3). **B** FATP6-driven ß-galactosidase activity is detected in mouse testes, placenta, and lung as measured by a luminescent assay (n=3). **C** ß-galactosidase staining in tissue sections demonstrates FATP6 promoter activity in testes spermatocytes and lung columnar epithelial cells, while there is non-specific staining in the decidua of the placenta. WAT = white adipose tissue. *$p < 0.05$. Error bars represent SEM.

Table 1. Body weight and blood metabolite levels in wild-type and FATP6$^{-/-}$ mice on a chow and high-fat diet.

	WT Chow	WT HFD	FATP6$^{-/-}$ Chow	FATP6$^{-/-}$ HFD
Body weight (g)	28.49 ± 0.55	47.24 ± 1.28^{+++}	35.13 ± 1.07***	46.72 ± 2.20^{++}
Blood glucose (mg/dL)	185.5 ± 7.98	200.8 ± 17.40	208.8 ± 8.83	191.4 ± 9.62
Serum TAG (mg/dL)	76.00 ± 7.07	79.42 ± 8.13	76.15 ± 10.54	92.20 ± 6.13
Serum FFA (mM)	0.9114 ± 0.041	0.8366 ± 0.084	0.8977 ± 0.17	1.073 ± 0.24
Serum insulin (ng/ml)	0.6242 ± 0.054	7.852 ± 1.90^{+}	1.789 ± 0.39*	7.364 ± 1.46^{+}

TAG = triglycerides, FFA = free fatty acids. *$p < 0.05$ versus wild-type, **$p < 0.005$ versus wild-type, ***$p < 0.001$ versus wild-type; $^{+}p < 0.05$ versus chow diet, $^{++}p < 0.005$ versus chow diet, $^{+++}p < 0.001$ versus chow diet. Mean is given with SEM.

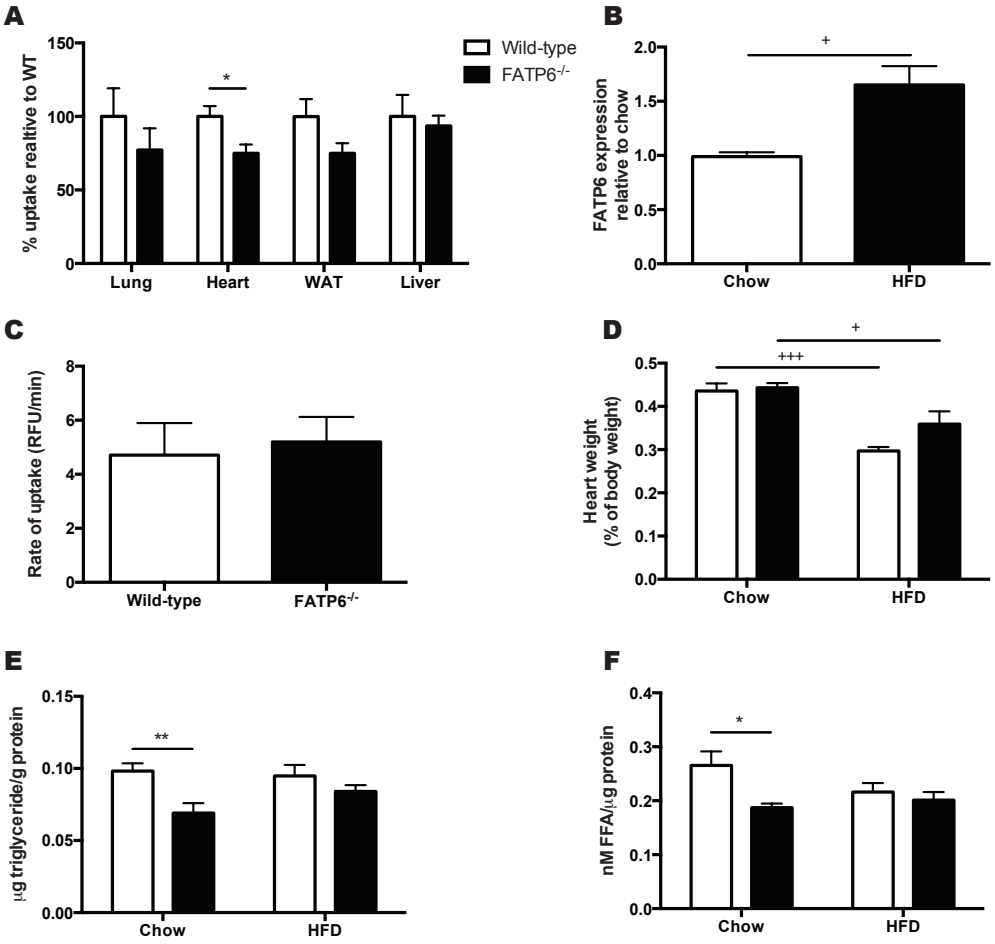

Figure 4. FATP6$^{-/-}$ mice have reduced BODIPY-fatty acid uptake and reduced lipid accumulation in the heart.

A FATP6$^{-/-}$ mice show a trend towards reduced fatty acid uptake in lung and white adipose tissue and have significantly reduced BODIPY-fatty acid uptake in the heart compared to wild-type mice (n=5). **B** Wild-type mice fed a high-fat diet for 16 weeks have enhanced expression of FATP6 in the heart compared to mice on a chow diet (n=6). **C** Neonatal cardiomyocytes isolated from FATP6$^{-/-}$ mice take up BODIPY-fatty acid at the same rate as neonatal cardiomyocytes isolated from wild-type mice (n=8). **D** FATP6$^{-/-}$ mice have hearts of similar weight in proportion to total body weight compared to wild-type mice when fed a chow or high-fat diet. High-fat diet feeding decreases the relative weight of the heart in proportion to total body weight in both wild-type and FATP6$^{-/-}$ mice (n=5-6). **E** FATP6$^{-/-}$ mice have lower heart triglyceride levels than wild-type mice on a chow diet. High-fat diet feeding ameliorates this effect (n=5-6). **F** FATP6$^{-/-}$ mice have lower heart free fatty acid levels than wild-type mice on a chow diet. High-fat diet feeding eliminates this effect (n=5-6). WAT = white adipose tissue, HFD = high-fat diet, RFU = relative fluorescent units, FFA = free fatty acids. *$p < 0.05$ versus wild-type, **$p < 0.005$ versus wild-type, $^{+}p < 0.05$ versus chow diet, $^{++}p < 0.005$ versus chow diet, $^{+++}p < 0.001$ versus chow diet. Error bars represent SEM.

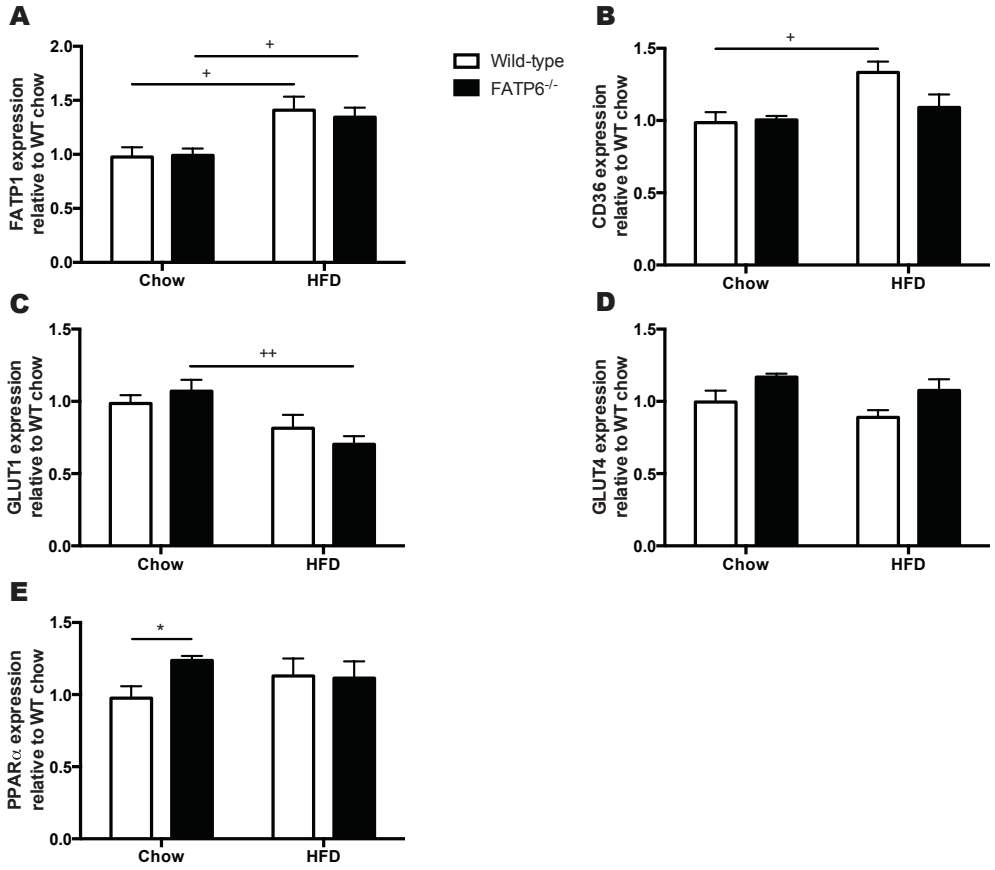

Figure 5. FATP6$^{-/-}$ mice express nutrient transporters in the heart at similar levels as wild-type mice.

A FATP1 expression in the heart increases upon high-fat feeding in both wild-type and FATP6$^{-/-}$ mice (n=5). **B** CD36 expression in the heart increases upon high-fat feeding in wild-type, but not FATP6$^{-/-}$ mice (n=5). **C** GLUT1 expression in the heart decreases upon high-fat feeding in mice (n=5). **D** GLUT4 expression trends towards increasing in FATP6$^{-/-}$ mice ($p = 0.050$ for chow diet and $p = 0.070$ for high-fat diet, n=5). **E** Cardiac PPARα expression is increased in FATP6$^{-/-}$ mice compared to wild-type mice on a chow diet (n=5). HFD = high-fat diet. $^{*}p < 0.05$ versus wild-type, $^{+}p < 0.05$ versus chow diet, $^{++}p < 0.005$ versus chow diet. Error bars represent SEM.

Table 2. Echocardiography results in wild-type and FATP6$^{-/-}$ mice

	WT Chow	WT HFD	FATP6$^{-/-}$ Chow	FATP6$^{-/-}$ HFD
IVSs (mm)	1.586 ± 0.096	1.684 ± 0.091	1.402 ± 0.048	1.630 ± 0.11
IVSd (mm)	1.048 ± 0.073	1.158 ± 0.045	0.9346 ± 0.030	1.091 ± 0.075
LVPWs (mm)	1.463 ± 0.12	1.461 ± 0.11	1.147 ± 0.096	1.345 ± 0.10
LVPWd (mm)	0.9701 ± 0.087	0.9946 ± 0.057	0.8415 ± 0.047	0.9168 ± 0.052
LVIDs (mm)	2.135 ± 0.20	1.992 ± 0.31	3.019 ± 0.18**	2.489 ± 0.19
LVIDd (mm)	3.565 ± 0.11	3.435 ± 0.22	4.278 ± 0.11**	3.696 ± 0.14^{+}
CI (ml/min/g BW)	0.5357 ± 0.019	0.3165 ± 0.031^{+++}	0.5486 ± 0.024	0.5443 ± 0.048**
SV (µl)	35.44 ± 1.54	33.76 ± 3.31	42.26 ± 2.32*	35.67 ± 3.88
EF (%)	68.52 ± 4.50	68.59 ± 4.69	54.69 ± 2.92*	60.95 ± 3.38
FS (%)	32.16 ± 3.79	34.21 ± 5.09	24.20 ± 1.74	27.24 ± 2.20
LV mass (mg/g BW)	3.838 ± 0.23	2.392 ± 0.10^{+++}	3.404 ± 0.098	2.431 ± 0.21^{++}

IVSs = intraventricular septum length at systole, IVSd = intraventricular septum length at diastole, LVPWs = left ventricular posterior wall thickness at systole, LVPWd = left ventricular posterior wall thickness at diastole, LVIDs = left ventricular internal diameter at systole, LVIDd = left ventricular internal diameter at diastole, CI = cardiac index, SV = stroke volume, EF = ejection fraction, FS = fractional shortening, LV = left ventricle, BW = body weight. *$p < 0.05$ versus wild-type, **$p < 0.005$ versus wild-type; $^{+}p < 0.05$ versus chow diet, $^{++}p < 0.005$ versus chow diet, $^{+++}p < 0.001$ versus chow diet. Mean is given with SEM.

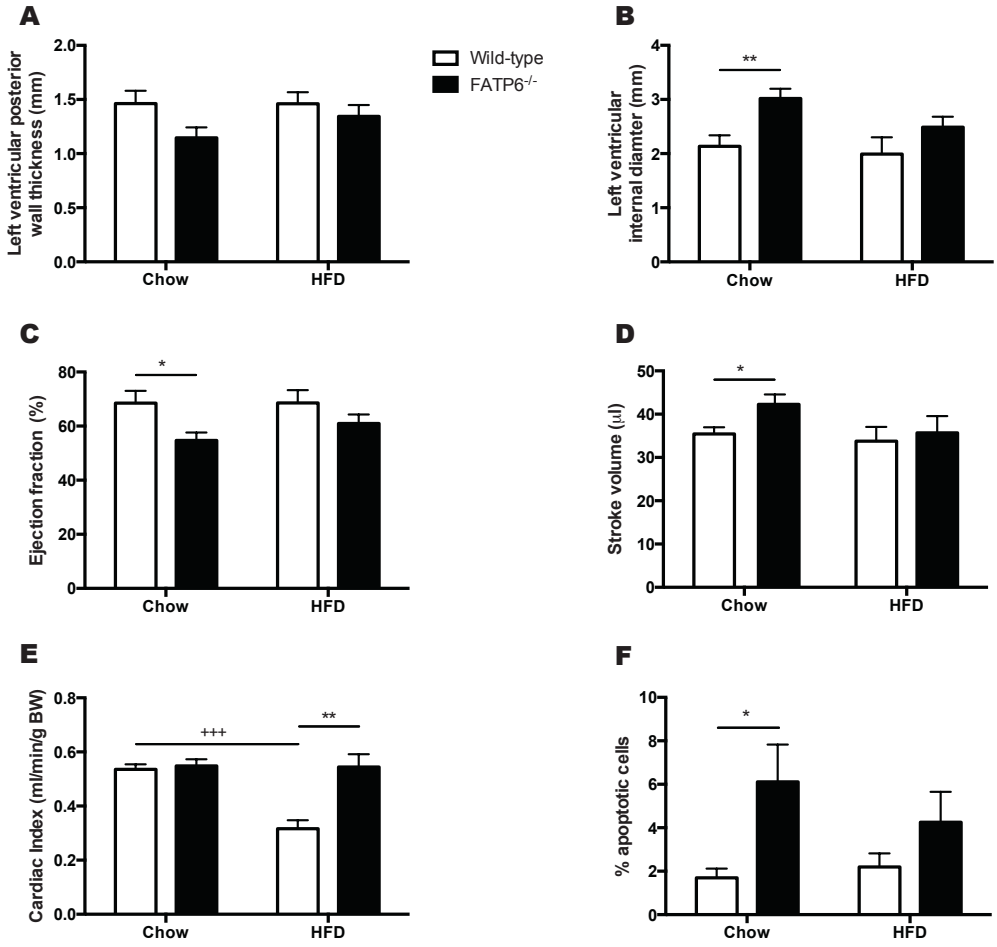

Figure 6. FATP6$^{-/-}$ mice have cardiac dilation, reduced systolic function, and enhanced levels of apoptosis in cardiomyocytes.

A On a chow diet, FATP6$^{-/-}$ mice show a trend towards decreased left ventricular posterior wall thickness at systole compared to wild-type mice, and this effect is reduced in mice fed a high-fat diet (n=5-6). **B** On a chow diet, FATP6$^{-/-}$ mice have larger left ventricular internal diameters during systole compared to wild-type mice, and this effect is reduced in mice fed a high-fat diet (n=5-6). **C** On a chow diet, FATP6$^{-/-}$ mice have significantly reduced ejection fraction compared to wild-type mice, and this effect is reduced in mice fed a high-fat diet (n=5-6). **D** On a chow diet, FATP6$^{-/-}$ mice have significantly increased stroke volume compared to wild-type mice, and this effect is reduced in mice fed a high-fat diet (n=5-6). **E** FATP6$^{-/-}$ mice have the same weight-adjusted cardiac output as wild-type mice on a chow diet, but FATP6$^{-/-}$ mice do not have the reduction in cardiac index observed in wild-type mice on a high-fat diet (n=5-6). **F** FATP6$^{-/-}$ mice on a chow diet have more apoptosis in cardiomyocytes than wild-type mice, while high-fat diet feeding alleviates this effect (n=5-6). HFD = high-fat diet, BW = body weight. *$p < 0.05$ versus wild-type, **$p < 0.005$ versus wild-type, $^{+}p < 0.05$ versus chow diet, $^{++}p < 0.005$ versus chow diet, $^{+++}p < 0.001$ versus chow diet. Error bars represent SEM.

Discussion

FATP6 facilitates the transport of fatty acids into cells. It is highly expressed in mouse testes, lung, and placenta, but may mediate fatty acid uptake in other peripheral tissues. Global deletion of FATP6 resulted in significantly reduced fatty acid uptake into cardiac tissue and FATP6$^{-/-}$ mice have reduced cardiac triglyceride and free fatty acid levels. We did not observe altered expression of other fatty acid transporters in the heart, but we did find a trend towards increased expression of glucose transporters. FATP6$^{-/-}$ mice show evidence of cardiac dilation, reduced systolic function, and enhanced cardiomyocyte apoptosis. While we did not directly measure beta-oxidation, glucose uptake, or glucose oxidation in our mice, our data suggests that FATP6$^{-/-}$ mice utilize fewer fatty acids in the heart than wild-type mice and unsuccessfully compensate for this reduction in fatty acid utilization with enhanced glucose utilization. Taken together, our data reveal a role for FATP6 in maintaining normal cardiac fatty acid metabolism and function.

FATP6$^{-/-}$ mice show evidence of systolic dysfunction suggesting dilated cardiomyopathy, including dilation of the left ventricle, reduced ejection fraction, and increased stroke volume. During dilated cardiomyopathy, the stroke volume of the heart increases to compensate for decreased ejection fraction in order to maintain cardiac output. Eventually, untreated dilated cardiomyopathy leads to the development of congestive heart failure[53]. This type of cardiomyopathy is the most prevalent form of cardiomyopathy and is the most common indicator for heart transplants in the United States[53].

FATP6$^{-/-}$ mice also have increased levels of apoptosis in cardiomyocytes. Although intracellular fatty acid accumulation itself is proposed to contribute to apoptosis and reduced cardiac function, cardiolipotoxicity is not well-documented in vivo and the mechanisms remain unclear[8]. Low levels of apoptosis in the heart have been shown to lead to dilated cardiomyopathy and heart failure in mice[78].

Feeding FATP6$^{-/-}$ mice a high-fat diet restored cardiac triglyceride and free fatty acid levels and ameliorated the changes we found in cardiac function, effectively rescuing the heart phenotype we observed. This suggests that reduced fatty acid availability in the heart drives the FATP6$^{-/-}$ heart phenotype. Hearts cannot fully compensate for reduced fatty acid oxidation with glucose oxidation[8]. Loss of FATP6 expression may result in reduced cardiac fatty acid utilization and overall reduced energy production, which could lead to cardiac inefficiency, dilated cardiomyopathy, and cardiomyocyte apoptosis.

Supporting this hypothesis, the FATP6$^{-/-}$ mouse heart phenotype mimics other mouse models and genetic human diseases in which there is a reduction in cardiac fatty acid utilization. The heart-specific lipoprotein lipase knockout mouse has reduced uptake of triglyceride-derived lipids in the heart, reduced palmitate oxidation, increased GLUT4 expression, increased glucose uptake, and increased glucose oxidation[61,79]. Heart-specific lipoprotein lipase knockout mice also show evidence of dilated cardiomyopathy, specifically left ventricular dilation and reduced fractional shortening, and the mice are unable to cope with ischemic stress[61]. CD36 knockout mice have reduced fatty acid uptake and oxidation in the heart[11,60,71], as well as reduced cardiac triglyceride levels[60] and increased glucose

oxidation[71], although they do not show signs of cardiomyopathy or reduced cardiac function. Some researchers have found that CD36 deficiency in humans, which also results in reduced fatty acid oxidation and enhanced glucose oxidation[80], is associated with hypertrophic cardiomyopathy, but this finding was not reproducible[81,82]. Heart-specific fatty acid binding protein knockout mice have reduced cardiac fatty acid utilization and enhanced glucose utilization as well, but they develop cardiac hypertrophy rather than dilated cardiomyopathy[59].

Several human genetic disorders that result in reduced expression and activity of genes involved in fatty acid oxidation result in dilated cardiomyopathy. Examples include deficiencies in malonyl-CoA decarboxylase, the enzyme that converts malonyl-CoA, an inhibitor of beta-oxidation, into acetyl-CoA[83]; deficiencies in very-long-chain acyl-CoA dehydrogenase, the first enzyme in the beta-oxidation pathway[84,85]; deficiencies in long-chain 3-hydroxyacyl-CoA dehydrogenase, the enzyme responsible for the third step in beta-oxidaiton[83], and systemic deficiencies in carnitine, the molecule that facilitates the transfer of fatty acids across the mitochondrial membrane[83].

Rodent models that result in increased fatty acid uptake in the heart, like cardiac overexpression of PPARα[63,73], FATP1[41], or acyl-CoA synthetase 1[65], or models of obesity like the db/db mouse[48] or obese ZDF rat[86] tend to result in the opposite heart phenotype. These mouse models show evidence of enhanced cardiac lipid accumulation, increased fatty acid oxidation, decreased glucose oxidation, and cardiac hypertrophy. Unlike the phenotype observed in the FATP6$^{-/-}$ mice, these metabolic abnormalities result in systolic as well as diastolic dysfunction and more closely resemble hypertrophic cardiomyopathy than dilated cardiomyopathy.

Clearly, it is important that hearts maintain a normal balance between fatty acid and glucose utilization and altering cardiac metabolism has profound effects on heart physiology and function. Equally apparent is that genes that control fatty acid availability play major roles in overall cardiac metabolism. In fact, it has been proposed that fatty acid uptake is the rate-limiting step of fatty acid utilization in the heart[45,66]. In the aforementioned mouse models and human genetic disorders, disruption of genes involved in cardiac fatty acid transport led to reduced fatty acid oxidation and gain-of-function of genes involved in cardiac fatty acid transport led to increased fatty acid oxidation. Although carnitine palmitoyltransferase-1 is viewed as the rate-limiting step in fatty acid utilization, its expression and activity do not correlate with fatty acid oxidation rates in the heart[66,87–89]. Here, a new mediator of fatty acid availability within cardiac tissue is described and its expression is shown to affect cardiac metabolism and overall function. To clearly demonstrate a link between FATP6 expression, fatty acid utilization, and cardiac function, future studies will need to measure cardiac fuel utilization in FATP6$^{-/-}$ mice.

We did not observe changes in fatty acid uptake in cardiomyocytes isolated from neonatal FATP6$^{-/-}$ mice compared to cardiomyoctyes from wild-type mice, but only in adult FATP6$^{-/-}$ hearts in vivo. This data, along with our expression data, suggests that the FATP6$^{-/-}$ mouse heart phenotype may be driven by global loss of FATP6 expression and not by deletion of FATP6 specifically in cardiac tissue. Alternatively, this data may indicate that FATP6 only mediates fatty acid uptake in

the hearts of adult mice rather than in neonatal mice. This hypothesis could be addressed by measuring fatty acid uptake in cardiomyocytes isolated from adult wild-type and FATP6$^{-/-}$ mice. It may also be the case that FATP6 activity requires factors that are present in vivo that we did not recapitulate in tissue culture. In order to better understand the location and mechanism of FATP6 in the heart, cardiac-specific FATP6 knockout mice could be generated using our current transgene and the phenotype of these mice could be compared to that of the whole-body FATP6 knockout mice.

Our data presents the possibility that FATP6 is playing a role in endothelial cell fatty acid transport. In support of this hypothesis, we observed a decrease or a trend towards decreased fatty acid uptake in tissues with continuous, non-porous endothelium, like the heart, lung, and white adipose tissue, while we did not observe any difference in fatty acid uptake in the liver, which has fenestrated endothelium. Fenestrated endothelium may allow albumin-bound fatty acid direct access to peripheral tissues, while tissues with continuous endothelium require the dissociation of fatty acids from albumin and the transport of fatty acids across the endothelial cell membrane prior to the fatty acids having access to peripheral tissues[66]. Secondly, our heart phenotype most closely resembles that of the heart-specific lipoprotein lipase mouse, which specifically results in reduced fatty acid availability to cardiomyocytes from the endothelium. Lipoprotein lipase is produced by peripheral tissues but acts in the surrounding capillaries[90]. Finally, our results coincide with a study published on a human FATP6 genetic variant with a single nucleotide polymorphism in the FATP6 gene that is proposed to result in constitutive binding of PPARα[42]. We would expect enhanced PPARα activity at the FATP6 promoter to result in increased FATP6 expression. Researchers in this study found reduced serum triglyercide and free fatty acid levels and increased left ventricular mass in men with the FATP6 variant compared to controls. While they did not measure the level or location of FATP6 expression in their subjects, it is tempting to speculate that the FATP6 variant resulted in increased expression of FATP6 and increased delivery of fatty acids from circulation into peripheral tissues, thereby reducing serum lipid levels and causing lipid accumulation and hypertrophy in the heart.

Researchers do not fully understand how circulating fatty acids traverse the endothelial wall and get taken up by peripheral tissues, but one study shows that two FATPs, FATP3 and FATP4, are expressed in endothelial cells and regulated by vascular endothelial growth factor[91]. This group went on to find significant physiological roles for FATP3 and FATP4 in mediating cellular fatty acid uptake in peripheral tissues, including the heart, but they did not thoroughly investigate the role of FATP6. FATP6 may also play a role in endothelial fatty acid transport and therefore systemic fatty acid availability to peripheral tissues.

Our expression data agrees with unbiased genetic screens in mice that found that FATP6 transcript is highly expressed in testes and lung[92]. This expression pattern deviates from the FATP6 expression pattern in humans. In humans, FATP6 is reported to be most highly expressed in the heart[35], and unbiased genetic and proteomic screens in humans confirm this finding[93–95]. While we do not detect robust expression of FATP6 in mouse heart, FATP6 does mediate fatty acid

availability in heart and thereby affects cardiac metabolism and physiology. Future studies will need to address what roles FATP6 plays in tissues where it is highly expressed in the mouse, like the testes, lung, and placenta.

Like other FATPs[4], FATP6 has fatty acid transport and acyl-CoA synthetase activity in vitro and mediates fatty acid availability in vivo. While we did not observe increased BODIPY-fatty acid uptake in HEK293 cells overexpressing FATP6, we did observe BODIPY-fatty acid acyl-CoA snythetase activity and uptake of C^{14}-oleate in vitro. In vivo, FATP6 mediated rapid BODIPY-fatty acid uptake. These data suggest that FATP6 does not necessarily have a substrate preference for oleate over other kinds of fatty acids, but rather that our cell system does not perfectly emulate biological fatty acid uptake conditions. Indeed, our lab has observed that stable cell lines expressing FATP6 sometimes lose fatty acid uptake capabilities over time[35].

In summary, FATP6 mediates fatty acid availability in vivo by enhancing the transport and activation of fatty acids. While it is highly expressed in the testes, lung, and placenta in the mouse, it is responsible for fatty acid uptake in the heart. We found that loss-of-function of FATP6 in mice led to reduced cardiac lipid accumulation, dilated cardiomyopathy, and cardiomyocyte apoptosis. Feeding the mice a high-fat diet diminished these effects, perhaps by increasing lipid levels enough to overcome the reduction in fatty acid import caused by lack of FATP6 activity. We hypothesize that FATP6 deletion results in reduced cardiac fatty acid utilization, which leads to reduced cardiac efficiency, and that this in turn leads to dilated cardiomyopathy and cell death. These findings constitute the first evidence for a physiological role of FATP6 in vivo. We are also the first to show that deletion of a fatty acid transporter results in diminished cardiac function. Targeting fatty acid transport may prove to be an effective method to restore normal cardiac metabolism and prevent the development of cardiomyopathy and other cardiac dysfunction in the event of excess or deficient fatty acid utilization.

Methods

Animal experiments

All animal procedures were approved by the University of California Berkeley Animal Care and Use Committee. C57BL/6J mice were purchased from the Jackson Laboratory (#000664). $FATP6^{-/-}$ mice were generated as described below. All animal experiments were performed in 6- to 24-week-old male mice. Mice were given free access to water and rodent chow (Harlan Teklad #2018) or 60% fat diet (Research Diets, Inc. #D12492) and housed under standard conditions. The 60% fat diet was maintained for 16 weeks. Blood glucose was measured with a glucometer (NovaMax #14). For serum analyses, 50 µl of blood was collected with a non-heparinized capillary tube and allowed to coagulate at room temperature for 15-30 minutes. The blood was centrifuged at 1500 x g for 10 minutes at 4°C and the serum was further analyzed.

Generation of transgenic mice

The FATP6 transgene was designed and developed by the Knockout Mouse Consortium (Project ID #CSD39430, **Fig. 2A**). Researchers at the Mouse Biology

Program at the University of California, Davis electroporated two distinct clones of knockout-first, promoter-driven vectors into JM8.N4 agouti stem cells and implanted the stem cells into C57BL/6J blastocysts. The location of the transgene in the stem cells was verified with long-range PCR (**Fig. 2B**). Chimeric mice were produced and bred to C57BL/6J mice to test for germline transmission. Germline transmission for both clones was confirmed with long-range PCR and quantitative PCR (**Fig. 2B**, **2C**, and **Table S1**; primers in **Table S2**). Heterozygous mice for each clone were bred together to generate FATP6$^{-/-}$ mice. Both colonies of mice were used in subsequent studies.

Echocardiography

Echocardiography was performed in mice using the Vevo2100 ultrasound (VisualSonics). Mice were anesthetized with 3% isoflurane and held under 1.5-2.5% anesthesia to maintain a heart rate of 400-500 beats per minutes. The fur covering the thorax was removed with a depilatory cream and body temperature was maintained at 37°C. Hearts were first imaged in B-mode in a parasternal long-axis view using a MS 550S transducer and then in M-mode in a short-axis view. At least two sets of time-lapse images were collected in each view for each mouse. Images were analyzed using the Vevo2100 software. A left ventricular trace was performed for B-mode and M-mode images. Intraventricular septum, left ventricular internal diameter, and left ventricular posterior wall thickness were measured in M-mode in four tandem cardiac cycles. The Vevo2100 software utilized these measurements to calculate cardiac output, stroke volume, ejection fraction, fractional shortening, and left ventricular mass with algorithms detailed in their manual. Replicate measurements and values were averaged for each mouse. Cardiac output was adjusted for animal body weight and presented as cardiac index. Left ventricular mass was also adjusted for animal body weight.

In vivo BODIPY-fatty acid uptake assay

Wild-type and FATP6$^{-/-}$ mice were fasted for three hours and injected with 20 μM BODIPY-fatty acid (Molecular Probes #D3823) bound to 1% bovine serum albumin at 0.125 μmol BODIPY per kilogram of body weight. Mice were euthanized and tissues were harvested 15 minutes later. Tissues were homogenized in radioimmunoprecipitation assay buffer (150 mM sodium chloride, 1% NP-40, 0.5% deoxycholic acid, 0.1% sodium dodecyl sulfate, 50 mM Tris, pH 8.0) and the fluorescence of the lysate was read at an excitation of 488 nm and emission of 515 nm using the SpectraMaxi3 plate reader (Molecular Devices). Protein content was quantified by the bicinchoninic assay (Pierce #23225). Relative fluorescence values were adjusted for lysate protein content.

Isolation and culture of neonatal cardiomyocytes

Neonatal mouse cardiomyocytes were isolated using a published protocol[96]. Briefly, hearts were extracted from one- to three-day-old mice and minced and digested overnight in 0.0125% trypsin supplemented with 20 mM 2,3-butanedione monoxime (Sigma #B-0753). The next day, hearts were further digested in 1.5

mg/ml collagenase/dispase (Roche #10269638001) in L-15 media supplemented with 20 mM 2,3-butanedione monoxime for 30-40 minutes while shaking at 37°C. The digest was filtered through a 100 μM cell strainer and centrifuged at 100 x *g* for 5 minutes to pellet cardiomyocytes. Cells were then plated in DMEM media with 19% M-199, 10% horse serum, 5% fetal calf serum, and 1% penicillin-streptomycin onto tissue culture plates for three hours to allow for the adherence of fibroblasts. The non-adherent cardiomyocytes were re-plated onto collagen-coated glass culture dishes (0.1% collagen solution from Sigma #I-6501, glass culture dishes from MatTek #P35GC-1.0-14-C). After 16 hours, the plating media was replaced with DMEM media with 17% M-199, 4% horse serum, 1% penicillin-streptomycin, 1 μM cytosine-B-D-arabinofuranoside hydrochloride (Sigma #C-6645), and 1 μM isoproterenol (Sigma #I-6501).

BODIPY-fatty acid uptake assay in isolated cardiomyocytes

18-24 hours after plating isolated cardiomyocytes, beating cells were imaged for BODIPY-fatty acid uptake using a Zeiss AxioObserver Z1 microscope. Cell media was replaced with a solution containing 1 mM trypan blue, 3.5 g/L glucose, 2 μM BODIPY-fatty acid, and 0.1% bovine serum albumin in Hank's buffered saline solution. Images were captured with a 20x objective every 30 seconds for 30 minutes. Images were processed with ImageJ. The mean fluorescence of individual cells was plotted over time and linear regression was performed to calculate the steady-state change in fluorescence.

β-galactosidase activity assay

β-galactosidase activity was measured in mouse tissue using the Galacto-Star™ System (Applied Biosystems #T1012). Wild-type and FATP6$^{-/-}$ tissues were homogenized in lysis buffer. The lysates were incubated at 48°C for one hour to inactivate endogenouse β-galactosidase activity. The lysates were diluted 1:10 into Galacto-Star™ reaction buffer and incubated for 30 minutes. The luminescence of each sample was detected with a SpecrtraMax i3 plate reader with an integration time of 0.1-1 second/well. Light signal was adjusted for protein concentration.

β-galactosidase staining

β-galactosidase activity was detected on tissue sections using a standard protocol. Wild-type and FATP6$^{-/-}$ mice were sacrificed and perfused with 50 ml of ice-cold 4% paraformaldehyde (Electron Microscopy Sciences #15710) through the left ventricle of the heart. Each organ was dissected and fixed in 4% paraformaldehyde for an additional 30 minutes at 4°C, washed in phosphate-buffered saline, then equilibrated in 30% sucrose overnight at 4°C. The tissues were cryopreserved in O.C.T Compound (Sakura #4583) in a cryomold and sectioned at 10 μM onto charged glass slides with a Leica CM3050S cryostat at -20°C. The resulting slides were stained in a solution containing 2 mM magnesium chloride, 0.01% deoxycholic acid, 0.02% IGEPAL CA-630, 0.1% 5-bromo-4-chloro-3-indolyl β-D-galactopyranoside (X-gal, Sigma #B4254) in dimethylfluoride, 5 mM potassium ferrocyanide, and 5 mM potassium ferricyanide overnight at 37°C. The slides were

rinsed in phosphate-buffered saline, post-fixed in 4% paraformaldehyde for one hour at 4°C, and counter-stained in Nuclear Fast Red (Sigma #N3020) for one minute. The slides were dehydrated in 50% ethanol, 70% ethanol, and 100% ethanol in succession, cleared in Xylenes, and mounted in Permount (Fisher #SP15-100). The slides were imaged with a Zeiss Axioimager M1 microscope.

Apoptosis assay

Hearts were dissected and fixed in 4% paraformaldehyde for one hour at 4°C, washed in phosphate-buffered saline, then equilibrated in 30% sucrose overnight at 4°C. The tissues were cryopreserved in O.C.T Compound in a cryomold and sectioned at 10 μM onto charged glass slides at -20°C. Heart sections were stained for apoptotic cells using the In Situ Cell Death Detection Kit (Roche #11684795910). Briefly, the slides were post-fixed in 4% paraformaldehyde for 20 minutes at room temperature, permeabilized with 0.1% Triton X-100 (Sigma Aldrich #234729) in 0.1% sodium-citrate for 5 minutes at room temperature, then incubated in TUNEL reaction mixture at 37°C for one hour. As a positive control for the reaction, a heart section was treated with DNase I for 10 minutes before the TUNEL stain. Slides were mounted in DAPI mountant (Life Technologies P36971) and imaged with a Zeiss LSM710 laser scanning confocal microscope. TUNEL-positive apoptotic cells and total number of cells were quantified with IMARIS.

Cell culture

HEK293 cells (ATCC #CRL-1573) were maintained in DMEM supplemented with 10% fetal bovine serum and 1% penicillin-streptomyocin and incubated at 37°C with 5% CO_2. The human FATP6 gene was cloned into pIRES-neo (Addgene #10835) and transfected into HEK293 cells with Fugene HD (Promega #E2311). FATP6-expressing cells were selected by growing cells in media containing G418 (Sigma #A1720). Cells were serially diluted to obtain single colonies of clonal cells. The clone expressing the highest level of FATP6 transcript was used in subsequent assays. Cells expressing human FATP5 were previously generated in the lab[40] and cells expressing ACSL4 were generated by transient transfection of the mouse ACSL4 gene into HEK293 cells.

Quencher-based real-time BODIPY-fatty acid uptake assay

The real-time fatty acid uptake assay was based on a previously published assay[97]. Cells were plated in a 96-well plate with 30,000 cells per well the day before the assay. Cell media was replaced with uptake solution containing 1 mM trypan blue, 3.5 g/L glucose, 2 μM BODIPY-fatty acid, and 0.1% bovine serum albumin in Hank's buffered saline solution. The cells were immediately placed into a SpectraMax i3 plate reader and the fluorescence was read at an excitation of 488 nm and emission of 515 nm every minute for two hours. The steady-state change in fluorescence over time was plotted.

C^{14}-oleate uptake assay

Cells were plated in a six-well plate the day before the assay. Cell media was replaced with uptake solution containing 20 μM C^{14}-oleate in 0.1% bovine serum albumin. The cells were incubated with uptake solution for ten minutes and the reaction was stopped by addition of ice-cold 0.2% bovine serum albumin. Cells were homogenized in radioimmunoprecipitation assay buffer and radiation was quantified in the cell lysate with a liquid scintillation counter. The values were adjusted for protein content.

BODIPY-fatty acyl CoA synthetase activity assay

Cells were trypsinized and lysed in 300 mM sucrose supplemented with 2 mM MOPS-sodium hydroxide, pH 7.4. The cell lysate was incubated with a solution containing 2 μM BODIPY-fatty acid (Molecular Probes #D3821), 20 μM Coenzyme A (Sigma #C3144), 10 mM ATP (Sigma #A2383), 10 mM magnesium chloride, and 150 mM tris-hydrochloride for 20 minutes at 37°C. The reaction was stopped by moving the lysates to Dole's reagent containing heptane:isopropanol:2 N sulfuric acid in a 10:40:1 ratio. Fatty acids were extracted by vortexing the lysates with Dole's reagent and centrifuging the samples to create an aqueous and organic layer. The aqueous layer was washed two times with additional heptane. The fluorescence of the aqueous layer was measured using a SpectraMax i3 plate reader at an excitation of 488 nm and emission of 515 nm. The values were adjusted for the protein content of the original lysates.

Quantitative PCR

1 μl of cDNA was used in a 20 μl PCR reaction along with 1 μl PrimeTime qPCR assay [Integrated DNA Technologies #Mm.PT.39a.1 for glyceraldehyde 3-phosphate dehydrogenase (GAPDH), #Hs.PT.58.40136242 for hsFATP6, #Mm.PT.58.43265938 for mmFATP6, #Mm.PT.53a.33622420 for mmFATP1, #Mm.PT.58.12375764 for mmCD36, #Mm.PT.58.7020742 for mmPPARα, #Mm.PT.58.9683859 for mmGLUT1, and #Mm.PT.58.9683859 for mmGLUT4] and 10 μl TaqMan Universal Master Mix II (Thermo Fisher Scientific #4440040). The PCR reactions were run and cycle thresholds were calculated with the Applied Biosystems 7500 Real Time PCR System. Fold change was calculated by comparing the difference in cycle thresholds between the gene of interest and the housekeeping gene for treated samples and control samples. For placenta samples, RNA was collected from e12.5 placentas.

Quantification of triglycerides, free fatty acids, and insulin in tissue lysate and serum

Triglycerides were quantified with the Infinity Triglycerides reagent (ThermoFisher Scientific #TR22421) according to the manufacturer's protocol. Serum or lysate samples were diluted 1:100 into the reagent and incubated for five minutes at 37°C. The absorbance of the samples was read at 500 nm with a SpectraMax i3 plate reader. Absolute triglyceride values were calculated by comparing the sample absorbance values to a known standard absorbance value. Tissue triglyceride content was adjusted for protein content.

Free fatty acids were quantified using the HR Series NEFA-HR (2) (Wako #999-34691, #999-34791, #999-34891, #999-35191) according to the manufacturer's protocol. The serum or lysate samples were diluted into color reagent A 1:50 and incubated for five minutes at 37°C. Color reagent B was added to the solutions at half the volume of color reagent A and allowed to incubate for five additional minutes at 37°C. The absorbance of the samples was read at 550 nm. Absolute free fatty acid values were calculated by comparing sample absorbance values to the absorbance values of oleic acid standards.

Insulin was quantified with a mouse insulin ELISA (CrystalChem #90080) according to the manufacturer's protocol. Serum samples were diluted into sample diluent and allowed to incubate on the microplate for 2 hours at 4°C. After extensive washing of the plate, anti-enzyme conjugate was added to each well and allowed to incubate for 30 minutes at room temperature. After more washing, enzyme substrate solution was added to the microplate and allowed to incubate for 40 minutes. The reaction was stopped by the addition of enzyme reaction stop solution and the absorbance of each well was measured at 450 nm using a plate reader. Absolute insulin values were calculated by comparing sample absorbance values to the absorbance values of insulin standards.

Statistical analysis

Differences between two groups were determined using an unpaired Student's *t* test with Welch's correction. Linear regression analysis was used to determine the change of values over time. Data are presented as mean values with error bars representing the standard error of the mean. Asterisks and plus signs indicate significant differences (*$p < 0.05$ versus wild-type or another group, **$p < 0.005$ versus wild-type or another group, **$p<0.001$ versus wild-type or another group, $^{+}p < 0.05$ versus chow diet, $^{++}p < 0.005$ versus chow diet, $^{+++}p < 0.001$ versus chow diet).

Supplemental Data

Supplemental Table 1. Genotyping strategy used to detect FATP6 transgene.

Genotyping Strategy			
Genotype	**Forward Primer**	**Reverse Primer**	**Amplicon size (bp)**
Floxed	CSD-loxF	CSD-Slc27a6-R	333
Pre-Cre	CSD-neoF	CSD-Slc27a6-ttR	584
Post-Cre	CSD-lacF	CSD-Slc27a6-R	631
Wild-type	CSD-Slc27a6-F	CSD-Slc27a6-ttR	591
Post-Flp	CSD-Slc27a6-F	CSD-Slc27a6-ttR	767
Post-Flp & -Cre	CSD-Slc27a6-F	CSD-Slc27a6-R	809
3' verification	CSD-LoxPcomF1	LR-Slc27a6-R3	5128
5' verification	5' Gene Specific (GF4)	5' Universal (LAR3)	5376

Supplemental Table 2. Genotyping primers used to detect FATP6 transgene.

Genotyping Primers
CSD-lacF: GCTACCATTACCAGTTGGTCTGGTGTC
CSD-neoF: GGGATCTCATGCTGGAGTTCTTCG
CSD-loxF: GAGATGGCGCAACGCAATTAATG
CSD-Slc27a6-R: AACAAAACCGAACAGGAATGCACCC
CSD-Slc27a6-ttR: AGCCCTGAAAGCATGTGAATACTGC
CSD-Slc27a6-F: TTGATGGCCAAGAGAAGAAGCAAGC
LR-Slc27a6-R3: ACACTGGCAAGCAGACACTCTCC
CSD-LoxPcomF1: GAGATGGCGCAACGCAATTAAT
5' Universal (LAR3): CACAACGGGTTCTTCTGTTAGTCC
5' Gene Specific (GF4): GATCAGGATTCTCTAATAAGGTAATCTCAG

Supplemental Table 3. Homozygous and heterozygous FATP6 transgenic mouse breeding from two clones of stem cells.

	Clone #1	**Clone #1**	**Clone #2**	**Clone #2**
	$FATP6^{-/-}$ x $FATP6^{-/-}$	**$FATP6^{-/-}$ x $FATP6^{-/+}$**	**$FATP6^{-/-}$ x $FATP6^{-/-}$**	**$FATP6^{-/-}$ x $FATP6^{-/+}$**
# of litters	8	4	3	4
Avg # of pups	6.25	7	5.67	6.25
% Male	36%	41%	53%	52%
% Female	64%	59%	47%	48%
% Heterozygous		61%		52%
% Knockout		39%		48%

Supplemental Video 1. Cultured neonatal mouse cardiomyocytes are viable and functional.

Supplemental Video 2. Neonatal mouse cardiomyocytes take up BODIPY-fatty acid and form intracellular lipid droplets over the course of 30 minutes.

Chapter 2: Deletion of FATP1 or FATP6 does not alter cardiac function in STZ-induced diabetic mice

Rationale

Nearly one-tenth of the United States population is diabetic, and rates of diabetes are expected to continue to rise over the next 20 years due to the prevalence of obesity and the metabolic syndrome[98,99]. Heart disease in the leading cause of morbidity and mortality in both type I and type II diabetic patients[100]. While heart failure is often a result of ischemic heart disease or hypertension in diabetic patients, it is estimated that nearly half of diabetic patients have diastolic dysfunction[101]. Impaired left ventricular function in the absence of coronary artery disease or hypertension has been clinically observed in diabetic patients[101,102] and is now recognized as a distinct clinical manifestation of diabetes termed diabetic cardiomyopathy[39,99,103]. Diabetic cardiomyopathy is characterized by cardiac hypertrophy[104–106] and diastolic dysfunction[107,108] with or without systolic dysfunction[109]. One-third of patients with diabetic cardiomyopathy develop heart failure or die within nine years of diagnosis[101].

The systemic metabolic changes during diabetes, including hyperglycemia, hyperlipidemia, insulin resistance in the case of type II diabetes, and hypoinsulinemia in the case of type I diabetes, lead to molecular changes within cardiac tissue that cause structural and functional abnormalities in the heart[98,99,103]. One of the molecular hallmarks of diabetic cardiomyopathy is increased fatty acid utilization[50,110–113]. The human heart normally relies on fatty acids for 70% of oxidative metabolism[43–45] and can adapt to ischemic conditions or increased workload by shifting to enhanced glucose or lactate utilization[55,114,115]. During diabetic cardiomyopathy, the heart loses metabolic flexibility and nearly 100% of ATP production comes from fatty acid oxidation[39,116]. In both type I and type II diabetes, lack of insulin action results in reduced glucose uptake, glycolysis, and glucose oxidation[113,117–120]. This reduced glucose utilization and the increased substrate availability from elevated triglyceride and fatty acid levels leads to enhanced fatty acid uptake, storage, and oxidation[39,98,99].

Rodent models have provided evidence that increased fatty acid utilization independently causes cardiac dysfunction in diabetes[38,39]. Lipid accumulation has been well-documented in patients[50,121,122] and in rodent models[123–125] and is an independent predictor of diastolic dysfunction in humans[126]. In rodents, lipid accumulation precedes the development of diabetic cardiomyopathy[125,127]. Reducing lipid accumulation by reducing fatty acid uptake[64], increasing intracellular triglyceride stores[128], or increasing fatty acid oxidation alleviates cardiac dysfunction[99]. Conversely, enhancing lipid accumulation causes cardiac hypertrophy in mice[8,65,129]. Enhanced fatty acid utilization causes an increase in oxygen consumption without an increase in cardiac contractility and therefore results in reduced cardiac efficiency[38,99,130]. Metabolic inflexibility also impairs the heart's ability to adapt to hypoxia or exercise[83]. It is thought that toxic lipid intermediates like ceramides, diacylglycerol, and oxidized phospholipids cause

cellular stress and cardiomyocte apoptosis and necrosis rather than neutral intracellular lipid stores themselves[8,99].

Fatty acid transport into cardiomyocytes is proposed to be the rate-limiting step in fatty acid utilization in the heart[45,66,87–89]. Fatty acid uptake across the sarcolemma membrane is saturable and primarily regulated by the activity of fatty acid transporters like fatty acid translocase (CD36), plasma membrane fatty acid binding protein (FABPpm), and fatty acid transport proteins 1 and 6 (FATP1, FATP6)[66–70]. Cardiac fatty acid transporter expression levels are upregulated in diabetic rats[66,70,131]. Much work has been done on the role of CD36 in cardiac fatty acid transport in the context of diabetes. Constitutive, rather than regulated, expression of CD36 on the sarcolemma membrane drives excess fatty acid import in the ZDF diabetic rat[132] and CD36 expression is correlated with the severity of insulin deficiency in streptozotocin-injected rats[133]. In a mouse model of diabetic cardiomyopathy in which peroxisome proliferator-activated receptor α (PPARα) was overexpressed in cardiac tissue, loss-of-function of CD36 reduced cardiac lipid accumulation, increased glucose utilization, diminished cardiac hypertrophy, and enhanced systolic function[64].

Less is known about the role of FATPs in the context of diabetes. One group overexpressed FATP1 in cardiac tissue and found increased fatty acid uptake and lipid accumulation in the hearts of transgenic mice as well as evidence of cardiac hypertrophy and diastolic dysfunction[41]. However, no one has investigated whether loss-of-function of FATP1 affects the heart phenotype in diabetic cardiomyopathy. FATP6 is also expressed in the heart[35] but has not been as thoroughly studied as other FATPs. In fact, we are the first to show evidence for a physiological role for FATP6 in cardiac fatty acid transport in vivo (Chapter 1). To better understand the impact of FATP1 and FATP6 expression on the development of diabetic cardiomyopathy, we developed a mouse model of diabetes, characterized the heart phenotype in this model, and evaluated the effect of loss-of-function of FATP1 and FATP6 in this context. Our diabetic mouse model did not result in sufficient changes in cardiac function to adequately test the role of FATPs and a more robust model of diabetic cardiomyopathy will have to be developed.

Results

A high-fat diet and two low-dose STZ injections results in diabetes

We chose to induce diabetes with two low-dose streptozotocin (STZ) injections in the context of a high-fat diet. STZ is a toxic glucose analog that is primarily taken up by pancreatic beta cells, selectively destroying the insulin-producing cells[134]. While elimination of beta cells more closely resembles a type I diabetic phenotype rather than a type II diabetic phenotype, we fed the mice a high-fat diet before and after the STZ injections to induce insulin resistance and maintain hyperlipidemia[134]. We also chose to inject the mice with two low doses of STZ rather than one high dose in order to preserve a portion of the beta cell mass[135].

After testing several different durations of high-fat diet feeding prior to STZ injections, we found that feeding mice a high-fat diet for a minimum of four weeks

prior to STZ injections reliably resulted in hyperglycemia, while feeding mice a high-fat diet for less than four weeks did not always make beta cells sufficiently sensitive to STZ-induced cell death (data not shown). As shown in **Figure 1A**, four weeks of a high-fat diet resulted in significant weight gain in mice. Four weeks of a high-fat diet followed by two low-dose STZ injections resulted in significant hyperglycemia within days of STZ injections, while feeding mice a high-fat diet alone or giving mice two low-dose STZ injections alone did not produce hyperglycemia (**Fig. 1B**). Diabetic mice lost body weight immediately after STZ injections, but maintained normal body weights for the rest of the study (**Fig. 1A**).

In addition to blood glucose levels, we measured glucose tolerance four weeks after the STZ injections. Compared to chow-fed mice, eight weeks of a high-fat diet and two low-dose STZ injections independently produced glucose intolerance in mice, but giving mice STZ injections in the context of a high-fat diet resulted in an even greater reduction in glucose tolerance (**Fig. 1C**).

Four weeks after the STZ injections, we measured insulin levels in the mice. Only the mice given STZ injections in the context of a high-fat diet had significantly reduced serum insulin levels compared to chow-fed mice (**Fig. 1D**). To investigate how STZ injections affected insulin production in pancreatic beta cells, we performed immunohistochemistry for insulin on sections of pancreas from the mice. As expected, we found that STZ injections in chow- and high-fat diet-fed mice decreased beta cell insulin content, while high-fat diet feeding without STZ injections resulted in increased beta cell insulin content (**Fig. 1E** and **F**).

Diabetes results in enhanced expression of fatty acid transport proteins and reduced expression of glucose transport proteins in the heart

During diabetic cardiomyopathy, fatty acid utilization increases and glucose utilization decreases in the heart[50,110–113]. This is associated with increased cardiac expression of fatty acid transport proteins and decreased cardiac expression of glucose transport proteins[66,70,73]. To assess whether we see evidence of this metabolic switch in our mouse model of diabetes, we measured the expression of fatty acid transport proteins and glucose transport proteins as well as the expression of PPARα. PPARα is a transcription factor that regulates the expression of many metabolic genes and its expression in increased in the heart in diabetic cardiomyopathy[63,72,73]. For this assay, we fed mice a high-fat diet for two weeks prior to STZ injections and measured changes in gene expression four weeks after STZ injections. This protocol to induce diabetes resulted in increased expression of the fatty acid transporters FATP1, FATP6, and CD36, enhanced expression of PPARα, and reduced expression of glucose transporter 1 (GLUT1) and glucose transporter 4 (GLUT4) (**Fig.2A**). Cumulatively, these results suggest a shift towards increased fatty acid utilization and decreased glucose utilization in our mouse model of diabetes.

Diabetic mice do not develop cardiac hypertrophy

If cardiac fatty acid uptake exceeds fatty acid oxidation, lipids accumulate in cardiomyocytes[41,65]. Lipid accumulation is a hallmark of diabetic cardiomyopathy and is associated with cardiac hypertrophy[8,65,129], lipotoxicity[8], and cardiac dysfunction[126]. We fed mice a high-fat diet for four weeks, injected the mice with two low-doses of STZ, and measured cardiac lipid accumulation and heart weight twelve weeks later. We found a trend towards increased heart triglycerides in diabetic mice, although this increase was not significant (**Fig. 2B**). Heart weight relative to total body weight decreased in mice fed a high-fat diet, but relative heart weight was restored in diabetic mice (**Fig. 2C**). We also measured left ventricular mass relative to body weight using echocardiocardiography. We found that both high-fat diet-fed mice and diabetic mice had decreased left ventricular mass compared to non-diabetic chow-fed mice, but that diabetic mice had greater relative left ventricular mass than high-fat diet-fed mice (**Fig. 2D** and **Table 1**). These changes in relative heart weight and left ventricular mass seem driven more by changes in body weight than by diet or diabetes. Taken together, these data suggest that although we see a trend towards enhanced cardiac triglyceride content, we do not see evidence of cardiac hypertrophy in our diabetic mouse model.

Diabetic mice do not show evidence of lipotoxicity

To further assess the effects of diabetes on cardiomyocytes, we measured levels of apoptosis and fibrosis 12 weeks after inducing diabetes in mice. Using a TUNEL stain for apoptotic cells, we did not detect changes in the rate of cardiomyocyte apoptosis in the context of a high-fat diet or diabetes (**Fig. 2E**). Using a Masson's Trichrome stain we also did not detect induction of fibrosis in high-fat diet-fed or diabetic mice (**Fig. 2F**). So, although we found evidence for increased fatty acid utilization in our mouse model of diabetes, we did not detect evidence for lipotoxicity.

Diabetic mice do show evidence of altered cardiac function

To assess cardiac function in diabetic mice, we performed echocardiography in mice 12 weeks after inducing diabetes. Echocardiography is the standard technique used to measure cardiac function in vivo and is now routinely and reliably performed in small rodents[74–77]. We found no difference in left ventricular wall thickness or left ventricular diameter with high-fat diet feeding or diabetes (**Table 1**). We found a significant decrease in weight-adjusted cardiac output in mice fed a high-fat diet, but weight-adjusted cardiac output was restored in diabetic mice. Again, this change seemed driven by changes in body weight rather than by induction of diabetes. We found no differences in measures of systolic function, including stroke volume, ejection fraction, or fractional shortening.

To summarize, although feeding mice a high-fat diet for four weeks and injecting with two low doses of STZ results in robust hyperglycemia and hypoinsulinemia as well as transcriptional changes suggesting increased fatty acid utilization, this

protocol does not produce cardiac hypertrophy, cardiolipotoxicity, or cardiomyopathy.

FATP1$^{-/-}$ mice develop diabetes like wild-type mice

Despite the fact that we did not observe a striking heart phenotype indicative of diabetic cardiomyopathy in mice made diabetic with our protocol, we evaluated the role of FATP1 and FATP6 within this context. We induced diabetes in wild-type and whole-body FATP1 and FATP6 knockout (FATP1$^{-/-}$ and FATP6$^{-/-}$) mice and assessed the hearts of these mice.

As shown in **Figure 3B**, STZ injections in the context of a high-fat diet produce hyperglycemia in FATP1$^{-/-}$ mice as in wild-type mice. For this study we fed mice a high-fat diet for only two weeks prior to STZ injections and analyzed the heart phenotypes of the mice eight weeks after STZ injections. FATP1$^{-/-}$ mice had similar body weights and serum insulin levels as wild-type mice (**Fig. 3A** and **3C**).

FATP1$^{-/-}$ mice have a diabetic heart phenotype comparable to wild-type mice

We assessed the heart phenotype in diabetic FATP1$^{-/-}$ and wild-type mice using the aforementioned assays. Diabetic FATP1$^{-/-}$ mice expressed other fatty acid transport proteins, glucose transport proteins, and PPARα at similar levels as diabetic wild-type mice, although there was an insignificant trend towards reduced expression of CD36 and PPARα in FATP1$^{-/-}$ mice (**Fig. 4A**). FATP1$^{-/-}$ mice also had similar cardiac triglyceride levels and relative heart weights as wild-type mice (**Fig. 4B** and **C**). FATP1$^{-/-}$ mice had a trend towards reduced rates of apoptosis in cardiomyocytes, but this difference was not significant (**Fig. 4D**). We did not detect appreciable levels of fibrosis in FATP1$^{-/-}$ or wild-type mice (**Fig. 4E**). Taken together, our data suggest that there is no difference in the heart phenotype of FATP1$^{-/-}$ mice compared to wild-type mice in the context of diabetes. It is important to point out that we had high variation in our findings and that this variation may be masking the effects of loss-of-function of FATP1.

FATP6$^{-/-}$ mice develop diabetes like wild-type mice

We also investigated the effect of FATP6 expression on the development of diabetic cardiomyopathy. For this study, we fed mice a high-fat diet for four weeks, injected mice with two low-doses of STZ, and analyzed the heart phenotypes of the mice 12 weeks after the STZ injections. As shown in **Figure 5B**, FATP6$^{-/-}$ mice develop hyperglycemia to the same extent as wild-type mice. Diabetic FATP6$^{-/-}$ mice have similar body weights and serum insulin, triglyceride, and free fatty acid levels as diabetic wild-type mice (**Fig. 5A** and **C-E**).

Diabetic FATP6$^{-/-}$ mice have dilated hearts compared to wild-type mice

FATP6$^{-/-}$ mice expressed fatty acid transporters, PPARα, and glucose transporters in the heart at the same level as wild-type mice in the context of diabetes (**Fig. 6A**). Diabetic FATP6$^{-/-}$ mice had similar cardiac triglyceride levels, relative heart weights, and left ventricular mass as wild-type mice (**Fig. 6B-D**). Surprisingly, diabetic

FATP6$^{-/-}$ mice showed a trend towards elevated levels of cardiomyocyte apoptosis, but this difference was not significant (**Fig. 6E**). We did not detect appreciable levels of fibrosis in either FATP6$^{-/-}$ or wild-type mice (**Fig. 6F**).

Using echocardiography, we found that FATP6$^{-/-}$ mice had thinner left ventricular walls and enhanced left ventricular internal diameters compared to wild-type mice in the context of diabetes (**Fig. 6G** and **H** and **Table 2**). These anatomical differences in FATP6$^{-/-}$ hearts did not translate into changes in systolic function in diabetic mice (**Table 2**). Weight-adjusted cardiac output, stroke volume, ejection fraction, and fractional shortening were similar between diabetic FATP6$^{-/-}$ and wild-type mice.

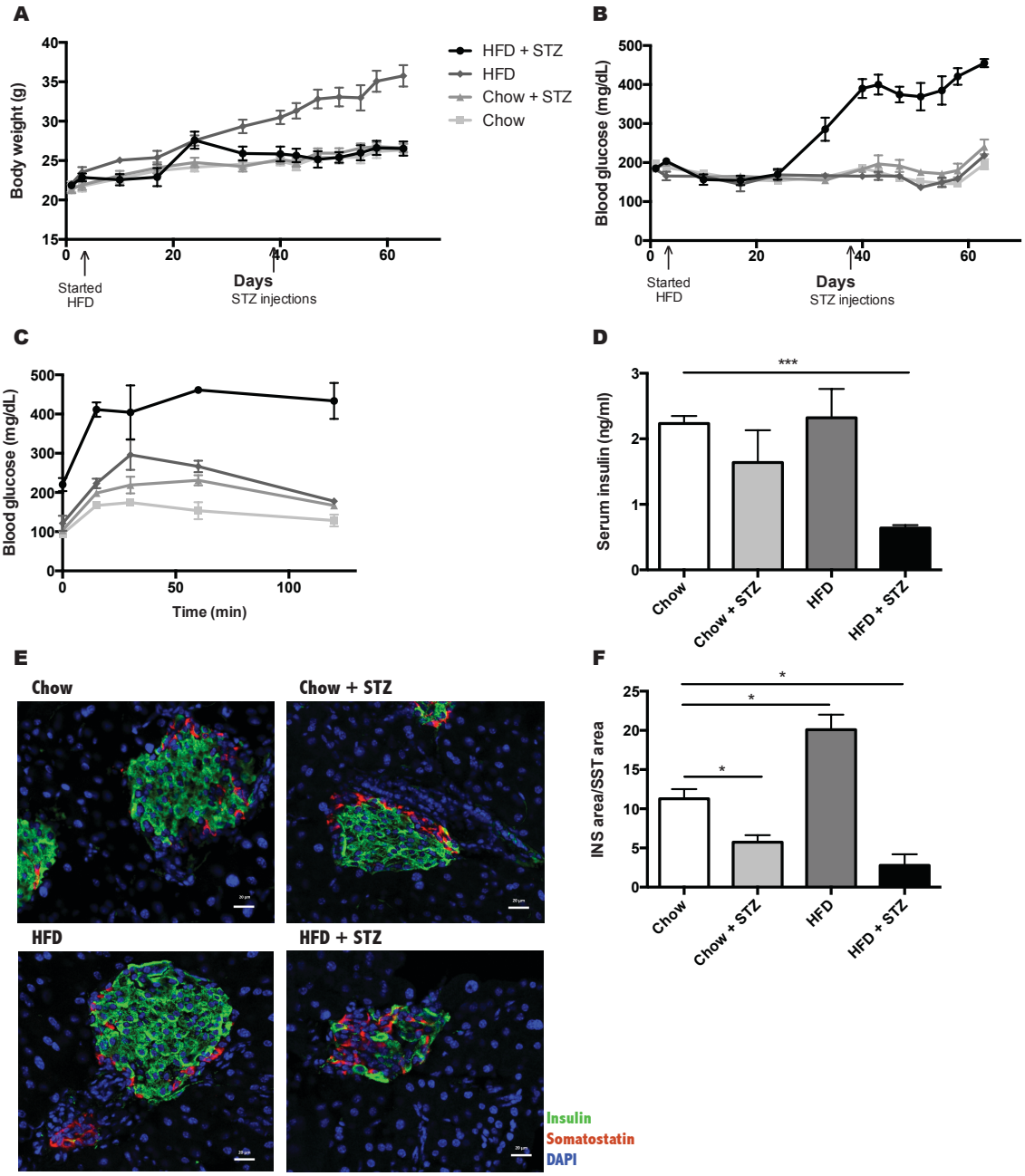

Figure 1. Four weeks of a high-fat diet followed by two low-dose STZ injections results in the onset on diabetes.

A Mice fed a high-fat diet for four weeks gain body weight. Weight gain in mice is attenuated by STZ injections (n=6). **B** Mice fed a high-fat diet for four weeks and injected with two low-doses of STZ develop hyperglycemia within days of STZ injections (n=6). **C** High-fat diet feeding as well as STZ injections independently produce glucose intolerance in mice, while high-fat diet feeding followed by STZ injections results in robust glucose intolerance (n=6). **D** Four weeks of a high-fat diet followed by two low-dose STZ injections results in reduced serum insulin levels

four weeks after STZ injections (n=6). **E** Eight weeks of a high-fat diet increases pancreatic beta cell insulin content, while injecting mice with two low doses of STZ reduces beta cell insulin content as measured by immunohistochemistry for insulin in pancreatic sections (representative images). **F** Quantification of (E) (n=6). HFD = high-fat diet, INS = insulin, SST = somatostatin. *$p < 0.05$, **$p < 0.005$, ***$p < 0.001$. Error bars represent SEM.

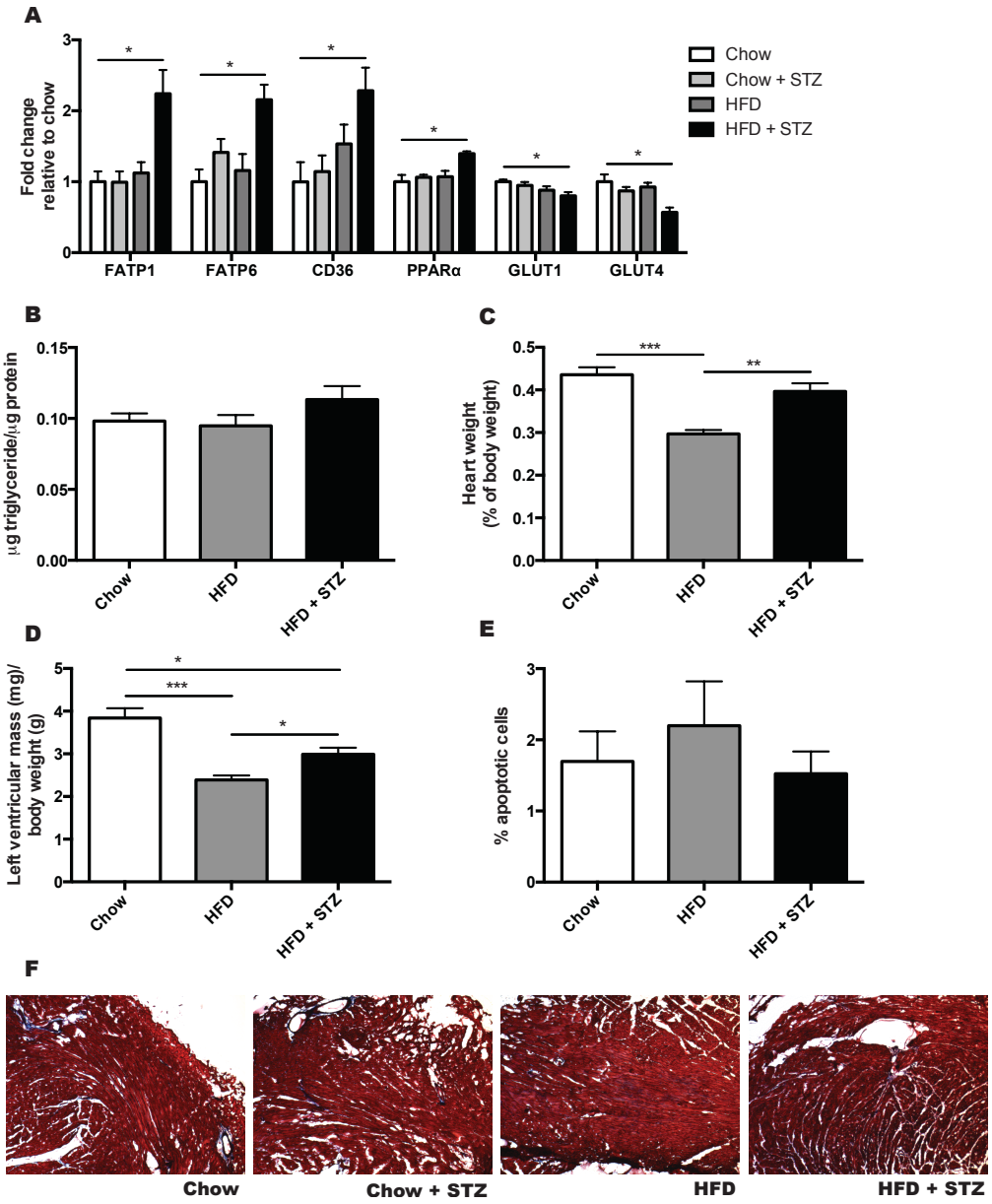

Figure 2. Diabetic mice show evidence for increased fatty acid utilization but do not develop cardiac hypertrophy or lipotoxicity.

A Feeding mice a high-fat diet for two weeks followed by two low-dose STZ injections results in increased fatty acid transporter and PPARα expression and decreased glucose transporter expression within four weeks of STZ injections (n=3). **B** Heart triglyceride content does not significantly change with 16 weeks of a high-fat diet or 12 weeks of diabetes (n=6). **C** Mice fed a high-fat diet have reduced heart weight in proportion to body weight, while diabetic mice have hearts of similar weight to chow-fed mice (n=6). **D** Both high-fat diet feeding and diabetes result in reduced left ventricular mass in proportion to total body weight (n=6). **E** Neither high-fat diet-fed mice nor diabetic mice show significant rates of apoptosis in

cardiomyocytes (n=6). **F** Neither high-fat diet-fed mice nor diabetic mice develop significant levels of fibrosis in the heart (representative images, n=6). HFD = high-fat diet. *p < 0.05, **p < 0.005, ***p < 0.001. Error bars represent SEM.

Table 1. Echocardiography in high-fat diet-fed and diabetic mice compared to chow-fed mice.

	Chow	HFD	HFD + STZ
IVSs (mm)	1.586 ± 0.096	1.684 ± 0.091	1.587 ± 0.082
IVSd (mm)	1.048 ± 0.073	1.158 ± 0.045	1.012 ± 0.042^{+}
LVPWs (mm)	1.463 ± 0.12	1.461 ± 0.11	1.466 ± 0.10
LVPWd (mm)	0.9701 ± 0.087	0.9946 ± 0.057	0.9652 ± 0.036
LVIDs (mm)	2.135 ± 0.20	1.992 ± 0.31	1.998 ± 0.19
LVIDd (mm)	3.565 ± 0.11	3.435 ± 0.22	3.419 ± 0.11
CI (ml/min/g BW)	0.5357 ± 0.019	0.3165 ± 0.031***	0.4633 ± 0.040^{+}
SV (µl)	35.44 ± 1.55	33.76 ± 3.31	34.94 ± 2.35
EF (%)	68.52 ± 4.50	68.59 ± 4.69	70.54 ± 4.01
FS (%)	32.16 ± 3.79	34.21 ± 5.09	33.79 ± 2.83
LV mass (mg/g BW)	3.838 ± 0.23	2.392 ± 0.10***	2.989 ± 0.16*/$^{+}$

IVSs = intraventricular septum length at systole, IVSd = intraventricular septum length at diastole, LVPWs = left ventricular posterior wall thickness at systole, LVPWd = left ventricular posterior wall thickness at diastole, LVIDs = left ventricular internal diameter at systole, LVIDd = left ventricular internal diameter at diastole, CI = cardiac index, SV = stroke volume, EF = ejection fraction, FS = fractional shortening, LV = left ventricle, BW = body weight. *$p < 0.05$, **$p < 0.005$, ***$p < 0.001$ versus chow-fed mice. $^{+}p<0.05$ versus high-fat diet fed mice. Mean is given with SEM.

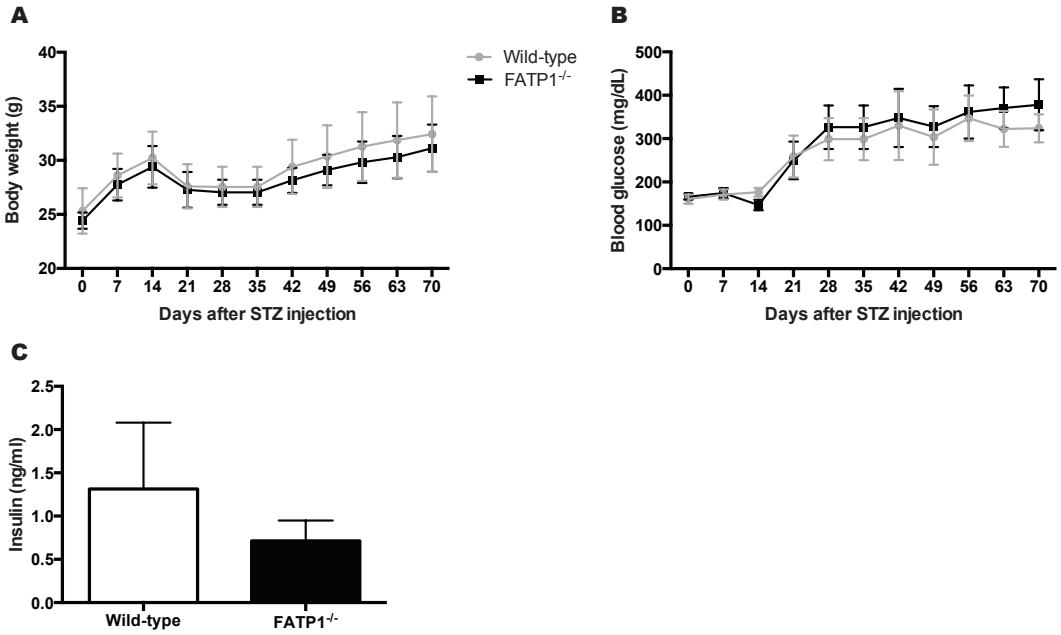

Figure 3. FATP1$^{-/-}$ mice become as diabetic as wild-type mice when fed a high-fat diet and injected with two low doses of STZ.

A After STZ injections, body weights were variable within each genotype, but there was no significant difference between wild-type and FATP1$^{-/-}$ mice (n=4). **B** Blood glucose levels increased for both wild-type and FATP1$^{-/-}$ mice after STZ injections (n=4). **C** Serum insulin levels were not significantly different between diabetic wild-type and FATP1$^{-/-}$ mice (n=4). Error bars represent SEM.

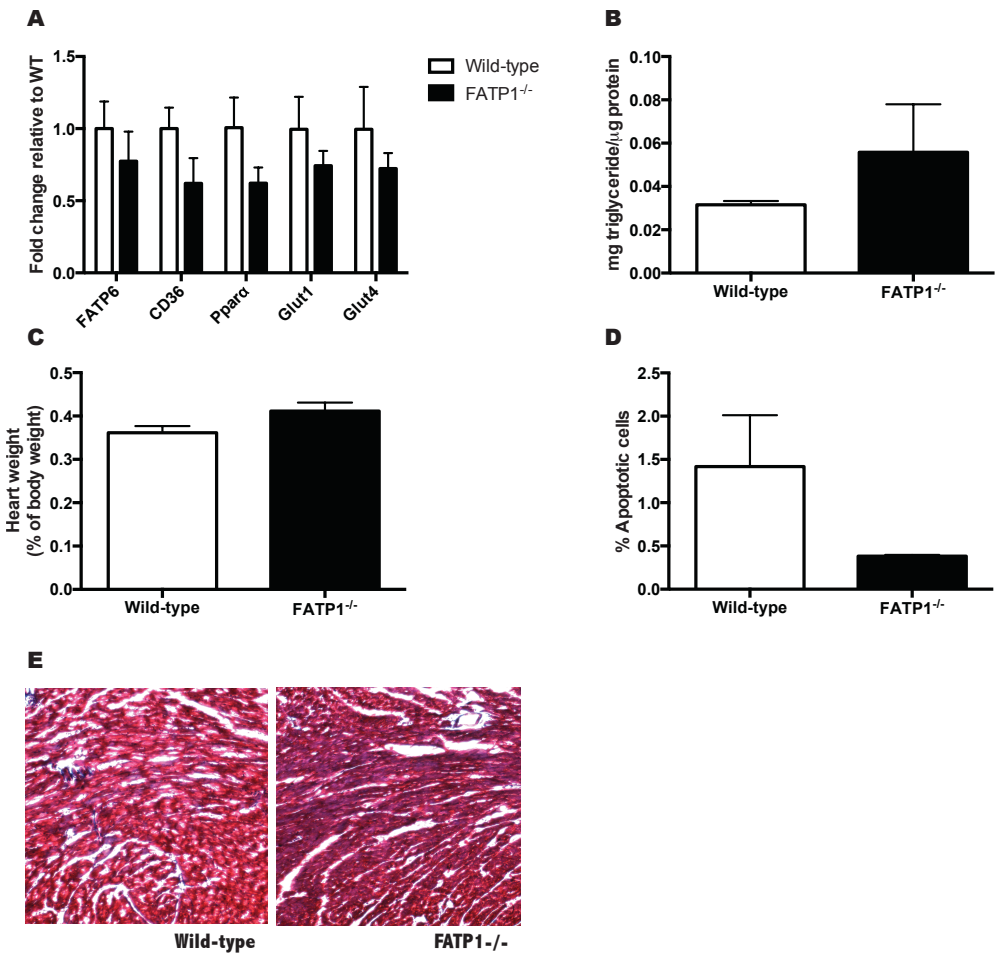

Figure 4. FATP1$^{-/-}$ mice have a similar diabetic heart phenotype as wild-type mice. **A** FATP1$^{-/-}$ mice have the same expression of fatty acid transporters and glucose transporters in the heart as wild-type mice in the context of diabetes (n=4). **B** Cardiac triglyceride levels are similar between diabetic wild-type and FATP1$^{-/-}$ mice (n=4). **C** The proportional weight of the heart in diabetic FATP1$^{-/-}$ mice is comparable to that of diabetic wild-type mice (n=4). **D** FATP1$^{-/-}$ diabetic hearts show a trend towards reduced levels of cardiomyocyte apoptosis as measured by a TUNEL stain, although this difference is not significant (n=4). **E** Neither FATP1$^{-/-}$ nor wild-type diabetic mice show evidence of fibrosis as detected by a Masson's Trichrome stain (representative images, n=4). Error bars represent SEM.

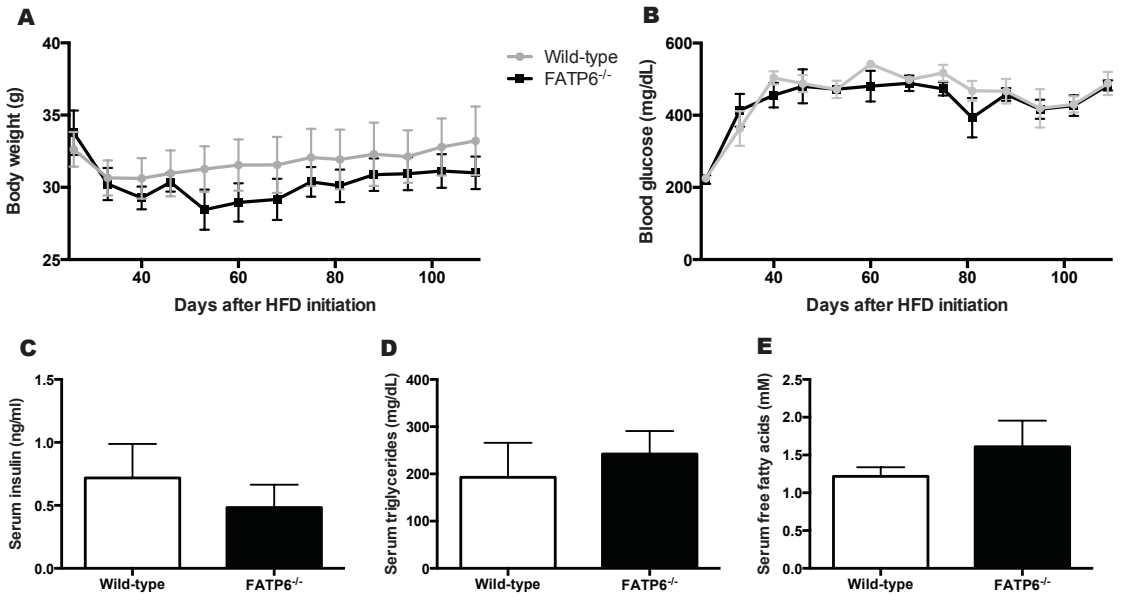

Figure 5. FATP6$^{-/-}$ mice become as diabetic as wild-type mice when fed a high-fat diet and given two low doses of STZ.

A Wild-type and FATP6$^{-/-}$ mice fed a high-fat diet and injected with two low doses of STZ have similar body weights (n=5-6). **B** Both wild-type and FATP6$^{-/-}$ mice develop hyperglycemia with our protocol to induce diabetes (n=5-6). **C** Wild-type and FATP6$^{-/-}$ diabetic mice have comparable serum insulin levels (n=5-6). **D** Wild-type and FATP6$^{-/-}$ diabetic mice have comparable serum triglyceride levels (n=5-6). **E** Wild-type and FATP6$^{-/-}$ diabetic mice have comparable serum free fatty acid levels (n=5-6). Error bars represent SEM.

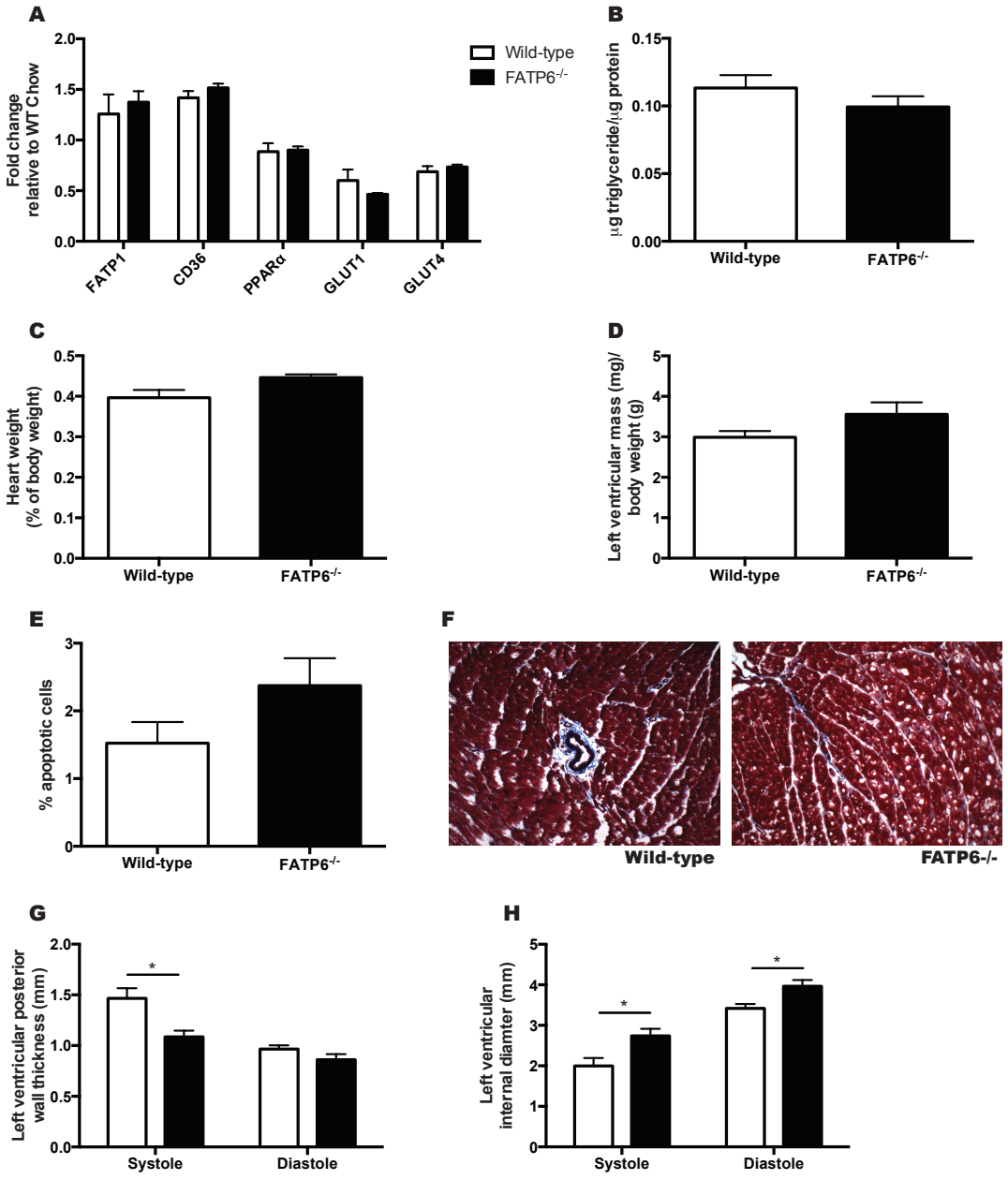

Figure 6. FATP6$^{-/-}$ diabetic mice show evidence for cardiac dilation, but the overall diabetic phenotype is similar to that of wild-type mice.

A FATP6$^{-/-}$ mice have the same expression of fatty acid transporters and glucose transporters in the heart as wild-type mice in the context of diabetes (n=5-6). **B** Cardiac triglyceride levels are similar between diabetic wild-type and FATP6$^{-/-}$ mice (n=5-6). **C** The proportional weight of the heart in diabetic FATP6$^{-/-}$ mice is comparable to that of diabetic wild-type mice (n=5-6). **D** Diabetic FATP6$^{-/-}$ mice and wild-type mice have comparable relative left ventricular mass (n=5-6). **E** Diabetic FATP6$^{-/-}$ mice show a trend towards elevated levels of apoptosis in cardiomyocytes, but this difference is not significant (n=5-6). **F** Neither wild-type nor FATP6$^{-/-}$ mice

develop significant levels of fibrosis in the heart in the context of diabetes (representative images, n=5-6). **G** During systole, diabetic FATP6$^{-/-}$ mice have thinner left ventricular posterior walls than wild-type diabetic mice (n=5-6). **H** During systole and diastole, FATP6$^{-/-}$ diabetic mice have larger left ventricular internal diameters than diabetic wild-type mice (n=5-6). *$p < 0.05$. Error bars represent SEM.

Table 2. Echocardiography in diabetic wild-type and FATP6$^{-/-}$ mice.

	Wild-type	FATP6$^{-/-}$
IVSs (mm)	1.587 ± 0.082	1.448 ± 0.081
IVSd (mm)	1.012 ± 0.042	0.9272 ± 0.020
LVPWs (mm)	1.466 ± 0.10	1.085 ± 0.063*
LVPWd (mm)	0.9652 ± 0.037	0.8612 ± 0.054
LVIDs (mm)	1.998 ± 0.19	2.738 ± 0.18*
LVIDd (mm)	3.419 ± 0.11	3.964 ± 0.16*
CI (ml/min/g BW)	0.4633 ± 0.040	0.3430 ± 0.037
SV (μl)	34.94 ± 2.35	38.65 ± 3.41
EF (%)	70.54 ± 4.01	57.95 ± 5.069
FS (%)	33.79 ± 2.83	25.36 ± 3.56
LV mass (mg/g BW)	2.989 ± 0.16	3.558 ± 0.29

IVSs = intraventricular septum length at systole, IVSd = intraventricular septum length at diastole, LVPWs = left ventricular posterior wall thickness at systole, LVPWd = left ventricular posterior wall thickness at diastole, LVIDs = left ventricular internal diameter at systole, LVIDd = left ventricular internal diameter at diastole, CI = cardiac index, SV = stroke volume, EF = ejection fraction, FS = fractional shortening, LV = left ventricle, BW = body weight. *$p < 0.05$. Mean is given with SEM.

Discussion

Feeding mice a high-fat diet and injecting with two low-doses of STZ results in diabetes, however, it does not produce diabetic cardiomyopathy. Using this model, we found genetic evidence of increased fatty acid utilization and decreased glucose utilization, but we did not see evidence of structural or functional changes in the heart. Unlike clinical cases of diabetic cardiomyopathy or other rodent models of diabetes[136,137], we did not observe enhanced lipid accumulation, cardiac hypertrophy, apoptosis, fibrosis, systolic dysfunction, or diastolic dysfunction. Loss-of-function of FATP1 and FATP6 did not significantly affect the heart phenotype of our diabetic mice. Because we did not observe robust diabetic cardiomyopathy in our mouse model of diabetes, we cannot make conclusions about the role of FATP1 and FATP6 in the development of this condition.

Fatty acid transporter proteins may still affect cardiac fatty acid utilization and cardiac function in the context of severe diabetic cardiac dysfunction. Loss-of-function of CD36 protects mice from diabetic cardiomyopathy produced by cardiac overexpression of PPARα. However, CD36 knockout mice do not show evidence of altered cardiac function in the absence of diabetes[8], despite having reduced cardiac fatty acid utilization and reduced cardiac lipid levels[11,60,71]. Aged wild-type mice show evidence of cardiac hypertrophy and systolic dysfunction and deletion of CD36 protects mice from these age-associated changes in heart structure and function[138]. Taken together, these studies suggest that manipulating CD36 activity only results in functional changes in the heart in the context of overt cardiac dysfunction. Clearly, CD36 is playing a physiological role in mediating fatty acid availability in vivo, but targeting CD36 only results in cardiac functional changes in a pathophysiological setting where fatty acid utilization is dysregulated. Similarly, we may expect to only see changes in cardiac function with loss-of-function of FATP1 or FATP6 in potent pathophysiological settings where fatty acid utilization is dysregulated. FATP1 expression is sufficient to drive cardiac fatty acid uptake and cardiac dysfunction as evidenced by a transgenic mouse model in which FATP1 was overexpressed in the heart[41]. FATP6 overexpression in the heart may also enhance fatty acid uptake and result in changes in cardiac function. To address this, a transgenic mouse model with cardiac-specific expression of FATP6 could be generated.

FATP1$^{-/-}$ mice and FATP6$^{-/-}$ mice developed diabetes to the same extent as wild-type mice in our studies. All mice developed hyperglycemia within days of STZ injections. All mice had reduced serum insulin levels like type I diabetic patients, but we fed them a high-fat diet throughout the study to maintain elevated lipid levels in the blood and induce insulin resistance. We expected that reduced insulin action would result in reduced glucose utilization and that this, along with increased fatty acid availability, would result in increased fatty acid utilization[39,98,99]. Indeed, we found increased expression of FATP1, FATP6, CD36, and PPARα and reduced expression of GLUT1 and GLUT4 in our mice. This gene expression pattern is also observed in other mouse models of diabetes, including the ZDF rat[86,132] and mice overexpressing PPARα in the heart[63,73]. These results suggest a shift towards increased cardiac fatty acid utilization and decreased cardiac glucose utilization in

our diabetic mouse model; however, we did not directly measure fatty acid or glucose uptake or oxidation. We observed a trend towards enhanced cardiac lipid accumulation in diabetic mice compared to control mice, but this difference was not significant. In the absence of marked lipid accumulation, we did not expect to see cardiac hypertrophy[8,65,129], lipotoxicity[8], or diastolic dysfunction[98,99,126]. We did not directly measure mitral valve function or left ventricle filling efficiency in order to assess diastolic dysfunction in our mice, but we did measure several parameters of systolic function. We did not observe any differences in the structure of function of the left ventricle in our diabetic mice compared to control mice.

We chose to make mice diabetic with high-fat diet feeding and two low-dose STZ injections for several reasons. First, STZ-induced diabetic mice have been reported to produce heart phenotypes with evidence of diabetic cardiomyopathy, including a metabolic shift towards enhanced fatty acid utilization in the heart, cardiac lipid accumulation, reduced cardiac efficiency, and reduced cardiac function[136]. Importantly, as seen in our study, cardiac hypertrophy is not observed in STZ-induced diabetic mice, so some of the downstream effects of cardiac hypertrophy, like diastolic dysfunction, would also not be expected in our mice[136]. We also chose STZ-induced diabetes as a model because it allowed us to investigate the effect of cardiac expression of FATPs in the context of diabetes without directly manipulating fatty acid metabolism to produce diabetic cardiomyopathy. The most striking mouse models of diabetic cardiomyopathy are models in which genes involved in fatty acid metabolism, like PPARα[63,73], acyl-CoA synthetase 1[65] or FATP1[41], are overexpressed in the heart. Evaluating the effects of deleting FATP1 or FATP6 in these contexts would be parallel to overexpressing a gene, and then deleting it to return to a normal level of expression. This would not provide us with useful information that can be applied to clinical cases of diabetic cardiomyopathy. We opted to investigate the role of FATP1 and FATP6 in the heart in a more physiological context by inducing systemic diabetes in our mice. Finally, pharmacological induction of diabetes with STZ injections provided a way for us to circumvent issues with genetic models of type II diabetes. FATP1$^{-/-}$ mice are resistant to high-fat diet-induced insulin resistance[17] and may not have developed diabetes to the same extent as control mice if we used a genetic model of type II diabetes like the *db/db* mouse or *ob/ob* mouse. These mouse models would also require more complicated crossbreeding strategies. However, despite these complications, *db/db* and *ob/ob* mice provide excellent models of diabetic cardiomyopathy. These mice increase fatty acid utilization in the heart, accumulate cardiac lipids, develop cardiac hypertrophy, have reduced cardiac efficiency, and have diastolic dysfunction, better mimicking the clinical manifestations of diabetic cardiomyopathy in humans than STZ-induced diabetic mouse models[136].

We did observe some changes in left ventricle structure in diabetic FATP6$^{-/-}$ mice compared to wild-type diabetic mice, including reduced left ventricular posterior wall thickness and increased left ventricular internal diameter. These changes also occur in chow-fed, non-diabetic FATP6$^{-/-}$ mice compared to wild-type mice (Chapter 1). In Chapter 1, we proposed that loss-of-function of FATP6 reduces fatty acid availability in the heart, causing cardiac dilation, perhaps by reducing fatty acid utilization and cardiac efficiency. Cardiac dilation is a hallmark of dilated

cardiomyopathy, not diabetic cardiomyopathy[39,53]. In the context of severe diabetic cardiomyopathy, loss-of-function of FATP6 may cause beneficial rather than detrimental effects on cardiac function by reducing fatty acid utilization and thereby reducing lipid accumulation, hypertrophy, and diastolic dysfunction. Future studies will need to address the role of FATP6 in a more robust model of diabetic cardiomyopathy than the model used in this study.

In summary, mice made diabetic by high-fat diet feeding and low-dose STZ injections do not develop diabetic cardiomyopathy. Using this mouse model, we could not determine the effects of FATP1 and FATP6 expression on the development of diabetic cardiomyopathy. It is clear that enhanced fatty acid utilization leads to lipid accumulation in diabetic hearts and that fatty acid transport is an important determinant of overall cardiac fatty acid utilization. It is highly likely that FATPs are involved in this process and that targeting these proteins would reduce the development or severity of diabetic cardiomyopathy. The effect of FATP1 and FATP6 activity should be evaluated in a more robust model of this condition.

Methods

Animal experiments

All animal procedures were approved by the University of California Berkeley Animal Care and Use Committee. C57BL/6J mice were purchased from the Jackson Laboratory (#000664). FATP1$^{-/-}$ mice were generated and maintained as previously described[139]. FATP6$^{-/-}$ mice were generated and maintained as described in Chapter 1. All animal experiments were performed in 6- to 24-week-old male mice. Mice were given free access to water and rodent chow (Harlan Teklad #2018) or 60% fat diet (Research Diets, Inc. #D12492) and housed under standard conditions.

Body weight and blood glucose were measured each week after STZ injections until the mice were sacrificed. Blood glucose was measured with a glucometer (NovaMax #14). Mice were sacrificed four to 12 weeks after STZ injections.

For serum analyses, 50 µl blood was collected with a non-heparinized capillary tube and allowed to coagulate at room temperature for 15-30 minutes. The blood was centrifuged at 1500 x g for 10 minutes at 4°C and the serum was further analyzed.

STZ injections

The high-fat diet was given to mice for six to 16 weeks and mice were injected with STZ or vehicle alone after zero to four weeks of high-fat diet feeding. For STZ injections, mice were fasted the day before the injections. Mice were anesthetized, then intraperitoneally injected with 75 mg STZ (Sigma-Aldrich #S0130) per kg body weight in a 0.1 M sodium citrate buffer, pH 4.5 and then given access to food. Injections were repeated 24 hours later at the same dose.

Glucose tolerance test

Mice were fasted the day before the assay. Mice were anesthetized, then intraperitoneally injected with 2 mg of glucose per g body weight. Blood glucose

was measured with a glucometer before the injection, and 15, 30, 60, and 120 minutes after the injections.

Echocardiography

Echocardiography was performed in mice using the Vevo2100 (VisualSonics). Mice were anesthetized with 3% isoflurane and held under 1.5-2.5% anesthesia to maintain a heart rate of 400-500 beats per minutes. The fur covering the thorax was removed with a depilatory cream and body temperature was maintained at 37°C. Hearts were first imaged in B-mode in a parasternal long-axis view using a MS 550S transducer and then in M-mode in a short-axis view. At least two sets of time-lapse images were collected in each view for each mouse. Images were analyzed using the Vevo2100 software. A left ventricular trace was performed for B-mode and M-mode images. Intraventricular septum, left ventricular internal diameter, and left ventricular posterior wall thickness were measured in M-mode in four tandem cardiac cycles. The Vevo2100 software utilized these measurements to calculate cardiac output, stroke volume, ejection fraction, fractional shortening, and left ventricular mass with algorithms detailed in their manual. Replicate measurements and values were averaged for each mouse. Cardiac output was adjusted for animal body weight and presented as cardiac index. Left ventricular mass was also adjusted for animal body weight.

Tissue fixation, cryopreservation, and cryosectioning

Pancreases and hearts were dissected and fixed in 4% paraformaldehyde (Electron Microscopy Sciences #15710) for one hour at 4°C, washed in phosphate-buffered saline, and then equilibrated in 30% sucrose overnight at 4°C. The tissues were cryopreserved in O.C.T Compound (Sakura #4583) in a cryomold and sectioned at 10 μM onto charged glass slides at -20°C.

Immunohistochemistry

Pancreas sections were post-fixed in 4% paraformaldehyde for 20 minutes at room temperature in a humidified chamber and blocked for one hour at room temperature in blocking buffer (3% normal donkey serum, .05% saponin, 1% bovine serum albumin, and 10% fetal bovine serum in PBS). Slides were then incubated in a solution containing antibodies for insulin and somatostatin (Abcam anti-insulin + proinsulin #ab8304 and anti-somatostatin #ab103790) in blocking buffer overnight at 4°C. Slides were then incubated with secondary antibodies to the primary antibodies [donkey anti-mouse or donkey anti-rabbit IgG (H+L) conjugated to Alexa Fluor 488 or 647, Thermo Fisher Scientific #A-21206 and #A-31573] and mounted in DAPI mountant (Life Technologies #P36971). Slides were imaged with a Zeiss LSM710 laser scanning confocal microscope. Images were processed on the software IMARIS.

Apoptosis assay

Heart sections were stained for apoptotic cells using the In Situ Cell Death Detection Kit (Roche #11684795910). Briefly, the slides were post-fixed in 4%

paraformaldehyde for 20 minutes at room temperature, permeabilized with 0.1% Triton X-100 (Sigma Aldrich #234729) in 0.1% sodium-citrate for 5 minutes at room temperature, then incubated in TUNEL reaction mixture at 37°C for one hour. As a positive control for the reaction, a heart section was treated with DNase I for 10 minutes before the TUNEL stain. Slides were mounted in DAPI mountant (Life Technologies P36971) and imaged with a Zeiss LSM710 laser scanning confocal microscope. TUNEL-positive apoptotic cells and total number of cells were quantified with IMARIS.

Masson's Trichrome stain for fibrosis

Heart sections were stained for fibrosis using a Masson's Trichrome staining kit (Thermo Scientific #87019). Briefly, slides were rinsed in phosphate buffered saline, then incubated in Boudin's Fluid for one hour, then washed in deionized water, then incubated in Working Weigert's Iron Hematoxylin Stain for ten minutes, then rinsed in deionized water, then incubated in Beibrich Scarlet-Acid Fuchsin Solution for seven minutes, then rinsed in deionized water, then incubated in Phosphotungstic-Phosphomolybdic Acid Solution for five minutes, then incubated in Aniline Blue Stain Solution for seven minutes, then incubated in 1% acetic acid for one minute, then rinsed in deionized water, then dehydrated in two changes of 95% ethanol, then dehydrated in two changes of 100% ethanol, then cleared in Xylenes, and finally, mounted in Permount (Fisher Chemical #SP15-100). Images were captured with a Zeiss AxioImager M1. Images shown are representative of each group analyzed.

Quantitative PCR

1 µl of cDNA was used in a 20 µl PCR reaction along with 1 µl PrimeTime qPCR assay [Integrated DNA Technologies #Mm.PT.39a.1 for glyceraldehyde 3-phosphate dehydrogenase (GAPDH), #Mm.PT.58.43265938 for FATP6, #Mm.PT.53a.33622420 for FATP1, #Mm.PT.58.12375764 for CD36, #Mm.PT.58.7020742 for PPARα, #Mm.PT.58.9683859 for GLUT1, and #Mm.PT.58.9683859 for GLUT4] and 10 µl TaqMan Universal Master Mix II (Thermo Fisher Scientific #4440040). The PCR reactions were run and cycle thresholds were calculated with the Applied Biosystems 7500 Real Time PCR System. Fold change was calculated by comparing the difference in cycle thresholds between the gene of interest and the housekeeping gene for treated samples and control samples.

Quantification of triglycerides, free fatty acids, and insulin in tissue lysate and serum

Triglycerides were quantified with the Infinity Triglycerides reagent (ThermoFisher Scientific #TR22421) according to the manufacturer's protocol. Serum or lysate samples were diluted 1:100 into the reagent and incubated for five minutes at 37°C. The absorbance of the samples was read at 500 nm with a SpectraMax i3 plate reader (Molecular Devices). Absolute triglyceride values were calculated by comparing the sample absorbance values to a known standard absorbance value. Tissue triglyceride content was adjusted for protein content.

Free fatty acids were quantified using the HR Series NEFA-HR (2) (Wako #999-34691, #999-34791, #999-34891, #999-35191) according to the manufacturer's protocol. Lysate samples were diluted into color reagent A 1:50 and incubated for five minutes at 37°C. Color reagent B was added to the solutions at half the volume of color reagent A and allowed to incubate for five additional minutes at 37°C. The absorbance of the samples was read at 550 nm. Absolute free fatty acid values were calculated by comparing sample absorbance values to the absorbance values of oleic acid standards.

Insulin was quantified with a mouse insulin ELISA (CrystalChem #90080) according to the manufacturer's protocol. Serum samples were diluted into sample diluent and allowed to incubate on the microplate for 2 hours at 4°C. After extensive washing of the plate, anti-enzyme conjugate was added to each well and allowed to incubate for 30 minutes at room temperature. After more washing, enzyme substrate solution was added to the microplate and allowed to incubate for 40 minutes. The reaction was stopped by the addition of enzyme reaction stop solution and the absorbance of each well was measured at 450 nm using a plate reader. Absolute insulin values were calculated by comparing sample absorbance values to the absorbance values of insulin standards.

Statistical analysis

Differences between two groups were determined using an unpaired Student's *t* test with Welch's correction. Data are presented as mean values with error bars representing the standard error of the mean. Asterisks and plus signs indicate significant differences (*$p < 0.05$ versus wild-type or another group, **$p < 0.005$ versus wild-type or another group, **$p<0.001$ versus wild-type or another group, $^{+}p < 0.05$ versus chow diet, $^{++}p < 0.005$ versus chow diet, $^{+++}p < 0.001$ versus chow diet).

Chapter 3: Deletion of fatty acid transport protein 1 protects beta cells from palmitate-induced apoptosis

Rationale

According to the most recent National Diabetes Fact Sheet, 21.3 million people in the Unites States have diabetes and 90 to 95 percent are type II diabetic[3]. The diabetes incidence rate has increased so drastically that if trends continue, by 2050, one in three people will have the disorder. While it is clear that there is a genetic predisposition to the disease, obesity is the most significant environmental risk factor. Ectopic fat accumulation in obesity causes peripheral insulin resistance that the body compensates for by increasing insulin secretion from the pancreatic beta cells. Eventually, the beta cells cannot handle the insulin demand and blood glucose levels rise, resulting in diabetes. The increased fatty acid levels in the plasma during obesity can also directly affect beta cell function. While short-term exposure of beta cells to fatty acids can induce insulin secretion, long-term exposure inhibits glucose-stimulated insulin secretion and induces beta cell apoptosis, further contributing to the development of diabetes[140–142]. Although one mechanism by which fatty acids can alter insulin secretion is by binding to cell surface receptors, the lipotoxic effects of fatty acids are thought to be dependent on their entry into the cell[141–144].

Fatty acid-induced apoptosis of pancreatic beta cells has been extensively demonstrated in vitro and in vivo[142,145–148]. Specifically, chronically elevated saturated fatty acid levels concurrent with elevated glucose levels leads to beta cell lipotoxicity[144,149]. A variety of mechanisms have been proposed to explain how fatty acids contribute to beta cell lipotoxicity, including fatty acid induction of ER stress,[150–153] ceramide formation,[153–155] reactive oxygen species production,[142,153] and a reduction in autophagy[153]. Induction of intracellular triglyceride formation and fatty acid oxidation are actually protective against fatty acid-induced cell death[144,149].

It is not yet understood how beta cells take up fatty acids. Although fatty acids are hydrophobic molecules that can potentially diffuse across the plasma membrane, the majority of long-chain fatty acid uptake is believed to be protein-mediated[4,9,10]. Fatty acid transport proteins (FATPs) are a group of six transmembrane proteins shown to mediate long-chain fatty acid uptake and fatty acid activation in vitro and in vivo[4,15]. FATP loss-of-function studies in animals have shown that targeted deletion of these proteins can protect against high-fat induced insulin resistance and hepatic steatosis,[17,19] while overexpression of FATP1 in the heart leads to cardiomyopathy[41].

Due to the physiological importance of FATPs in other metabolic tissues, we investigated whether fatty acid transport proteins mediated fatty acid uptake in pancreatic beta cells and therefore played a role in beta cell lipotoxicity and the development of diabetes. We found that FATPs are differentially expressed in the endocrine pancreas, with FATP1 localizing to beta cells, FATP3 to delta cells, and FATP4 to alpha cells. Loss-of-function of FATP1 protected beta cells from palmitate-

induced lipotoxicity despite normal levels of fatty acid uptake and palmitate-induced ER stress.

Results

Long-term exposure of islets to palmitate induces apoptosis

To verify that we see induction of apoptosis in pancreatic beta cells in response to chronic palmitate treatment, we incubated whole islets isolated from male C57BL/6J mice with 1 mM palmitate complexed to albumin for 48 hours. We then fixed, cryopreserved, and sectioned the islets and performed an in situ TUNEL assay to stain apoptotic cells. We quantified apoptotic cells and adjusted for total cell number with the program IMARIS. We found that islets exposed to palmitate had about 3.5 times more apoptotic cells than islets incubated with albumin only (**Fig. 1A** and **B**).

It has also been reported that islets are more susceptible to apoptosis when exposed to high levels of palmitate in the presence of high levels of glucose, a phenomenon termed glucolipotoxicity[156,157]. We incubated islets in 1 mM palmitate, 30 mM glucose, 1 mM plamitate and 30 mM glucose, or bovine serum albumin alone for 48 hours and quantified apoptosis using the in situ TUNEL assay described. Islets incubated with both palmitate and glucose had about four times more apoptotic cells than islets incubated with albumin alone (**Fig. 1C**) and had more apoptotic cells than islets incubated with glucose or palmitate alone.

Long-term exposure of MIN6 cells to palmitate induces cell death

MIN6 cells are an islet-derived mouse cell line commonly used to study beta cell biology[158]. To study palmitate effects on MIN6 cells, we incubated the cells with 1mM palmitate for the indicated time and quantified apoptosis using the Cell Death Detection Kit (Roche). After 24 hours of palmitate exposure, MIN6 cells exposed to palmitate had 1.5 times higher levels of apoptosis as cells incubated in albumin only (**Fig. 1D**).

Since we did not see as robust of an induction of apoptosis in response to long-term palmitate treatment in MIN6 cells as we observed in islets, we tested whether the cells were susceptible to general cell death with a cell viability assay. We exposed MIN6 cells to 1 mM palmitate complexed to albumin at increasing palmitate to albumin molar ratios to create a gradient of free fatty acid levels. After 48 hours, we saw a dose-dependent decrease in cell viability, with a 75% reduction in cell viability in the cells exposed to 5:1 palmitate:albumin compared to cells exposed to albumin only (**Fig 1E**).

We also tested whether MIN6 cells are more susceptible to glucolipotoxicity than lipotoxicity. We incubated MIN6 cells with 1 mM palmitate, 30 mM glucose, 1 mM palmitate and 30 mM glucose, or albumin only for 16, 24, or 48 hours and measured cell viability with an XTT assay. The cells exposed to palmitate alone and palmitate with gluose had a similar time-dependent reduction in cell viability compared to

cells exposed to albumin only (**Fig. 1F**), suggesting that unlike isolated islets, MIN6 cells are no more susceptible to glucolipotoxicity than lipotoxicity.

FATP1, FATP3, and FATP4 are expressed in pancreatic islets

While it is clear that excess fatty acids affect beta cell biology, no one has reported whether members of the fatty acid transport protein family play a role in beta cell function. We first determined whether fatty acid transport proteins were expressed in pancreatic islets by collecting RNA from islets isolated from male C57BL/6J mice and performing quantitative PCR for all six members of the FATP family. While we could not detect expression of FATP2, FATP5, and FATP6, we did detect expression of FATP1, FATP3, and FATP4 (data not shown).

We then measured the copy number of each FATP transcript by performing absolute quantification PCR and generating standard curves for each transporter and a housekeeping gene (**Fig. S1**). FATP1 seemed to be the most highly expressed FATP, followed by FATP4 and FATP3 (**Fig. 2A**). The FATP transcript levels in MIN6 cells were similar to those in islets, although in MIN6 cells, FATP4 seemed to be the most highly expressed (**Fig. 2A**). We also compared the amount of FATP transcripts in isolated islets to the amount in tissues known to express high levels of each transporter. The levels of FATP transcript in islets were lower than the levels of FATP transcripts in the control tissues (**Fig. 2B**).

FATP1 expression is induced in response to glucose and palmitate treatment

FATPs are differentially regulated and some FATPs are regulated by metabolic signals[4]. We measured FATP transcript levels in response to short-term and long-term glucose and palmitate treatments using the conditions we employed in our apoptosis assays. We incubated isolated islets with 30 mM glucose, 1 mM palmitate, or albumin only for five or 24 hours, collected RNA, and then performed quantitative PCR for the fatty acid transport proteins. FATP1 expression was induced in a time-dependent manner in response to both glucose and palmitate treatment, although the magnitude of induction in response to glucose was much larger (**Fig. 2C**). FATP3 and FATP4 expression were not affected by glucose or palmitate treatment.

FATP1 is expressed in beta cells, FATP3 in delta cells, and FATP4 in alpha cells

We used immunohistochemistry to identify where our fatty acid transport proteins are expressed within pancreatic islets. We fixed, cryopreserved, and sectioned isolated islets, then stained the islets for each fatty acid transport protein. Islets are made up of four different cell types, each secreting a unique hormone. We co-stained for individual hormones to identify specific cell types within pancreatic islets. We found that FATP1 colocalized with insulin, FATP3 colocalized with somatostatin, and FATP4 colocalized with glucagon, indicating that FATP1 is expressed in beta cells, FATP3 in delta cells, and FATP4 in alpha cells (**Fig. 2D**).

Loss of FATP1 protects beta cells from palmitate-induced apoptosis.

Because of the role of beta cell lipotoxicity in the development of diabetes, we were particularly interested in FATP1 expression in beta cells. We decided to utilize whole-body FATP1$^{-/-}$ mice[139] to study the effects of loss-of-function of FATP1 in pancreatic beta cells. We first confirmed loss of FATP1 protein in islets by running a Western blot for FATP1 in islets isolated from wild-type and FATP1$^{-/-}$ mice. We used white adipose tissue as a control for FATP1 expression. We detected FATP1 protein in wild-type islets, while it is absent in islets isolated from FATP1$^{-/-}$ mice (**Fig. 3A**).

FATP1 mediates long-chain fatty acid uptake in vivo[159]. We hypothesized that FATP1 would mediate intracellular fatty acid availability in beta cells and therefore promote beta cell lipotoxicity. We first investigated whether loss-of-function of FATP1 affected palmitate-induced apoptosis in isolated islets. We exposed islets isolated from wild-type and FATP1$^{-/-}$ mice to 1 mM palmitate for 48 hours and performed the in situ TUNEL assay previously described. We found that palmitate-induced apoptosis was abolished in FATP1$^{-/-}$ islets (**Fig. 3B**). Deletion of FATP1 protected beta cells from lipotoxicity.

Loss of FATP1 does not affect fatty acid uptake in islets

To test whether loss-of-function of FATP1 resulted in changes in intracellular fatty acid availability, we evaluated islet fatty acid uptake in vivo and ex vivo. For the in vivo assay, we injected mice with 20 mM BODIPY-fatty acid bound to 1% bovine serum albumin. After an indicated amount of time, we isolated islets from the mice, homogenized the islets in RIPA buffer, and then measured the tissue lysate for fluorescence using a plate reader. We saw an increase in lysate fluorescence over time in the wild-type mice (**Fig. S2A**), indicating an accumulation of the BODIPY-fatty acid in the tissue. We performed the in vivo uptake assay in wild-type and FATP1$^{-/-}$ mice, collecting islets one hour after injection of the BODIPY-fatty acid. We did not detect a significant difference in islet lysate fluorescence from wild-type and FATP1$^{-/-}$ mice (**Fig. 3C**), suggesting that the FATP1$^{-/-}$ mice maintained normal levels of fatty acid uptake in the endocrine pancreas, despite loss of the transport protein.

We also evaluated fatty acid uptake in islets isolated from wild-type and FATP1$^{-/-}$ mice using a novel fatty acid uptake assay we developed in our lab. We crossed FATP1$^{-/-}$ mice with L2G85 mice expressing luciferase (luc^{+}). We then isolated islets from wild-type luc^{+} and FATP1$^{-/-}$ luc^{+} mice, incubated the islets with a fatty acid conjugated to luciferin[160], and measured the amount of light emitted from the islets with a luminometer. The amount of light emitted corresponds to the amount of luciferin-fatty acid being processed by the luciferase enzyme within the islet cells. When we incubated wild-type luc^{+} islets with increasing concentrations of the luciferin-fatty acid, we saw a dose-dependent increase in emitted light (**Fig. S2B**). We incubated wild-type luc^{+} and FATP1$^{-/-}$ luc^{+} islets with 20 μM luciferin-fatty acid bound to 0.2% bovine serum albumin for one hour and did not see a difference in

the light emitted between the two groups (**Fig. 3D**), suggesting that loss of FATP1 also does not affect ex vivo islet fatty acid uptake.

Compared to wild-type islets, FATP1$^{-/-}$ islets differentially store lipids in response to long-term palmitate treatment

We also measured lipid accumulation in isolated islets treated with palmitate or albumin alone. We incubated wild-type and FATP1$^{-/-}$ islets with 1 mM palmitate or albumin only for 48 hours, and then fixed, cryopreserved, sectioned, and stained the islets with BODIPY neutral lipid stain. We found that wild-type islets store neutral lipid in the basal state and that lipid levels are reduced in response to palmitate treatment (**Fig. 3E** and **F**). FATP1$^{-/-}$ islets have lower levels of intracellular lipid than wild-type islets in the basal state, but accumulate, rather than reduce, intraceullar lipid after palmitate treatment. Therefore, deletion of FATP1 reduces basal lipid accumulation, but results in differential lipid storage in response to palmitate treatment.

Like wild-type islets, FATP1$^{-/-}$ islets undergo ER stress in response to palmitate treatment

One of the proposed mechanisms for palmitate-induced apoptosis is an induction of ER stress in response to chronic exposure to excess lipids[150–153]. We wanted to investigate whether FATP1$^{-/-}$ islets were protected from palmitate-mediated ER stress since they are protected from palmitate-induced apoptosis. To this end, we incubated islets isolated from wild-type and FATP1$^{-/-}$ mice with palmitate for 48 hours, homogenized the islets, then ran a Western blot for CCAAT/-enhancer-binding protein homologous protein (CHOP), a protein upregulated in palmitate-induced ER stress. CHOP expression was induced in both wild-type and FATP1$^{-/-}$ islets in response to palmitate treatment (**Fig. 3E**), suggesting that FATP1$^{-/-}$ islets undergo palmitate-mediated ER stress to the same extent as wild-type islets.

In summary, FATP1$^{-/-}$ islets are protected from palmitate-induced apoptosis. This protection from cell death is not mediated by a reduction in islet fatty acid uptake or palmitate-mediated ER stress, but may be due to reduced lipid accumulation in the basal state or differential storage or metabolism of lipids upon palmitate treatment.

Gain-of-function of FATP1 in MIN6 cells leads to enhanced fatty acid uptake

In an attempt to better understand the role of FATP1 in beta cells, we created a gain-of-function model in MIN6 cells. We cloned the mouse FATP1 gene into a lentiviral vector, created lentivirus containing the FATP1 gene or vector only, and infected MIN6 cells with the lentivirus. We isolated individual clones of infected cells and used a clone with robust transcript (**Fig. 4A**) and protein (**Fig. 4B** and **C**) expression of FATP1 for our studies. We then evaluated fatty acid uptake in MIN6 cells expressing FATP1. We incubated MIN6 cells expressing FATP1 or vector only with 2 μM BODIPY-fatty acid bound to 0.1% bovine serum albumin for one hour and measured cell fluorescence using a flow cytometer. Cells expressing FATP1

accumulated significantly more BODIPY-fatty acid than cells expressing vector alone (**Fig. 4D**), showing that FATP1 facilitates fatty acid uptake in MIN6 cells.

Gain-of-function of FATP1 in MIN6 cells does not affect susceptibility to palmitate-induced cell death

We hypothesized that gain-of-function of FATP1, which leads to increased fatty acid uptake, would lead to enhanced beta cell sensitivity to palmitate-induced cell death. To test this, we incubated MIN6 cells expressing FATP1 or vector only with increasing amounts of palmitate for 48 hours and measured cell viability with an XTT assay. The cells expressing FATP1 were just as susceptible to palmitate-induced cell death as cells expressing vector only (**Fig. 4E**).

We also evaluated how FATP1-expressing cells accumulated lipid when exposed to palmitate. We incubated MIN6 cells expressing FATP1 or vector only with increasing amounts of palmitate and stained the cells with BODIPY neutral lipid stain. Both cell types accumulated lipid in a dose-dependent manner to a similar degree, although there was a trend toward reduced lipid accumulation in FATP1-expressing cells exposed to the highest concentration of palmitate ($p=0.06$) (**Fig. 4F**).

In summary, MIN6 cells overexpressing FATP1 are susceptible to palmitate-induced cell death, despite having enhanced fatty acid uptake. They show a trend towards reduced lipid accumulation in response to palmitate treatment.

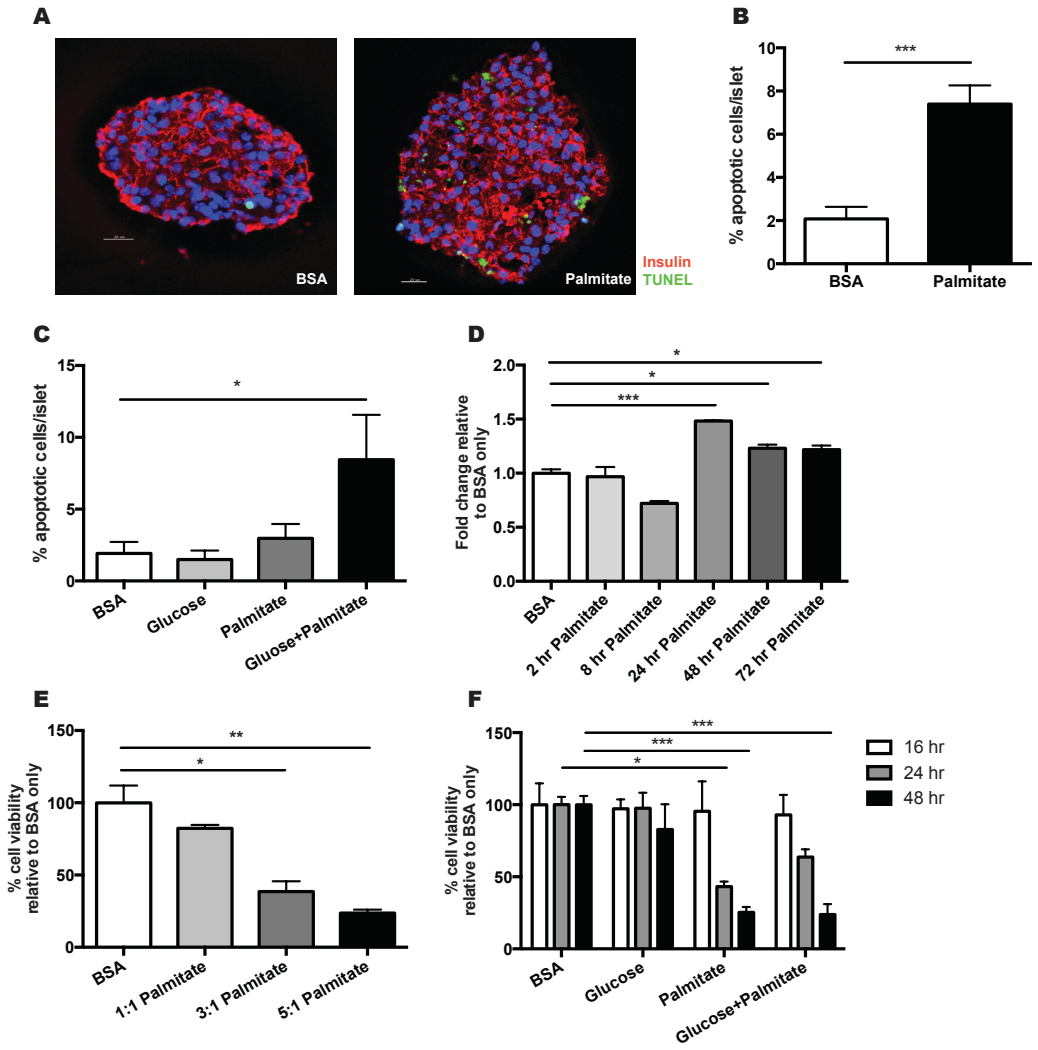

Figure 1. Treating isolated islets or MIN6 cells with 1 mM palmitate induces cell apoptosis.

A Islets isolated from mice and exposed to 1 mM palmitate for 48 hours have higher levels of apoptosis than islets exposed to albumin only as measured by an in situ TUNEL assay (representative images). **B** Quantification of (A) (n=8). **C** Isolated islets incubated with elevated glucose and palmitate levels for 48 hours have more apoptotic cells than islets incubated with glucose or palmitate alone (n=4). **D** MIN6 cells exposed to 1 mM palmitate for at least 24 hours undergo more apoptosis than MIN6 cells exposed to albumin only (n=3). **E** MIN6 cells exhibit reduced cell viability in response to palmitate treatment in a dose-dependent manner (n=3). **F** Elevated glucose and palmitate levels do not induce more cell death in MIN6 cells than elevated palmitate levels alone (n=3). BSA = bovine serum albumin. *$p < 0.05$, **$p < 0.005$, ***$p < 0.001$. Error bars represent SEM.

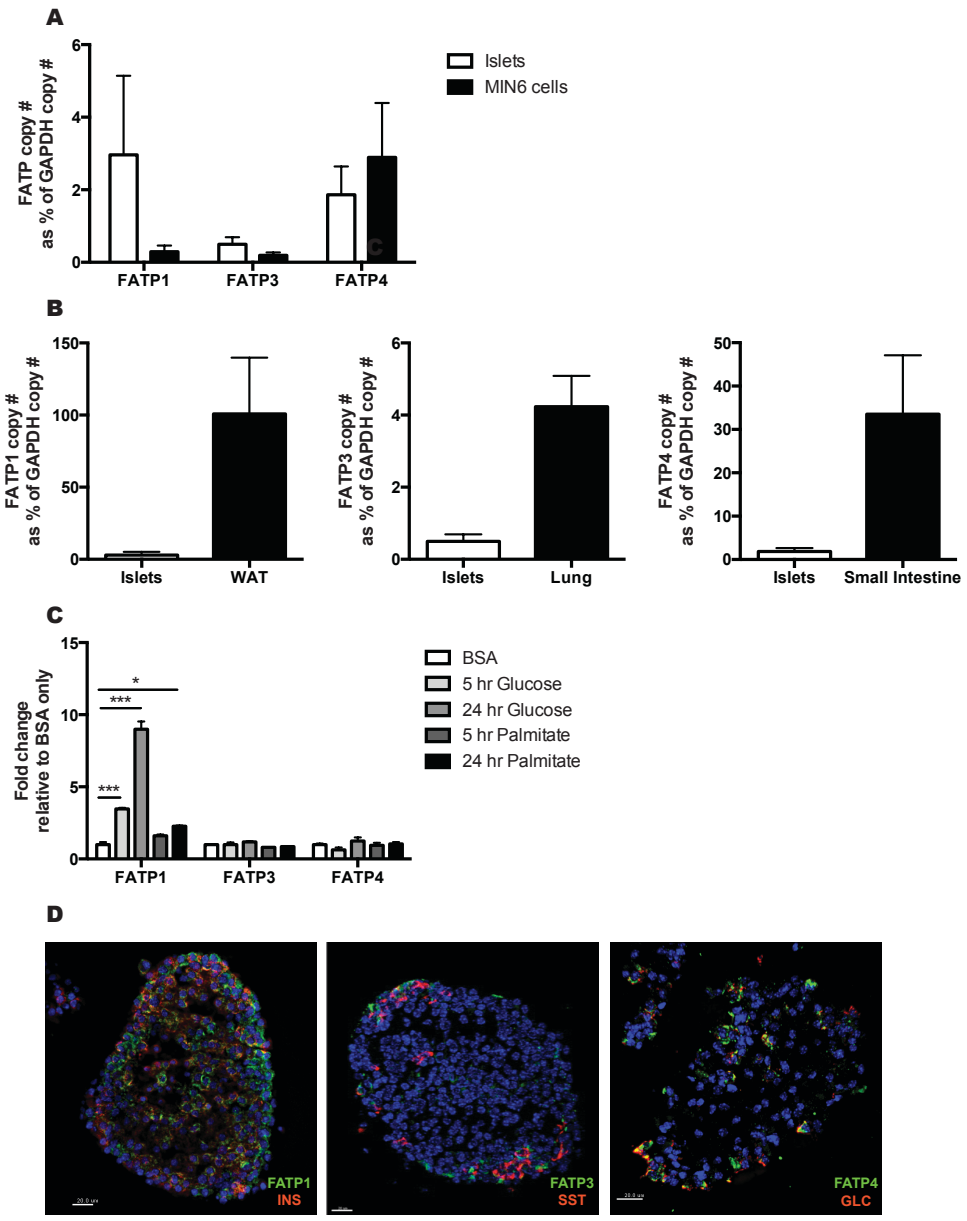

Figure 2. FATPs are differentially expressed in the endocrine pancreas.
A FATP1, FATP3, and FATP4 transcript is expressed in isolated islets and MIN6 cells as determined by absolute quantification PCR (n=3). **B** The amount of FATP transcript expressed in isolated islets is lower than the amount expressed in control tissues for FATP1, FATP3, and FATP4 (n=3). **C** FATP1 expression is induced in response to glucose and palmitate treatment (n=3). **D** FATP1 is expressed in beta cells, FATP3 is expressed in delta cells, and FATP4 is expressed in alpha cells of pancreatic islets, as determined by the colocalization of FATPs with the hormones secreted by those cells. WAT = white adipose tissue, BSA = bovine serum albumin, INS = insulin, SST = somatostatin, GLC = glucagon. *p < 0.05, **p < 0.005, ***p < 0.001. Error bars represent SEM.

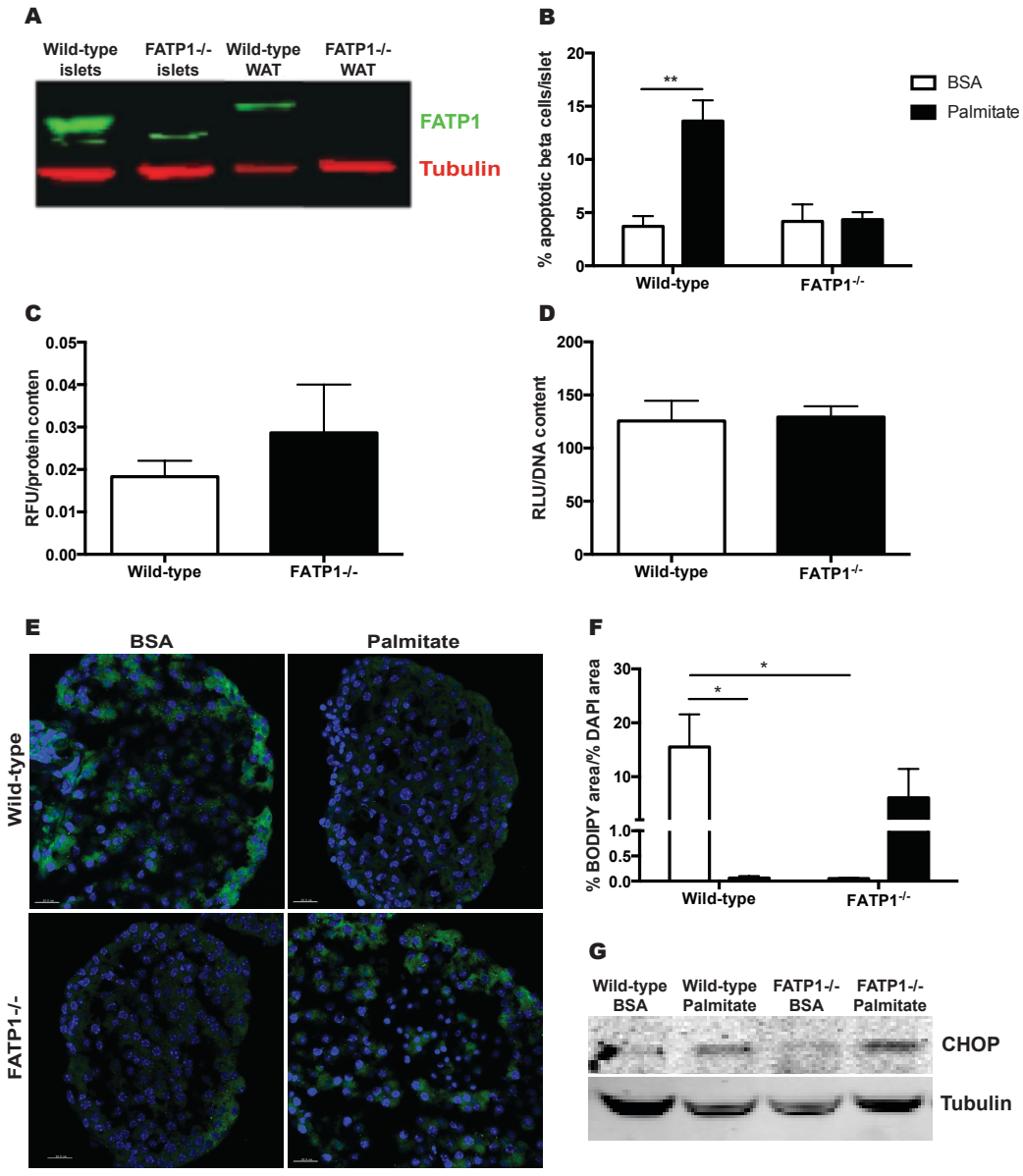

Figure 3. FATP1$^{-/-}$ islets are protected from palmitate-induced apoptosis and differentially accumulate lipids in response to metabolic signals.

A FATP1 protein is expressed in isolated islets and absent from FATP1$^{-/-}$ islets. **B** FATP1$^{-/-}$ islets are protected from palmitate-induced apoptosis (n=3). **C** Wild-type and FATP1$^{-/-}$ islets take up the same amount of BODIPY-fatty acid in vivo (n=6). **D** Islets isolated from wild-type luc^{+} and FATP1$^{-/-}$ luc^{+} mice take up the same amount of luciferin-fatty acid (n=3). **E** Wild-type islets and FATP1$^{-/-}$ islets differentially accumulate lipid in response to palmitate treatment (representative images). **F** Quantification of (E) (n=4). **G** Wild-type and FATP1$^{-/-}$ islets both undergo palmitate-induced ER stress. WAT = white adipose tissue, BSA = bovine serum albumin, RFU = relative fluorescent units, RLU = relative luminescent units. *p < 0.05, **p < 0.005, Error bars represent SEM.

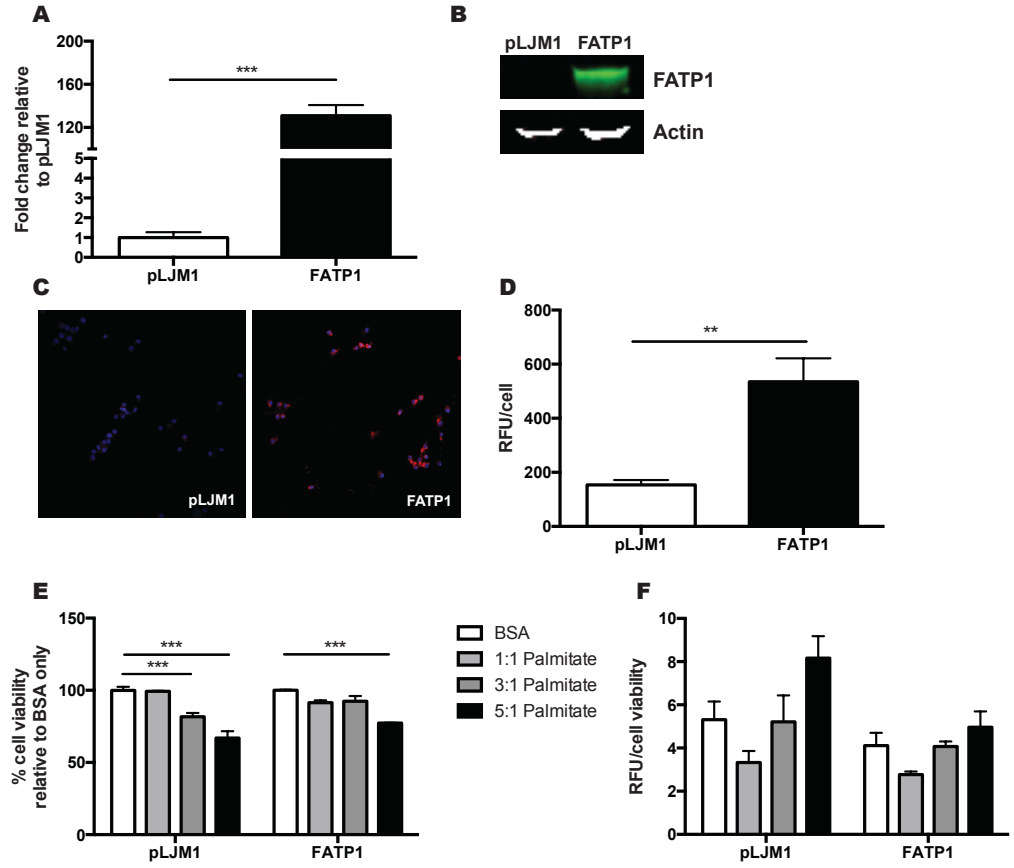

Figure 4. MIN6 cells overexpressing FATP1 have enhanced fatty acid uptake but are just as susceptible to palmitate-induced cell death as cells expressing empty vector
A MIN6 cells infected with FATP1 lentivirus express more FATP1 transcript than cells infected with empty vector (n=6). **B** MIN6 cells infected with FATP1 lentivirus express more FATP1 protein than cells infected with empty vector, as measured by Western blot. **C** MIN6 cells infected with FATP1 lentivirus express more FATP1 protein than cells infected with empty vector, as measured by immunohistochemistry. **D** MIN6 cells overexpressing FATP1 show enhanced BODIPY-fatty acid uptake compared to cells expressing vector alone (n=6). **E** FATP1-expressing MIN6 cells are just as susceptible to palmitate-induced cell death as cells expressing vector alone (n=3). **F** FATP1-expressing MIN6 cells show a trend towards reduced lipid accumulation when incubated with palmitate (p=0.06) (n=3). RFU = relative fluorescent units, BSA = bovine serum albumin. *p < 0.05, **p < 0.005, ***p < 0.001. Error bars represent SEM.

Discussion

FATPs are expressed in the endocrine pancreas, with FATP1 localizing to pancreatic beta cells, FATP3 to delta cells, and FATP4 to alpha cells. Loss-of-function of FATP1 protects beta cells from palmitate-induced apoptosis. FATP1$^{-/-}$ islets had the same level of fatty acid uptake as wild-type islets, but differentially stored intracellular lipid in response to metabolic cues. FATP1-overexpressing MIN6 cells are just as susceptible to palmitate-induced cell death as control cells, but also show a trend towards differential lipid storage in response to palmitate. FATP1 seems to be playing a role in directing fatty acids towards specific metabolic fates within beta cells and may protect beta cells from the lipotoxic effects of fatty acids.

We are the first to show that FATPs are expressed in the endocrine pancreas. We detected FATP1, FATP3, and FATP4 transcript in islets isolated from mouse pancreas. Although the absolute transcript levels of the FATPs were low compared to the transcript levels we see in other tissues, we were able to localize FATP protein expression to specific cell types within the pancreas. FATP1 is expressed in beta cells, FATP3 in delta cells, and FATP4 in alpha cells. Perhaps the reason we see low absolute levels in whole islets in that we are evaluating RNA from a pool of various cell types rather than individual cell species.

We focused our attention on FATP1's role in pancreatic beta cells. While there is some evidence that dysregulated glucagon secretion plays a role in the development of diabetes,[161–164] and that fatty acids affect alpha cell function,[165,166] loss of beta cell mass and insulin production, secretion, and action is central to the development of diabetes[148]. Future work will need to address the role of FATP3 and FATP4 in delta cell and alpha cell metabolism and function respectively. We utilized FATP1 whole-body knockout mice[17] to study FATP1's function in pancreatic beta cells. FATP1$^{-/-}$ mice have normal weight gain and fatty acid uptake in peripheral tissues on a chow diet. However, loss of FATP1 protects mice from skeletal muscle insulin resistance caused by a high-fat diet[17]. This is due to a reduction in insulin-stimulated fatty acid uptake and intracellular lipid accumulation in skeletal muscle and white adipose tissue in FATP1$^{-/-}$ mice[17,21]. In order to investigate FATP1 action specifically in beta cells and to avoid confounding data from FATP1 action in skeletal muscle and white adipose tissue, we performed the majority of our experiments ex vivo in islets isolated from FATP1$^{-/-}$ mice. However, it is important to note that the islets isolated from FATP1$^{-/-}$ mice may have had a lower demand for insulin production and secretion in vivo than islets isolated from wild-type mice and this may have resulted in changes in the overall metabolism and function of islets from FATP1$^{-/-}$ mice.

We hypothesized that loss-of-function of FATP1 would lead to reduced fatty acid transport into beta cells and therefore reduced lipotoxicity. We found that indeed, deletion of FATP1 protected pancreatic beta cells from palmitate-induced apoptosis. To explore the mechanism behind this finding, we examined fatty acid uptake, lipid accumulation, and induction of ER stress in FATP1$^{-/-}$ islets. First, we measured fatty acid uptake in wild-type and FATP1$^{-/-}$ islets using an in vivo and ex vivo assay. We did not detect alterations in fatty acid uptake in FATP1$^{-/-}$ islets in either assay. FATP1 mediates long-chain fatty acid uptake in vitro[13,16] and we

verified this by overexpressing FATP1 in an islet-derived cell line. FATP1-expressing MIN6 cells showed enhanced BODIPY-fatty acid uptake compared to cells expressing empty vector. In vivo, there are no changes in basal skeletal muscle fatty acid uptake in FATP1$^{-/-}$ mice compared to wild-type mice[17]. However, insulin-stimulated fatty acid uptake is diminished in muscle strips and adipocytes from FATP1$^{-/-}$ mice[21]. We found that FATP1 is transcriptionally regulated by glucose and palmitate in islets. It may be that as in other tissues, metabolic signals regulate the majority of beta cell FATP1 activity, and we will not see changes in fatty acid uptake in the basal state in FATP1$^{-/-}$ islets. Beta cells may maintain optimal glucose sensing and utilization in the basal state by downregulating other nutrient transporters[167]. It may also be the case that FATP1 expression in beta cells is relatively low and that global loss of FATP1 expression led to changes in beta cell biology that resulted in reduced susceptibility of beta cells to palmitate-induced apoptosis ex vivo. In this case, we would not expect that loss of FATP1 activity in other peripheral tissues like skeletal muscle and adipose tissue would result in a reduction in fatty acid uptake in beta cells. To differentiate the effects of FATP1 expression in beta cells from the effects of whole-body deletion of FATP1, a beta cell-specific FATP1 knockout mouse model could be developed.

The fatty acid uptake assays we employed measured fatty acid uptake over the course of one hour. Since we saw changes in apoptosis after incubating islets with palmitate for 48 hours, we wanted to investigate whether FATP1 affected long-term lipid accumulation. To this end, we measured lipid levels in wild-type and FATP1$^{-/-}$ islets, applying the same conditions we used in our apoptosis assays. We found that in the basal state, FATP1$^{-/-}$ islets store fewer intracellular lipids than wild-type islets, suggesting that lack of FATP1 activity results in reduced lipid uptake and storage. Interestingly, when we treat wild-type islets with palmitate, we see a reduction in lipid stores compared to the basal state, but in FATP1$^{-/-}$ islets, we see an increase in lipid stores. Also, in our MIN6 cell model, FATP1-overexpressing cells had a trend towards reduced lipid accumulation in response to palmitate compared to control cells. It seems that FATP1 expression is inversely correlated with palmitate-induced intraceullular lipid stores. Palmitate does not form intracellular triglycerides in islets as readily as unsaturated fatty acids like oleate[149], and actually, the ability of islets to form neutral lipid stores may help protect beta cells from toxic lipid intermediates that lead to apoptosis. Cnop et al. found an inverse correlation between apoptosis rates and triglyceride accumulation in islet cells[149]. It is not well understood where fatty acids are channeled within a cell and what regulates the metabolic fate of specific fatty acids[168]. In wild-type islets, palmitate taken up by the beta cells may be oxidized directly or turned into toxic lipid intermediates that in turn lead to apoptosis. In FATP1$^{-/-}$ islets, fatty acids may not be targeted to these lipotoxic metabolic fates. Perhaps other fatty acid transporters are upregulated that direct palmitate to neutral lipid stores, thereby protecting beta cells from palmitate-induced apoptosis. Future work needs to address which fatty acid species change in FATP1$^{-/-}$ islets in the basal state as well as in lipotoxic conditions and what compensatory mechanisms may be responsible for these changes.

Finally, we also evaluated whether FATP1 affected palmitate-induced ER stress in beta cells. Long-term exposure of beta cells to saturated fatty acid induces ER stress and this is sufficient, although not necessary, to cause beta cell apoptosis[169–171]. CHOP is the most well studied molecular target linking ER stress to lipotoxicity. We measured CHOP protein levels as a way to quantify ER stress in islets. We found that both wild-type and FATP1$^{-/-}$ islets upregulate expression of CHOP, suggesting that FATP1$^{-/-}$ islets are not protected from palmitate-induced ER stress. We did not measure ER stress by other methods, but more recently, studies have demonstrated CHOP-independent mechanisms linking lipotoxicity to ER stress that might also be at work in our model[152]. Also, since ER stress is not the sole mechanism by which saturated fatty acids induce apoptosis, FATP1 expression may have more directly affected other pathways responsible for lipotoxicity, such as ceramide or reactive oxygen species formation.

We utilized another model to investigate the mechanism of FATP1's role in pancreatic beta cells. By means of lentiviral infection, we overexpressed FATP1 in MIN6 cells. We hypothesized that gain-of-function of FATP1 would lead to an increase in fatty acid uptake and therefore make the cells more susceptible to palmitate-induced cell death. As expected, overexpression of FATP1 led to enhanced BODIPY-fatty acid uptake in MIN6 cells compared to cells expressing empty vector. However, this did not make FATP1-expressing MIN6 cells more susceptible to palmitate-induced cell death. Other groups have reported a weak induction of apoptosis in MIN6 cells[172]. Lipotoxicitiy mechanisms in MIN6 cells may be distinct from those in pancreatic islets, and it may be the case that FATP1 mediates specific apoptotic effects in islets but does not impact necrotic pathways in MIN6 cells.

In summary, beta cell lipotoxicity contributes to the development of diabetes and targeting fatty acid transport remains a promising therapeutic strategy to reduce beta cell destruction caused by hyperlipidemia[148]. We show that FATP1 is expressed in beta cells and that FATP3 and FATP4 are also expressed in pancreatic islets. Loss-of-function of FATP1 protects beta cells from palmitate-induced apoptosis. While the mechanism of this effect remains unclear, it may be due to lack of FATP1-mediated metabolic targeting of fatty acids to liptoxic fates. Future work should address which fatty acid-derived metabolites mediate apoptosis in beta cells and how fatty acid transporters affects overall beta cell fatty acid metabolism.

Methods

Animal experiments

All animal procedures were approved by the University of California Berkeley Animal Care and Use Committee. C57BL6/J mice were purchased from the Jackson Laboratory (#000664). FATP1$^{-/-}$ mice were generated as previously described[139]. Heterozygous FATP1$^{-/+}$ mice were bred to produce FATP1$^{-/-}$ and wild-type littermates. Mice were genotyped using a published PCR assay[139]. FATP1$^{-/-}$luc^{+} animals were generated by crossing FATP1$^{-/-}$ animals with D1.FVB(Cg)-Tg(CAG-luc,-GFP)L2G85Chco/FathJ animals (Jackson Laboratory #010548). The resulting litters were genotyped for the FATP1 transgene as described as well as for the luciferase

transgene by following the distributor's published protocol. All animal experiments were performed in 6- to 20-week-old male mice. Mice were given free access to water and rodent chow (Harlan Teklad #2018) and housed under standard conditions.

Isolation of islets from mice

Islets were isolated by a standard protocol[173]. Briefly, mice were euthanized and the pancreas was perfused via the bile duct with 3 ml of 0.8 mg/ml collagenase P (Roche Applied Science) in a washing buffer [10 mM HEPES, 10 μg Dnase I (Roche #10104159001), 1% penicillin-strepomyocin, 1.7 mM calcium chloride, and 1.2 mM magnesium chloride in Hank's buffered saline solution]. Then, the pancreas was digested at 37°C for 15 minutes. The digested pancreas was washed, strained through a tea strainer, and then subjected to density centrifugation in Histopaque (Sigma-Aldrich #11191). The layer containing the islets was moved to a 6-cm culture plate and the islets were handpicked using a dissecting microscope for further culture. Islets were maintained in RPMI 1640 supplemented with 10% fetal bovine serum, 1% penicillin-streptomyocin, 25 mM HEPES, and 1% non-essential amino acids (Invitrogen 11140) and used in experiments the day after isolation.

Cell culture

MIN6 cells were maintained in DMEM with high glucose supplemented with 15% fetal bovine serum, 1% penicillin-streptomyocin, and 71.5 μM 2-mercaptoethanol. Mouse FATP1 was expressed in MIN6 cells via lentiviral infection.

Lentiviral expression of FATP1

The mouse FATP1 gene was cloned into the lentiviral vector pLJM1 (Addgene #19319). To make lentivirus, HEK293 cells were transfected with pLJM1-FATP1 or empty vector, and the lentiviral packaging vectors psPAX2 and pMD2.G according to Addgene's protocol. Two days later, the media containing lentivirus was obtained from the cells. MIN6 cells were plated in a 6-well plate in media containing 8 μg/ml polybrene and infected with 500 μl of lentivirus housing FATP1 or empty vector. After two days, 1 μg/ml puromyocin was added to the maintenance media to select for cells expressing the infected vector. Single cells were obtained by serial dilution to make clonal cell lines, and the clone expressing the highest level of FATP1 transcript was used in experiments.

Palmitate preparations and treatments

Albumin-bound palmitate solutions were prepared as previously described[174]. Sodium palmitate (Sigma Aldrich #P9767) was dissolved in 1:1 ethanol:water to a concentration of 150 mM and incubated at 65°C for 15 minutes. This 150 mM sodium palmitate stock was diluted into a solution containing 10% bovine serum albumin (Akron Biotech #8909) in serum-free cell maintenance media at a molar ratio of 5:1 palmitate:albumin. For MIN6 cell experiments, 3:1 and 1:1 palmitate:albumin solutions were also prepared. These solutions were incubated

for 1 hour at 37°C in a shaking water bath. The resulting albumin-bound palmitate stock solutions were sterile-filtered, aliquoted, and stored at -20°C.

Isolated islets were treated with palmitate at a 5:1 palmitate:albumin ratio by diluting the described 5:1 palmitate:albumin stock to 1 mM in serum-free islet maintenance media. MIN6 cells were incubated with palmitate by diluting the described 5:1, 3:1, or 1:1 palmitate:albumin stock to 1 mM in serum-free MIN6 maintenance media. Islets and MIN6 cells were incubated in 1 mM palmitate, 30 mM glucose (Sigma Aldrich #G6152), 1 mM palmitate plus 30 mM glucose, or bovine serum albumin alone for up to 72 hours.

RNA isolation

RNA was isolated from 100-500 islets at a time by vortexing islets in 1 ml Trizol, incubating them for five minutes at room temperature, and then adding 0.2 ml chloroform and shaking vigorously for 15 seconds. Samples were then centrifuged at 12,000 x g for 10 minutes at 4°C and the aqueous phase was moved to a new tube. One volume of 70% ethanol was added to the aqueous phase and the solutions were mixed by pipetting up and down. This was applied to a column from the Qiagen RNeasy kit (#74104) and the rest of the isolation was carried out according to the manufacturer's protocol, including the on-column DNase digestion. RNA was eluted from the column in 30 µl RNase-free water. RNA was isolated from other tissues and cells using the Aurum Total RNA Fatty and Fibrous Tissue Module (Bio Rad #7326870) according to the manufacturer's protocol. cDNA was synthesized using the Maxima First Strand cDNA Synthesis Kit for RT-qPCR (Thermo Fisher Scientific #K1642) with 0.5-1 µg RNA per 20 µl reaction.

Absolute and relative quantification PCR

For relative quantification real-time quantitative PCR, 1 µl of cDNA was used in a 20 µl PCR reaction along with 1 µl PrimeTime qPCR assay [Integrated DNA Technologies #mm.pt.39a.1 for glyceraldehyde 3-phosphate dehydrogenase (GAPDH), #mm.pt.53a.33622420 for FATP1, #mm.pt.53a.7014435.g for FATP3, and #mm.pt.53a.14045996 for FATP4] and 10 µl TaqMan Universal Master Mix II (Thermo Fisher Scientific #4440040). The PCR reactions were run and cycle thresholds were calculated with the Applied Biosystems 7500 Real Time PCR System. Fold change was calculated by comparing the difference in cycle thresholds between the gene of interest and the housekeeping gene for treated samples and control samples.

For absolute quantification PCR, the mass of plasmids containing the mouse GAPDH, FATP1, FATP3, and FATP4 cDNA were calculated by assuming that each base pair weighed 1.096×10^{-21} g. The concentration of each plasmid needed to obtain 300,000 copies of the gene of interest per PCR reaction was calculated and the plasmids were serially diluted ten-fold to obtain 30,000, 3,000, 300, and 30 copies of the gene per PCR reaction. Standard curves of cycle threshold values were generated based on the gene copy number in each PCR reaction (**Fig. S1**). The cycle

threshold values for individual samples were plotted on the standard curve to determine the number of copies of the gene for a given amount of RNA.

Immunohistochemistry

Isolated islets were fixed in 4% paraformaldehyde (Electron Microscopy Sciences #15710) for 20 minutes at room temperature, washed in phosphate-buffered saline, then cryopreserved in O.C.T Compound (Sakura #4583) in a cryomold. Islets were then sectioned at 10 μm onto charged glass slides with a Leica CM3050S cryostat at -19°C. The resulting slides were post-fixed in 4% paraformaldehyde for 20 minutes at room temperature in a humidified chamber and blocked for one hour at room temperature in blocking buffer (3% normal donkey serum, .05% saponin, 1% bovine serum albumin, and 10% fetal bovine serum in phosphate-buffered saline). Slides were then incubated in primary antibody solutions in blocking buffer overnight at 4°C. Polyclonal antibodies against FATPs were developed in house[175]. Monoclonal antibodies against hormone markers of islets cells were purchased from Abcam (anti-insulin + proinsulin #ab8304, anti-glucagon #ab10988, and anti-somatostatin #ab103790). Insulin and glucagon were co-stained with the FATPs. Serial sections of islets were stained for FATPs and somatostatin, since both antibodies were raised in rabbits. Slides were then incubated with secondary antibodies to the primary antibodies [donkey anti-rabbit or anti-mouse IgG (H+L) conjugated to Alexa Fluor 488 or 647, Thermo Fisher Scientific #A-21206 and #A-31573] and mounted in DAPI mountant (Life Technologies #P36971). Slides were imaged with a Zeiss LSM710 laser scanning confocal microscope. Images were processed on the software IMARIS.

MIN6 cells were grown on glass coverslips in a 6-well plate and fixed and stained in the plate. After staining, the coverslips were mounted onto glass slides with DAPI mountant and imaged as described.

Western blot

Tissues or cells were lysed in radioimmunoprecipitation assay buffer (150 mM sodium chloride, 1% NP-40, 0.5% deoxycholic acid, 0.1% sodium dodecyl sulfate, 50 mM Tris, pH 8.0). Protein content was quantified by the bicinchoninic assay (Pierce #23225). 25-50 μg of protein were loaded onto a 4-20% Tris-Glycine gel (Novex #EC60285) and run at 130 volts in Tris-glycine running buffer (25 mM Tris-HCl, 250 mM glycine, 0.1% sodium dodecyl sulfate) for two hours. The gels were transferred to nitrocellulose membranes using the iBlot system (Thermo Fischer Scientific). The membranes were blocked in Odyssey Blocking Buffer (Licor #92740000) for one hour at room temperature, and then stained in primary antibody solutions in blocking buffer with 0.1% Tween-20 (Sigma Aldrich P7949) overnight at 4°C. (Anti-FATP1 antibody developed in house[175], diluted 1:1000; anti-GADD 153, Santa Cruz Biotechnology #sc-575, diluted 1:200; anti-beta-tubulin/E7, Developmental Studies Hybridoma Bank, diluted 1:1000; anti-beta-actin, Santa Cruz Biotechnology #sc-47778). The membranes were then washed and stained in Licor secondary antibody (IRDye 680LT #926-68022 or IRDye 800CW #926-32211, diluted

1:20,000) in blocking buffer with 0.1% Tween-20 for one hour at room temperature. Western blots were imaged with the Licor Odyssey system.

Apoptosis assay in isolated islets

Isolated islets were treated as indicated. Islets were fixed, cryopreserved, and sectioned as described. Islet sections were stained for apoptotic cells using the In Situ Cell Death Detection Kit (Roche #11684795910). Briefly, the slides were post-fixed in 4% paraformaldehyde for 20 minutes at room temperature, permeabilized with 1% Triton X-100 (Sigma Aldrich #234729) in 0.1% sodium-citrate for 5 minutes at room temperature, then incubated in TUNEL reaction mixture at 37°C for one hour. As a positive control for the reaction, islet sections were treated with DNase I for 10 minutes before the TUNEL stain. After washing slides in phosphate-buffered saline, the sections were co-stained for insulin as described. Slides were mounted in DAPI mountant and imaged with a Zeiss LSM710 laser scanning confocal microscope. TUNEL-positive apoptotic cells, insulin-positive beta cells, and total number of cells were quantified with IMARIS. Results are shown as percent of apoptotic cells per islet section.

Apoptosis assay in MIN6 cells

MIN6 cells were plated at 70,000 cells per well of a 24-well plate and treated as indicated. Apoptosis was measured with the Cell Death Detection ELISA PLUS kit (Roche #11774425001) according to the manufacturer's protocol. Briefly, cells were lysed in 250 µl of lysis buffer and 20 µl of the lysate was applied to the ELISA plate supplied. At the end of the assay, the absorbance in each well was quantified with a SpectraMaxi3 plate reader (Molecular Devices) and the values for the experimental samples were given relative to the values for the control samples.

XTT assay in MIN6 cells

MIN6 cells were plated onto a 96-well plate with 50,000 cells per well and treated as indicated. XTT solution was prepared immediately before the assay according to the manufacturer's protocol (Biotium #30007). 25 µl of XTT solution was added to each well. The cells were incubated with the XTT solution for four hours. The absorbance of the samples was measured using a SpecrtraMaxi3 plate reader. The absorbance of the experimental groups was compared to the absorbance of the samples treated with vehicle only.

In vivo BODIPY-fatty acid uptake assay

Wild-type or FATP1$^{-/-}$ mice were fasted for three hours and injected with 20 µM BODIPY-fatty acid (Molecular Probes #D3823) bound to 1% bovine serum albumin at 0.125 µmol BODIPY per kilogram of body weight. After the indicated time, the mice were euthanized and islets were isolated as described. Islets were homogenized in radioimmunoprecipitation assay buffer and the fluorescence of the lysate was read at an excitation of 488 nm and emission of 515 nm using a SpectraMaxi3 plate reader. Relative fluorescence values were adjusted for lysate protein content.

Ex vivo luciferin-fatty acid uptake assay

Islets were isolated from wild-type and FATP1$^{-/-}$luc^{+} mice as described. Islets were seeded into a 96-well opaque plate at 10 islets per well and exposed to uptake solution containing 10 μM luciferin-fatty acid[160] in 0.1% bovine serum albumin. The emitted luminescence was recorded in real-time using a plate reader (Molecular Devices SpectraMaxL). Steady-state values were reached within 30 minutes. At the end of the assay, the islets were homogenized in phosphate-buffered saline containing 0.1% Tween-20 and 0.2% propidum iodide (Invitrogen #P3566) to quantify the amount of DNA in each well. The fluorescence was quantified with a SpectraMaxi3 plate reader. The steady-state relative luminescence values for the luciferin-fatty acid were adjusted for the relative fluorescence of the propdium iodide stain.

BODIPY-fatty acid uptake assay by FACS

The day before the assay, MIN6 cells were plated at 250,000 cells per well in a 6-well plate. Cells were then incubated with uptake solution containing 2 μM BODIPY-fatty acid and 0.1% bovine serum albumin in Hank's buffered saline solution for one hour at 37°C. Cells were trypsinized, washed in ice-cold buffer containing 0.2% bovine serum albumin, and sent through a flow cytometer (BD FACS Calibur). Cells were gated on forward and side scatter and the mean FL1 fluorescence was plotted.

Neutral lipid stain

Sections of wild-type and FATP1$^{-/-}$ islets treated with 1 mM palmitate or bovine serum albumin alone for 48 hours were stained with 10 μg/ml BODIPY neutral lipid stain (Thermo Fisher Scientific #D3922) for one hour at room temperature. Slides were washed in PBS, mounted with DAPI mountant, and imaged with a Zeiss LSM710 laser scanning confocal microscope. The BODIPY and DAPI signals were quantified with ImageJ and the BODIPY signal was adjusted for total cell number.

MIN6 cells were treated with palmitate or albumin only as indicated and stained with 10 μg/ml BODIPY neutral lipid stain for ten minutes at room temperature. The fluorescence of the samples was quantified with a SpectraMaxi3 plate reader and the relative fluorescence was adjusted for cell viability.

Statistical analysis

Differences between two groups were determined using unpaired Student's *t* test. Linear regression analysis was used to determine the rate of change of values over time. Data are presented as mean values with error bars representing the standard error of the mean. Asterisks indicate significant differences (*$p < 0.05$, **$p < 0.005$, ***$p < 0.001$).

Supplementary Data

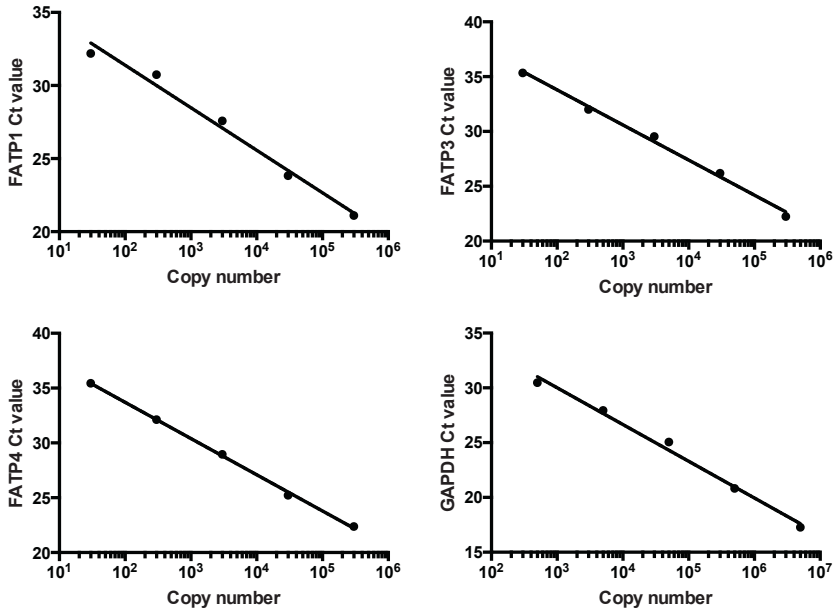

Supplementary Figure 1. Standard curves for absolute quantification PCR for FATP1, FATP3, FATP4, and GAPDH.

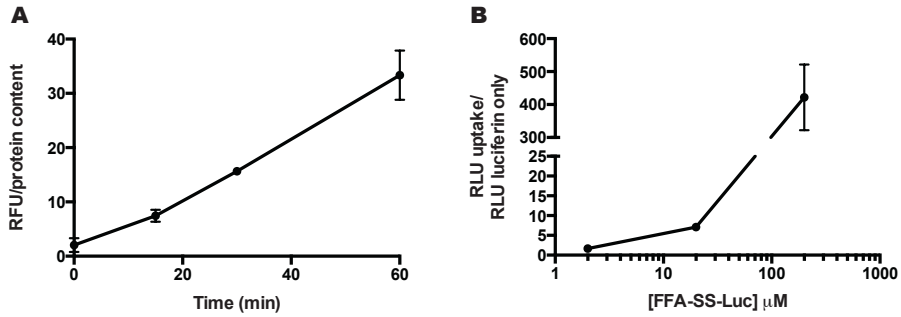

Supplementary Figure 2.
A After injecting mice with BODIPY-fatty acid, the fluorescence in isolated islet lysate increases over time (n=3). **B** Incubating isolated islets that express luciferase with a luciferin-fatty acid results in a dose-dependent increase in light production (n=6).

Chapter 4: Rationally designed FATP inhibitors and 4-aryl-3,4-dihydropyrimidin-2(1H)-one, an identified FATP4 inhibitor, do not reduce endogenous FATP-mediated fatty acid uptake

Additional Contributors:

Satoshi Shuto, *Hokkaido University* – synthesized phospholipid-based compounds

Vladislav Dubikovsky, *Intrace Medical* – synthesized 4-aryl-3,4-dihydropyrimidin-2(1H)-one

Rationale

Fatty acids are important molecules that are involved in a variety of biological processes. Besides being a major fuel source, they also activate intracellular signal transduction cascades, regulate metabolic enzymes, bind transcription factors, provide substrates for posttranslational protein modification, and are precursors to components of the cell membranes and mediators of the immune response[4,5]. While fatty acids are essential to maintain normal biological function, excess fatty acids in circulation and in peripheral tissues can become pathophysiological. Ectopic lipid accumulation in tissues like skeletal muscle, liver, heart, and pancreatic beta cells can lead to insulin resistance and lipotoxicity. Although the mechanisms of lipotoxicity are unclear, it seems that excess levels of fatty acids in these tissues results in the formation of toxic fatty acid intermediates that induce ER stress and ultimately, apoptosis and cell death[4,6–8].

Because of the detrimental effects of excess fatty acids, much effort has been made to understand how fatty acids enter cells and whether this process is regulated. We now know that while some fatty acids can diffuse across the plasma membrane, the majority of fatty acid uptake into cells is protein-mediated[4,9,10]. Fatty acid transport proteins (FATPs)[4], fatty acid translocase (CD36)[11], and plasma membrane fatty acid binding protein (FABPpm)[12] have been shown to facilitate fatty acid uptake into cells. Genetic studies in mice have shown a categorical role for these proteins in mediating tissue fatty acid uptake and lipid accumulation in vivo[4]. In fact, loss-of-function of specific FATPs can protect animals from the development of insulin resistance[17] and hepatosteatosis[19], while overexpression in the heart can lead to cardiomyopathy[41].

Metabolic diseases like diabetes, heart disease and nonalcoholic fatty liver disease are globally prevalent and represent a major public health concern. FATPs, therefore, are an attractive therapeutic target for these conditions. There are six members of the FATP family[4]. Because each FATP is uniquely expressed and regulated, targeting specific FATP's may be an effective way to target tissue-specific fatty acid uptake without affecting whole body lipid metabolism and producing undesirable side effects.

Some effort has been made to find small molecule inhibitors of FATPs. Two groups have developed high-throughput screening techniques utilizing a fluorescent BODIPY-fatty acid to identify compounds that reduced fatty acid uptake in cells[176–

[178]. Using these techniques, investigators have identified and validated triazole-based compounds as inhibitors of FATP1[179,180] tricyclic, phenothiazine-derived drugs as inhibitors of FATP2[176,181–183], dihydropyrimidinone-based drugs as inhibitors of FATP4[178,184], and secondary bile acids as inhibitors of FATP5[40,178]. Chemically optimized triazole-based FATP1 inhibitors effectively reduced fatty acid uptake in vitro and were bioavailable in vivo, but did not affect tissue lipid accumulation in mice[180]. Two phenothiazine-derived FATP2 inhibitors, called Grassofermata and Lipofermata, have been shown to reduce fatty acid uptake and lipotoxicity in a variety of cell lines from metabolic tissues[182,183]. A chemically optimized FATP4 inhibitor has been shown to reduce fatty acid uptake in 3T3-L1 adipocytes and in isolated enterocytes, which exclusively express FATP4[178]. Deoxycholic acid, a secondary bile acid, has been shown to inhibit fatty acid uptake and lipid accumulation in the liver in vivo[40].

While progress has been made towards finding small molecule inhibitors for FATPs, we still do not have inhibitors for all of the FATPs and many of the current inhibitors have not been validated in multiple cell models or in vivo. In order to address these concerns and to explore other potential inhibitors, we collaborated with two different groups that created potential FATP inhibitors. One group rationally designed and developed novel compounds with a phospholipid moiety and a fatty acid moiety. They predicted that these compounds would be targeted to cell membranes and would competitively inhibit general FATP activity. Another group provided our laboratory with one of the dihydropyrimidone-based FATP4 inhibitors that they identified by a high-throughput screen and chemically optimized to inhibit FATP4. We tested the ability of these compounds to reduce fatty acid uptake in multiple in vitro and ex vivo models and found that the phospholipid-based compounds did not inhibit FATP activity at reasonable concentrations and the dihydropyrimidone-based inhibitor effectively reduced FATP1- and FATP4-mediated fatty acid uptake in overexpression cell models, but did not affect endogenous FATP1 or FATP4 activity in other cell models.

Results

Phospholipid-based compounds are cytotoxic at some concentrations

A group of medicinal chemists synthesized six compounds with a phospholipid moiety conjugated to a fatty acid via an ether bond (unpublished, **Fig. 1A**) with the rationale that the phospholipid moiety would insert into the plasma membrane and the fatty acid moiety would competitively block fatty acid transporters. The six compounds are distinct in the length of the ether bonds connecting the two moieties (**Fig. S1**). Our goal was to test whether the compounds could effectively inhibit general FATP activity in mammalian cells. The fatty acid moiety in the compounds is based on arachidic acid, which we have shown competes with BODIPY-fatty acid in FATP4-expressing cells[34]. Therefore, we used arachidic acid as a positive control for competitive inhibition of FATP activity in our cell models.

We first tested the cytotoxicity of these compounds at concentrations ranging from 2 nM to 20 μM in HEK293 cells stably expressing human FATP5. Using an XTT assay

for cell viability, we found that treating the cells with compound 1, 2, 4, and 5 reduced cell viability at some but not all of the concentrations of the compounds tested (**Fig. 1B**). Compound 6, the compound with the longest ether bond, and arachidic acid were not toxic to the cells at any of the concentrations tested.

Phospholipid-based compounds do not inhibit FATP5-mediated BODIPY-fatty acid uptake.

We used HEK293 cells stably expressing human FATP5 as a model to test whether the synthesized compounds could inhibit general FATP-mediated fatty acid uptake. These cells consistently show elevated BODIPY-fatty acid uptake relative to cells expressing an empty vector as measured by a quencher-based real-time uptake assay (**Fig. 1C**)[97]. This real-time uptake assay is one of the methods used in high-throughput screens for FATP inhibitors[177,178].

We pre-incubated the FATP5-expressing cells for 30 minutes with the compounds varying in concentration from 2 nM to 20μM to allow the compounds to associate with the plasma membrane and potentially bind FATPs before we introduced bovine serum albumin. Albumin may bind phospholipid analogs and prevent them from incorporating into the plasma membrane[185]. We also incubated the cells with deoxycholic acid, a bile acid which we have shown inhibits BODIPY-fatty acid uptake in HEK293 cells expressing FATP5[40]. We replaced the pre-incubation media with uptake solution containing 2 μM BODIPY-fatty acid bound to 0.1% bovine serum albumin in the presence of 1 mM quencher and the compounds at the indicated concentrations. We measured the relative fluorescence emitted from the cells over the course of two hours and calculated the change in relative fluorescence over time. While deoxycholic acid effectively reduced BODIPY-fatty acid uptake in the FATP5-expressing cells, the synthesized compounds and arachidic acid either had no effect on BODIPY-fatty acid uptake compared to cells treated with vehicle alone or they enhanced uptake (**Fig. 1D**).

Phosholipid-based compounds do not inhibit BODIPY-fatty acid uptake in differentiated 3T3-L1 cells.

Since the synthesized compounds are designed so that the fatty acid moiety will compete for FATP activity, we only expect the compounds to be effective in model systems where arachidic acid inhibits FATP-mediated fatty acid uptake. Arachidic acid did not effectively inhibit FATP5-mediated fatty acid uptake at the concentrations we tested. Since FATP5 may have a substrate preference for bile acids rather than fatty acids[40], we turned to a new cell model that expresses different FATPs to test our compounds.

When differentiated into adipocytes, 3T3-L1 cells show increased expression of FATP1 and FATP4 and enhanced cellular fatty acid uptake (**Fig. 1E**)[16]. To test whether our phospholipid-based compounds could inhibit fatty acid uptake mediated by FATP1 or FATP4, we treated differentiated 3T3-L1 adipocytes with the compounds varying in concentration from 2 nM to 20μM and measured subsequent

BODIPY-fatty acid uptake using the quencher-based assay described. The compounds did not affect the rate of BODIPY-fatty acid uptake and 20 μM arachidic acid again increased BODIPY-fatty acid uptake relative to vehicle-treated cells (**Fig. 1F**).

We have shown that exogenous fatty acids can actually increase labeled fatty acid uptake when the exogenous fatty acids are only ten times more concentrated than the labeled fatty acid[186]. We believe that this increase in uptake is due to fatty acid competition on albumin, which may result in a higher concentration of free, labeled fatty acid and therefore make the labeled fatty acid more bioavailable for cellular uptake. Once exogenous fatty acids are 100 times more concentrated that labeled fatty acid, exogenous fatty acids can competitively inhibit labeled fatty acid uptake[34,186]. Therefore, we tried incubating differentiated 3T3-L1 cells with 200 μM arachidic acid, 100 times the concentration of the BODIPY-fatty acid. We saw reduced BODIPY-fatty acid uptake, proving that we need at least 100 times more exogenous fatty acid than labeled fatty acid in order to competitively inhibit uptake (**Fig. 1F**). Like arachidic acid, the synthesized compounds may need to be used at higher concentrations in order to be effective. Because small molecule inhibitors are more likely to interact with off-target proteins at higher concentrations[187], we did not test whether the compounds were effective at higher doses.

4-aryl-3,4-dihydropyrimidin-2(1H)-one inhibits FATP4-mediated fatty acid uptake

Since we did not detect any inhibition of fatty acid uptake by the phospholipid-based compounds at feasible concentrations, we next tried a different compound that was shown to inhibit FATP4 activity. 4-aryl-3,4-dihydropyrimidin-2(1H)-one is a dihdropyrimidinone-based inhibitor with a cyclopentyl group that was identified by a high-throughput screen and chemically optimized for specific inhibition of FATP4 (**Fig. 2A**)[184]. We verified that this compound was effective in inhibiting FATP4 activity in our laboratory by incubating HEK293 cells expressing human FATP4, human FATP5, or empty vector with the compound and measuring BODIPY-fatty acid uptake with the quencher-based method described. We saw a significant increase in BODIPY-fatty acid uptake in cells expressing FATP4 that was attenuated by treating the cells with the compound (**Fig. 2B**). However, the FATP5-mediated BODIPY-fatty acid uptake was unaffected by treatment with the compound. This verifies that the compound is effective in inhibiting FATP4- but not FATP5-mediated BODIPY-fatty acid uptake.

4-aryl-3,4-dihydropyrimidin-2(1H)-one inhibits FATP1-mediated fatty acid uptake

Of all the FATPs, FATP1 and FATP4 are the most homologous and share 60.3% of their amino acid sequence[188]. Therefore, we wanted to test whether 4-aryl-3,4-dihydropyrimidin-2(1H)-one could also inhibit FATP1-mediated fatty acid uptake. To this end, we incubated MIN6 cells expressing mouse FATP1 or vector only with the compound and measured BODIPY-fatty acid uptake using flow cytometry. FATP1-expressing MIN6 cells showed enhanced BODIPY-fatty acid uptake that was reduced by treating the cells with the compound in a dose-dependent manner (**Fig.**

2C). Therefore, 4-aryl-3,4-dihydropyrimidin-2(1H)-one inhibits both FATP1- and FATP4-mediated fatty acid uptake.

4-aryl-3,4-dihydropyrimidin-2(1H)-one does not inhibit endogenous FATP activity in 3T3-L1 adipocytes

Next, we wanted to test whether 4-aryl-3,4-dihydropyrimidin-2(1H)-one effectively inhibited endogenous FATP activity. We used 3T3-L1 adipocytes as a model since these cells endogenously express both FATP1 and FATP4 when differentiated[16]. We incubated 3T3-L1 adipocytes with varying concentrations of the compound and measured BODIPY-fatty acid uptake with the quencher-based method described. Again, we saw significantly enhanced BODIPY-fatty acid uptake in differentiated 3T3-L1 cells compared to undifferentiated cells. Counter to what we observed in the FATP overexpressing models, 0.25 μM 4-aryl-3,4-dihydropyrimidin-2(1H)-one significantly enhanced BODIPY-fatty acid uptake, while higher concentrations of the compound did not affect the rate of BODIPY-fatty acid uptake (**Fig. 2D**). We used phloretin, a broad fatty acid transporter inhibitor, as a positive control for inhibition of endogenous FATP activity.

4-aryl-3,4-dihydropyrimidin-2(1H)-one does not inhibit endogenous FATP activity in isolated enterocytes

We also tested whether the compound could inhibit endogenous FATP4 expression in isolated enterocytes, which express FATP4 on the apical membrane and exhibit fatty acid uptake capacity ex vivo[34]. We incubated isolated enterocytes with the compound, DMSO alone, or phloretin, and measured BODIPY-fatty acid uptake by flow cytometry. While BODIPY-fatty acid uptake in isolated enterocytes increases over time, 12.5 μM 4-aryl-3,4-dihydropyrimidin-2(1H)-one did not affect BODIPY-fatty acid uptake, while 200 μM phloretin effectively reduced uptake (**Fig. 2E**).

4-aryl-3,4-dihydropyrimidin-2(1H)-one does not inhibit endogenous FATP activity in isolated islets

We also tested whether the compound could inhibit endogenous FATP expression in isolated islets. Islets are mostly made up of beta cells and alpha cells, with fewer amounts of delta cells and PP-cells[189]. Beta cells express FATP1, while alpha cells express FATP4, and delta cells express FATP3 (Chapter 3). We incubated isolated islets with varying concentrations of the dihydroyrimidone-based compound in the presence of a luciferin-fatty acid analog developed by some of our collaborators[186]. We measured fatty acid uptake in these cells by measuring the accumulation of light over time. We found that 4-aryl-3,4-dihydropyrimidin-2(1H)-one did not affect luciferin-fatty acid uptake in isolated islets (**Fig 2F**).

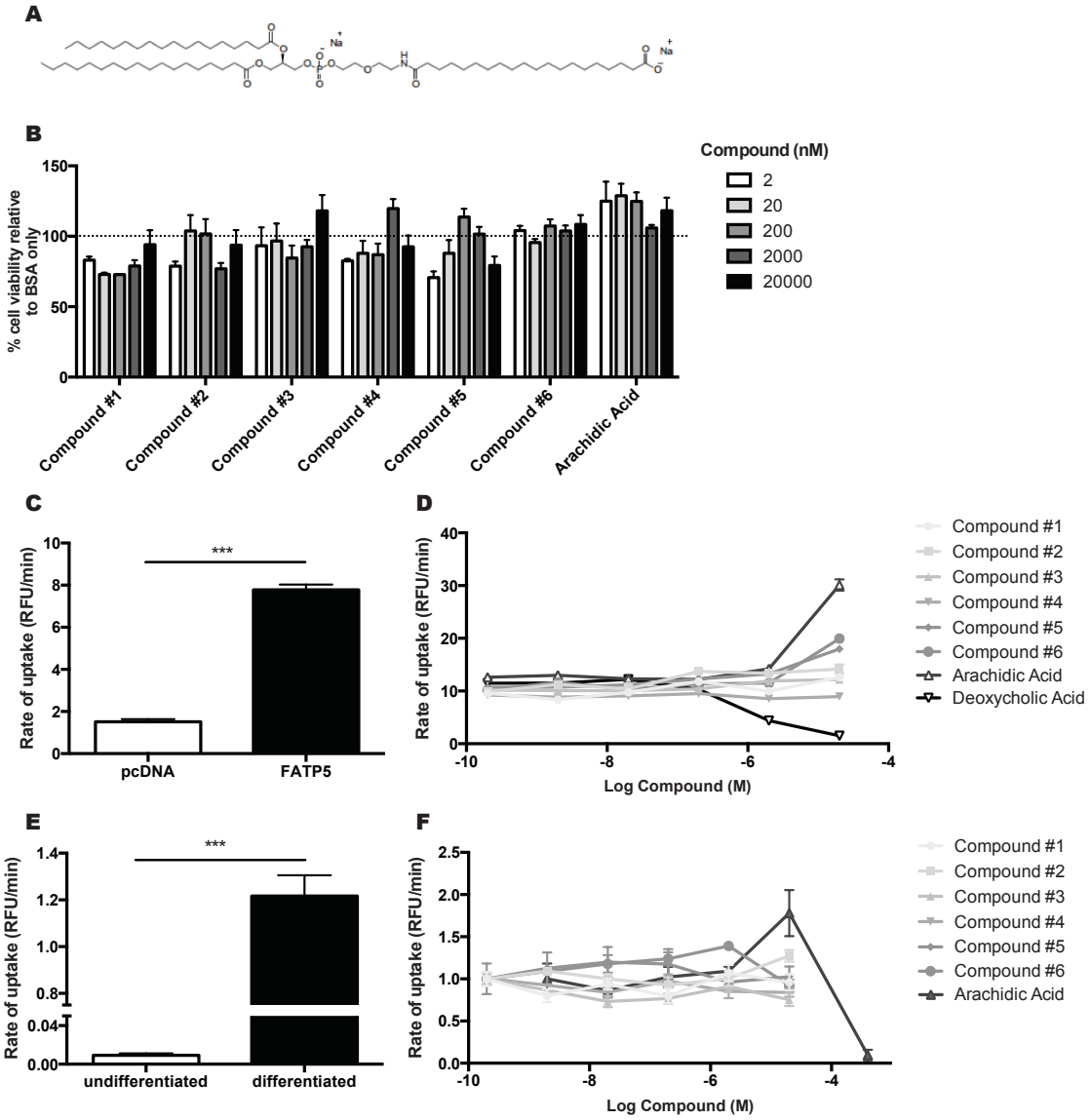

Figure 1. Phospholipid-based compounds do not inhibit BODIPY-fatty acid uptake. **A** Chemical structure of the phospholipid-based compounds containing a phospholipid moiety conjugated to a fatty acid moiety with an ether bond. (See supplementary figures for the structures of the other phospholipid-based compounds.) **B** Treating FATP5-overexpressing cells with the compounds resulted in slightly reduced cell viability for some compounds at some concentrations, while no changes in cell viability were detected for compound #6 or arachidic acid (n=3). **C** HEK293 cells overexpressing FATP5 have significantly enhanced BODIPY-fatty acid uptake compared to cells expressing empty vector (n=8). **D** In FATP5-overexpressing cells, 20 μM of compound #5, compound #6, and arachidic acid enhanced BODIPY-fatty acid uptake, while 20 μM deoxycholic acid inhibited BODIPY-fatty acid uptake (n=8). **E** Differentiated 3T3-L1 cells show significantly enhanced BODIPY-fatty acid uptake compared to undifferentiated 3T3-L1 cells

(n=8). **F** In differentiated 3T3-L1 cells, the phospholipid-based compounds did not affect BODIPY-fatty acid uptake, while 200 μM oleic acid inhibited BODIPY-fatty acid uptake (n=8). BSA = bovine serum albumin, RFU = relative fluorescent units. *$p < 0.05$, **$p < 0.005$, ***$p < 0.001$. Error bars represent SEM.

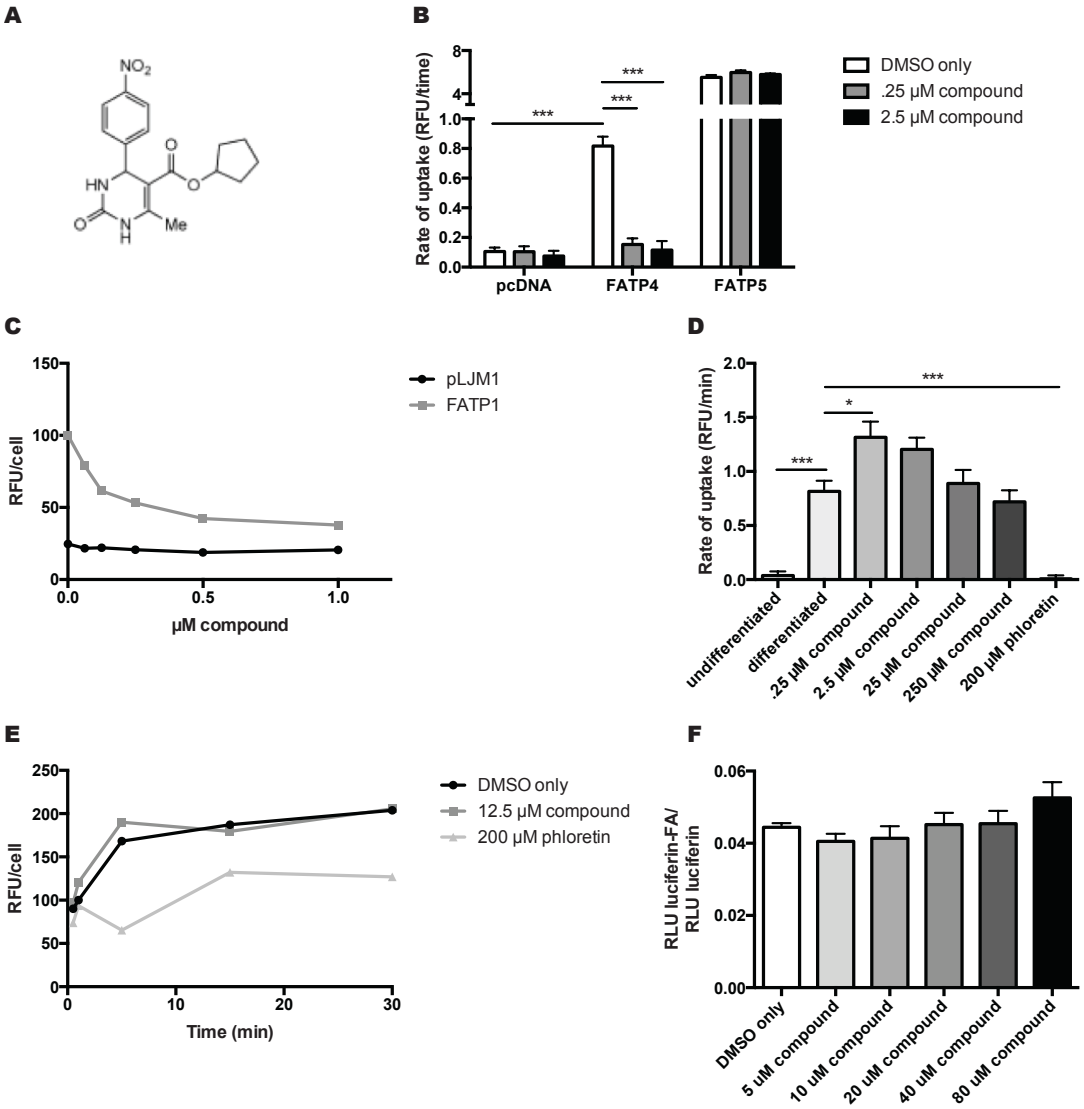

Figure 2. 4-aryl-3,4-dihydropyrimidin-2(1H)-one inhibits exogenous FATP1 and FATP4 activity, but does not inhibit endogenous FATP activity.

A 4-aryl-3,4-dihydropyrimidin-2(1H)-one is a dihdropyrimidinone-based compound with a cyclopentyl group that has been chemically optimized for inhibition of FATP4. **B** HEK293 cells overexpressing FATP4 have significantly enhanced BODIPY-fatty acid uptake compared to cells expressing empty vector. The dihydropyrimidinone-based compound specifically inhibits FATP4-mediated BODIPY-fatty acid uptake (n=8). **C** MIN6 cells overexpressing FATP1 have enhanced BODIPY-fatty acid uptake compared to cells expressing empty vector. The dihydropyrimidinone-based compound inhibits FATP1-mediated BODIPY-fatty acid uptake (n=1, representative of four experiments). **D** In differentiated 3T3-L1 cells, the compound enhanced BODIPY-fatty acid uptake at lower concentrations, while 200 μM phloretin significantly reduced BODIPY-fatty acid uptake (n=8). **E** In

isolated enterocytes, 12.5 μM compound does not affect BODIPY-fatty acid uptake as measured by flow cytometry, while 200 μM phloretin reduces uptake (n=1, representative of five experiments). **F** In isolated islets, the dihydropyrimidone-based compound does not affect luciferin-fatty acid uptake (n=4). RFU = relative fluorescent units, RLU = relative luminescent units. *p < 0.05, **p < 0.005, ***p < 0.001. Error bars represent SEM.

Discussion

We tested two different types of compounds for their ability to reduce FATP-mediated fatty acid uptake in select cell models. One class of compounds was rationally designed and synthesized by our collaborators. The other compound was identified by a high-throughput screen for inhibitors of FATP4 and was chemically optimized for inhibition of fatty acid uptake. The rationally designed phospholipid-based compounds were not capable of reducing fatty acid uptake at reasonable concentrations in the cell models tested. The FATP4 inhibitor 4-aryl-3,4-dihydropyrimidin-2(1H)-one effectively reduced FATP1- and FATP4-mediated fatty acid uptake in cell models in which the transport proteins were exogenously expressed, but was unable to reduce fatty acid uptake in cell models with endogenous expression of FATPs.

We did not observe any inhibition of BODIPY-fatty acid uptake with the phospholipid-based compounds at concentrations ranging from 2 nM to 20 μM, nor did we observe a trend towards dose-dependent effects on fatty acid uptake. We did observe that at 20 μM, the compounds slightly increased BODIPY-fatty acid uptake in the FATP5-expressing cells and the intensity of this effect seemed dependent on the length of the ether bond connecting the phospholipid and fatty acid moieties, with the compounds containing the longer ether bonds showing a more robust increase in BODIPY-fatty acid uptake. In both the FATP5-expressing cells and the 3T3-L1 adipocytes, arachidic acid increased BODIPY-fatty acid uptake more than any of the compounds tested. As mentioned, we believe this is due to competition on albumin in the uptake solution. If arachidic acid outcompetes BODIPY-fatty acid for albumin binding sites, more free BODIPY-fatty acid would be in the aqueous solution, effectively increasing the local concentration of the BODIPY-fatty acid that the cells are exposed to. Indeed, in this study and in previous studies, we have observed that when we incubate cells with exogenous fatty acids at ten times the concentration of a labeled fatty acid, we see a spike in labeled fatty acid uptake[186]. It is only when we add exogenous fatty acids at 100 times the concentration of labeled fatty acid that we see a reduction in fatty acid uptake[34,186].

We did not test whether the phospholipid-based compounds were effective at concentrations higher than 20 μM. Small molecule inhibitors are more likely to interact with off-target proteins at concentrations higher than 10 μM[187]. High concentrations of the compounds may also begin to affect membrane fluidity or have other unspecific biological effects. We hypothesized that since the compounds were designed with a phospholipid moiety to target the compounds to the plasma membrane, we would theoretically enhance the local concentration of the compounds at the cell surface and therefore be able to dose cells with lower concentrations of the compounds than are necessary for exogenous free fatty acids to inhibit FATPs. However, this was not the case.

Different FATPs may prefer different substrates, and the substrate specificity of FATPs remains largely unknown[190]. FATP5, for example, is unique among the FATP family in being a bile-CoA ligase and utilizing bile acids as substrates[191,192]. For this reason, we wanted to test our phospholipid-based compounds on a variety of

cell lines expressing different FATPs. However, the compounds were not effective against cells expressing FATP1 and FATP4 or FATP5-expressing cells.

The exact mechanism of FATP-mediated fatty acid transport is not clear. FATPs have fatty acyl-CoA synthetase activity and can activate fatty acids into fatty acyl-CoA thioesters that can then be further metabolized or used within a cell. Some of this enzymatic activity may be driving overall fatty acid influx into cells[188]. It may be that the phospholipid-based compounds could not be utilized as substrates for FATP-mediated fatty acid activation. Stahl et al.[34] found that while long-chain and very-long chain fatty acids could compete for FATP4-mediated BODIPY-fatty acid uptake, esters of long-chain fatty acids and lipid-soluble vitamins and hormones did not, suggesting that they are not substrates for FATP4. Because we do not have the crystal structure for any of the FATPs, we do not know which part of a fatty acid a FATP binds to. The phospholipid compounds may not be able to access FATPs the way that endogenous fatty acids interact with the proteins.

4-aryl-3,4-dihydropyrimidin-2(1H)-one was identified using a high-throughput screen for small molecule inhibitors that selectively reduced FATP4-mediated BODIPY-fatty acid uptake and not FATP2- or FATP5-mediated uptake[184]. We verified that the compound was specific to FATP4-mediated uptake by testing its ability to reduce BODIPY-fatty acid uptake in HEK293 cells overexpressing FATP4, FATP5, or empty vector. Indeed, the compound inhibited FATP4-, but not FATP5-mediated BODIPY-fatty acid uptake.

While this compound was chosen for it's selectivity for FATP4, we wanted to test whether it could also inhibit FATP1-mediated uptake, since FATP1 shares 60.3% of its amino acid sequence with FATP4[188]. We found that, indeed, 4-aryl-3,4-dihydropyrimidin-2(1H)-one did inhibit FATP1-mediated BODIPY-fatty acid uptake in HEK293 cells overexpressing FATP1. We are the first to show that this type of compound is effective against FATP1 activity.

While 4-aryl-3,4-dihydropyrimidin-2(1H)-one was effective against FATP1 and FATP4 in the nanomolar range in cell lines overexpressing these transporters, we could not detect any inhibition of fatty acid uptake in 3T3-L1 adipocytes, isolated enterocytes, or isolated islets, all cell lines which express FATPs endogenously. It is unclear why the inhibitors are not effective against endogenous FATPs. FATP1 is expressed on the plasma membrane in 3T3-L1 adipocytes, especially in response to insulin treatment[13,16]. Stahl et al.[34] found that FATP4 localized to the plasma membrane in enterocytes, while Milger et al.[20] found that FATP4 localized to the ER. Overexpressing proteins in cell lines often results in accumulation of the protein in the ER. Perhaps the localization or orientation of the exogenously expressed FATPs differed from endogenous FATP localization or orientation and the compound could not access or interact with the endogenous protein.

Blackburn et al.[184], the group that originally identified the compound, found that the compound did not affect intestinal lipid levels in mice. They fed mice a high-fat diet and treated mice with 4-aryl-3,4-dihydropyrimidin-2(1H)-one. While they could detect the compound in circulation and within the small intestine, they did not find differences in intestinal lipid levels in mice treated with the compound versus mice treated with vehicle alone. Mice treated with Orlistat, a well-known inhibitor of fat absorption, had decreased fat absorption and reduced lipid levels in

the small intestine. So 4-aryl-3,4-dihydropyrimidin-2(1H)-one seems to be ineffective in vivo as well as in our cell models with endogenous expression of FATP1 and FATP4.

Another group utilized one of these dihydropyrimidinone-based compounds identified by Blackburn et al. to validate their high-throughput screen assay for FATP inhibitors[178]. They found that their dihydropyrimidinone-based compound did inhibit fatty acid uptake in 3T3-L1 adipocytes and isolated enterocytes. The IC_{50} of the compound in cells overexpressing FATP4 was .63 μM, while the IC50 was 3.6 μM in 3T3-L1 adipocytes and 21 μM in isolated enterocytes. So while the compound was effective in these cell models, it seemed to be less effective in cell lines with endogenously expressed FATPs and more effective in the FATP4-overexpressing cell line. It is unclear which dihydropyrimidinone-based compound this group used, as they do not provide the chemical structure.

In conclusion, the rationally designed phospholipid-based inhibitors did not inhibit FATP-mediated BODIPY-fatty acid uptake in the models we tested. Using fatty acids as part of the FATP inhibitor design may not work unless the compounds can be specifically targeted to FATPs, otherwise, the concentration of the compound required to reduce fatty acid uptake will be too high. 4-aryl-3,4-dihydropyrimidin-2(1H)-one can reduce FATP1- and FATP4-mediated fatty acid uptake in cells overexpressing these proteins, but it is not effective in cell models that endogenously express these proteins. Perhaps dihydropyrimidinone-based compounds can be further optimized to target endogenous FATPs. Developers of FATP inhibitors should consider that inhibitors of FATP1 might also inhibit FATP4 activity and vice versa. It is essential that investigations for FATP inhibitors continue, not only to find potential therapeutic drugs to treat metabolic diseases, but also to find biological tools for manipulating FATP expression in order to better understand this important family of proteins.

Methods

Animal experiments

All animal procedures were approved by the University of California Berkeley Animal Care and Use Committee. C57BL6/J mice and D1.FVB(Cg)-Tg(CAG-luc,-GFP)L2G85Chco/FathJ were purchased from the Jackson Laboratory (#000664 and #010548). All animal experiments were performed in 6- to 20-week-old male mice. Mice were given free access to water and rodent chow (Harlan Teklad #2018) and housed under standard conditions.

Cell culture

HEK293 cells (ATCC #CRL-1573) were maintained in DMEM supplemented with 10% fetal bovine serum and 1% penicillin-streptomyocin and incubated at 37°C with 5% CO_2. Cells expressing human FATP4 and FATP5 were previously generated in the lab[34,40].

Undifferentiated 3T3-L1 cells were maintained in DMEM supplemented with 10% fetal bovine serum and 1% penicillin-streptomyocin. To differentiate the cells, cells

were first grown to confluency. Two days later, the maintenance media was replaced with maintenance media plus 0.25 μM dexamethasone, 0.5 mM 3-isobutyl-1methylxanthine, and 1 μg/ml insulin. Four days after confluency, this media was replaced with maintenance media plus 1 μg/ml insulin. Six days after confluency, this media was again replaced with normal maintenance media. Cells were used in experiments eight to ten days after confluency.

MIN6 cells were maintained in DMEM with high glucose supplemented with 15% fetal bovine serum, 1% penicillin-streptomyocin, and 71.5 μM 2-mercaptoethanol. Mouse FATP1 was expressed in MIN6 cells via lentiviral infection.

Lentiviral expression of FATP1

The mouse FATP1 gene was cloned into the lentiviral vector pLJM1 (Addgene #19319). To make lentivirus, HEK293 cells were transfected with pLJM1-FATP1 or empty vector, and the lentiviral packaging vectors psPAX2 and pMD2.G according to Addgene's protocol. Two days later, the media containing lentivirus was obtained from the cells. MIN6 cells were plated in a 6-well plate in media containing 8 μg/ml polybrene and infected with 500 μl of lentivirus housing FATP1 or empty vector. After two days, 1 μg/ml puromyocin was added to the maintenance media to select for cells expressing the infected vector. Single cells were obtained by serial dilution to make clonal cell lines, and the clone expressing the highest level of FATP1 transcript was used in experiments.

Isolation of primary cells

Enterocytes from 2-month old male C57Bl6/J mice were isolated using a standard protocol[193]. Briefly, small intestines were washed in phosphate-buffered saline, then cut into 1 cm segments and stirred at room temperature for 30 minutes in Hank's buffered saline solution containing 0.1 M sucrose and 20 mM EDTA. Cells were strained through cheesecloth and a 100 μM cell strainer, then plated in RPMI 1640 supplemented with 10% fetal bovine serum and allowed to recover for 30 minutes before initiation of the assay.

Islets from mice expressing the L2G85 transgene luciferase were isolated by a standard protocol[173]. Briefly, the mice were euthanized and the pancreas was perfused with 3 ml of 0.8 mg/ml collagenase P (Roche Applied Science) in a washing buffer [10 mM HEPES, 10 μg Dnase I (Roche #10104159001), 1% penicillin-strepomyocin, 1.7 mM $CaCl_2$, and 1.2 mM $MgCl_2$ in Hank's buffered saline solution] via the bile duct. Then, the pancreas was digested at 37°C for 15 minutes. The digested pancreas was washed with washing buffer, strained through a tea strainer, and then subjected to density centrifugation in Histopaque (Sigma-Aldrich #11191). The layer containing the islets was moved to a 6-cm culture plate and the islets were handpicked for further culture. Islets were maintained in RPMI 1640 supplemented with 10% fetal bovine serum, 1% penicillin-streptomyocin, 25 mM HEPES, and 1% non-essential amino acids (Invitrogen #11140) and used within two days of isolation.

Compound solutions

The phospholipid-based compounds (custom synthesis), arachidic acid, and deoxycholic acid (Sigma-Aldrich #D2510) were dissolved in dimethyl sulfoxide (DMSO):ethanol 1:1 as a 2 mM stock solution. Compounds were then diluted into 0.1% bovine serum albumin to the desired concentration. 4-aryl-3,4-dihydropyrimidin-2(1H)-one (Intrace Medical, custom synthesis) was dissolved in DMSO to make a 12.5 mM stock. This stock was diluted into cell media or uptake solution to the desired concentration. Phloretin (Sigma-Aldrich #P7912) was diluted in deionized water to obtain a 200 mM stock.

XTT assay

The day before the assay, HEK293 cells expressing FATP5 were plated onto a 96-well plate with 20,000 cells per well. Cells were incubated with the indicated concentration of the phospholipid-based compounds in 100 µl of 0.1% bovine serum albumin in DMEM for 30 minutes. XTT solution was prepared immediately before the assay according to the manufacturer's protocol (Biotium #30007). 25 µl of XTT solution was added to each well. The cells were incubated with the XTT solution for four hours. The absorbance of the samples was measured using a plate reader spectrophotometer (SpectraMax i3, Molecular Devices). The absorbance in the wells with cells treated with the compounds was compared to the absorbance in the wells with cells treated with DMSO alone.

Quencher-based real-time BODIPY-fatty acid uptake assay

The assay was based on previously published assay[97]. Cells were plated in a 96-well plate with 30,000 cells per well a day before the assay. Cells were pre-incubated with the compound of interest for 30 minutes. Then, the media was replaced with uptake solution containing 1 mM trypan blue, 3.5 g/L glucose, 2 µM BODIPY-fatty acid (Molecular Probes #D3823), and 0.1% bovine serum albumin in Hank's balanced saline solution with the indicated concentration of compound. The cells were immediately placed into a SpectraMax i3 plate reader and the fluorescence was read at an excitation of 488 nm and emission of 515 nm every minute for two hours. The steady-state change in fluorescence over time was plotted.

BODIPY-fatty acid uptake assay by flow cytometry

The day before the assay, MIN6 cells were plated at 250,000 cells per well in a 6-well plate. Cells were pre-treated with the compound at the indicated concentration for 15 minutes. Cells were then incubated with uptake solution containing 2 µM BODIPY-fatty acid 0.1% bovine serum albumin, and the indicated concentration of the compound in Hank's balanced saline solution for one hour at 37°C. Cells were then trypsinized, washed in ice-cold buffer containing 0.2% bovine serum albumin, and sent through a flow cytometer (BD FACS Calibur). Cells were gated on forward and side scatter and the mean FL1 fluorescence was plotted.

Enterocytes were incubated in a 15 ml conical tube containing RPMI 1640 with the compound of interest or DMSO only at 37°C for 30 minutes. The cells were then

resuspended in uptake solution containing 2 μM BODIPY-fatty acid, 0.1% bovine serum albumin, and the indicated compound in RPMI 1640 and incubated for the indicated time. To stop the uptake assay, aliquots of the cells were resuspended in ice-cold 0.2% bovine serum albumin with propidium iodide to label dead cells. The cells were gated on forward and side scatter as well as for the absence of the FL3 signal from cells stained with propidium iodide. Mean FL1 fluorescence was plotted.

Luciferin-fatty acid uptake assay

Islets were seeded into a 96-well opaque plate, with 10 islets per well and incubated with the compound of interest at the indicated concentration in Hank's buffered saline solution for 15 minutes. The islets were then exposed to uptake solution containing 10 μM luciferin-fatty acid in 0.1% bovine serum albumin and placed in a SpectraMax i3 plate-reader to record luminescence in real-time. Steady-state values were reached within 30 minutes. At the end of the assay, 1 mM luciferin was added to the islets to quantify the amount of luciferase-expressing cells. Steady-state values were reached within 10 minutes. The steady-state relative luminescence values for the luciferin-fatty acid were adjusted for the steady-state relative luminescence values for luciferin.

Statistical analysis

Differences between two groups were determined using unpaired Student's *t* test. Linear regression analysis was used to determine the rate of change of values over time. Data are presented as mean values with error bars representing the standard error mean. Asterisks indicate significant differences (*$p < 0.05$, **$p < 0.005$, ***$p < 0.001$).

Supplemental Data

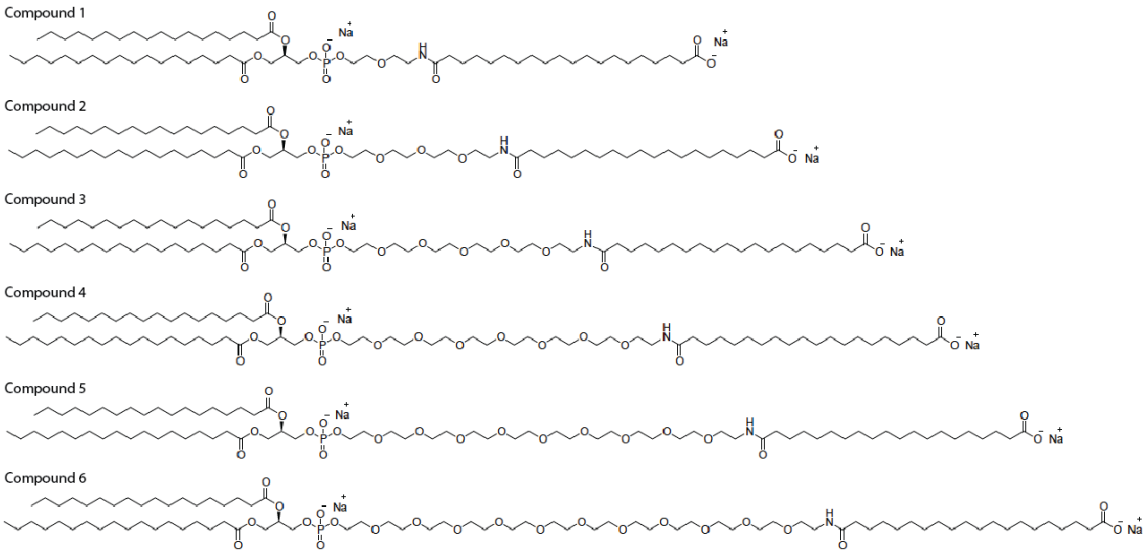

Supplementary figure 1. Chemical structures of phospholipid-based compounds.
Six different phospholipid-based compounds were synthesized, each with a different length ether bond between the phospholipid and fatty acid moieties.

Conclusion

Overall, our work contributes to the growing body of evidence that has established a role for FATPs in fatty acid transport in vivo and supports the notion that FATPs are implicated in the development of diet-related diseases. Specifically, we present a novel role for FATP6 in cardiac metabolism and function and FATP1 in pancreatic beta cell metabolism and function.

In Chapter 1, the creation of a FATP6 knockout mouse model that we used to study the physiological role of FATP6 was reported. We found that FATP6 mediated fatty acid uptake in vivo and was responsible for fatty acid availability in the heart. Deletion of FATP6 resulted in reduced cardiac lipid levels, cardiac dilation, reduced systolic function, and elevated rates of apoptosis in cardiomyocytes. This phenotype resembled dilated cardiomyopathy and was rescued by high-fat diet feeding. While the location and mechanism of FATP6 activity have not been fully defined, we hypothesize that lack of FATP6 expression leads to reduced cardiac fatty acid utilization, which in turn leads to reduced cardiac function. Future studies will need to clarify the link between FATP6 expression, cardiac fuel utilization, and cardiac function as well as explore the impact of FATP6 expression on other peripheral tissues.

In Chapter 2, our efforts to determine the role of FATP1 and FATP6 in the development of diabetic cardiomyopathy were described. Fatty acid transporters facilitate fatty acid uptake into the heart and are therefore likely involved in the development of diabetic cardiomyopathy. We used a combination of a high-fat diet and two low-dose streptozotocin injections to induce diabetes in wild-type and FATP1 and FATP6 knockout mice. While this protocol resulted in hyperglycemia, it did not result in diabetic cardiomyopathy. Without a strong heart phenotype in our diabetic mice, we were not able to detect significant differences in cardiac metabolism or function with loss of FATP activity. A more robust model of diabetic cardiomyopathy is needed in order to adequately evaluate the role of FATP1 and FATP6 in this condition.

In Chapter 3, a novel role for FATPs in the endocrine pancreas was presented. Excess import of saturated fatty acids into pancreatic beta cells leads to lipotoxicity and is thought to contribute to the development of diabetes. We found that FATPs are differentially expressed in the endocrine pancreas, with FATP1 localizing to beta cells, FATP3 to delta cells, and FATP4 to alpha cells. Loss-of-function of FATP1 protected beta cells from palmitate-induced lipotoxicity, despite the fact that islets from FATP1 knockout mice had normal levels of fatty acid uptake and palmitate-induced ER stress. Although the mechanism explaining this protection from lipotoxicity is not clear, it may be due to the fact that islets from FATP1 knockout mice accumulate neutral lipids differently than islets from wild-type mice. More work needs to be done in order to better understand FATP-mediated fatty acid uptake in beta cells and how this process affects the development of diabetes.

In Chapter 4, our attempts to characterize small molecule inhibitors of FATPs were portrayed. As membrane-bound proteins that can contribute to the

development of metabolic diseases, fatty acid transport proteins are enticing therapeutic targets. Some effort has been made towards finding small molecule inhibitors of FATPs, but many of the compounds have not been thoroughly tested or validated in vivo. We investigated the ability of two classes of potential FATP inhibitors to inhibit FATP activity in FATP-overexpressing cells and in cells that endogenously express FATPs. The first class of compounds, phospholipid-based inhibitors, did not reduce FATP-mediated fatty acid uptake at feasible concentrations. The second class of compound, a dihydropyrimidone-based inhibitor, effectively reduced FATP1- and FATP4-mediated fatty acid uptake in cell models overexpressing these proteins but did not affect endogenous FATP1 or FATP4 activity in other cell models. We still need to discover and verify FATP inhibitors that effectively reduce endogenous FATP activity and can be used in vivo.

Our work established roles for FATPs in the heart and in beta cells, but it also presented new questions and left many existing questions unanswered. In the heart, we found a novel function for FATP6 in mediating cardiac fatty acid uptake. The heart relies on fatty acids for the majority of its energy production[43–45] and dysregulated fatty acid utilization is pathophysiological, leading to cardiac inefficiency[47,50], diabetic cardiomyopathy[48], dilated cardiomyopathy[53], and heart failure[52,58]. FATP1 is also expressed in the heart and may mediate fatty acid uptake[41]. It is unclear how FATP1, FATP6, and other proteins involved in fatty acid metabolism coordinate in the heart to maintain normal fatty acid uptake rates. Because fatty acid transport is proposed as the rate-limiting step in fatty acid utilization in the heart[45,66], it is important to fully understand cardiac fatty acid uptake and further explore how we can target this process to treat metabolic diseases. It is especially pertinent to study FATPs in the context of diabetic cardiomyopathy due to the prevalence of diabetes[3] and the unequivocal role of fatty acid uptake in the development of this condition[38,39]. Unfortunately, we were not able to analyze the effects of FATP1 and FATP6 expression in the mouse model of diabetes that we employed.

In both the heart and in beta cells, we found that deletion of FATPs resulted in reduced intracellular lipid accumulation or a trend towards reduced intracellular lipid accumulation. In the heart, this was associated with reduced cardiac function, while in beta cells, reduced lipid stores in the basal state and elevated lipid stores in lipotoxic conditions were associated with enhanced cell viability. We do not know whether FATP activity targets fatty acids to specific metabolic fates within cells or how altering FATP activity changes the overall metabolic profile of cells. Future studies should address how gain- or loss-of-function of FATPs impacts specific lipid species within the cell. Formation of neutral lipids and beta-oxidation are important determinants of whether fatty acids have beneficial or detrimental effects within cells[8,144,149], so research should specifically address how FATPs affect triglyceride formation and fuel utilization in metabolic tissues.

We reported FATP expression in multiple tissues that we have yet to study further. We discovered FATP6 expression in mouse testes, lung, and placenta, FATP3 expression in pancreatic delta cells, and FATP4 expression in pancreatic alpha cells. We still need to delineate how FATP activity affects fatty acid metabolism in these tissues as well as how that activity affects overall physiology.

Another tissue that warrants further investigation is the endothelium. The endothelium is responsible for systemic fatty acid availability and we do not fully understand how fatty acids are transported across it and how peripheral tissues regulate that process. Only one other group has reported on FATP activity in the endothelium[91] and based on our findings in FATP6 knockout mice, we hypothesize that FATP6 may be involved in in this process.

Targeting FATPs remains an attractive therapeutic strategy to treat diet-related diseases. To adequately assess the potential of FATPs as therapeutic targets, several advances still need to be made. First, we need a better understanding of the balance between excess fatty acids and insufficient fatty acids in metabolic tissues. In the heart, lack of FATP6 activity lead to reduced cardiac function, while in the pancreas, lack of FATP1 activity protected beta cells from lipotoxicity. Does each tissue require a specific amount of fatty acid flux to function properly? If so, what is that amount and how does manipulating FATP activity affect this balance? We also need to determine how obesity and existing metabolic diseases like diabetes and cardiovascular disease affect intracellular lipids levels. Secondly, to sufficiently evaluate FATPs as therapeutic targets, we need better mouse models of metabolic diseases. Mice are resistant to many diet-related diseases like diabetes and heart disease and so we rely on genetic models to emulate human conditions. These models often do not perfectly represent the metabolic environment of the human disease. For example, inducing diabetes in mice with a high-fat diet and two low-dose STZ injections did not produce diabetic cardiomyopathy, so we could not assess the role of FATPs in the development of this condition using this model. We could more effectively evaluate the potential for FATPs as therapeutic targets in contexts that better mimic human biology. Finally, we need to make progress in specifically and effectively targeting FATP activity. We still do not have a small molecule inhibitor for FATPs that reduces fatty acid uptake in vivo. Also, compounds may broadly reduce fatty acid transport or distinctly affect the activities of different FATPs. Ideally, we will find specific inhibitors for each FATP that do not produce off-target effects on fatty acid metabolism in other tissues.

In summary, this work demonstrates that FATP1 and FATP6 mediate fatty acid uptake in vivo. It also unveils novel roles for these proteins in cardiac function and beta cell viability. There are still many unanswered questions regarding how FATP activity affects physiology and disease. These proteins are important determinants of intracellular metabolism, are clearly implicated in the development of diet-related diseases, and are therefore promising therapeutic targets for some of our country's most pressing health concerns.

References

1. Centers for Disease Control and Prevention (CDC) & National Center for Health Statistics (NCHS). National Health and Nutrition Examination Survey Data. (2009).
2. Centers for Disease Control and Prevention (CDC). Heart disease fact sheet. (2013).
3. Centers for Disease Control and Prevention (CDC). National diabetes fact sheet: national estimates and general information on diabetes and prediabetes in the United States. (2011).
4. Anderson, C. M. & Stahl, A. SLC27 fatty acid transport proteins. *Mol. Aspects Med.* **34,** 516–528 (2013).
5. Schäffler, A. & Schölmerich, J. Innate immunity and adipose tissue biology. *Trends Immunol.* **31,** 228–235 (2010).
6. Boden, G. & Shulman, G. I. Free fatty acids in obesity and type 2 diabetes: defining their role in the development of insulin resistance and β-cell dysfunction. *Eur. J. Clin. Invest.* **32,** 14–23 (2002).
7. Leamy, A. K., Egnatchik, R. A. & Young, J. D. Molecular mechanisms and the role of saturated fatty acids in the progression of non-alcoholic fatty liver disease. *Prog. Lipid Res.* **52,** 165–174 (2013).
8. Drosatos, K. & Schulze, P. C. Cardiac Lipotoxicity: Molecular Pathways and Therapeutic Implications. *Curr. Heart Fail. Rep.* **10,** 109–121 (2013).
9. Schwenk, R. W., Holloway, G. P., Luiken, J. J. F. P., Bonen, A. & Glatz, J. F. C. Fatty acid transport across the cell membrane: Regulation by fatty acid transporters. *Prostaglandins Leukot. Essent. Fat. Acids PLEFA* **82,** 149–154 (2010).
10. Black, P. N., Sandoval, A., Arias-Barrau, E. & DiRusso, C. C. Targeting the fatty acid transport proteins (FATP) to understand the mechanisms linking fatty acid transport to metabolism. *Immunol. Endocr. Metab. Agents Med. Chem.* **9,** 11–17 (2009).

11. Coburn, C. T. *et al.* Defective Uptake and Utilization of Long Chain Fatty Acids in Muscle and Adipose Tissues of CD36 Knockout Mice. *J. Biol. Chem.* **275,** 32523–32529 (2000).
12. Huang, H., Starodub, O., McIntosh, A., Kier, A. B. & Schroeder, F. Liver Fatty Acid-binding Protein Targets Fatty Acids to the Nucleus REAL TIME CONFOCAL AND MULTIPHOTON FLUORESCENCE IMAGING IN LIVING CELLS. *J. Biol. Chem.* **277,** 29139–29151 (2002).
13. Schaffer, J. E. & Lodish, H. F. Expression cloning and characterization of a novel adipocyte long chain fatty acid transport protein. *Cell* **79,** 427–436 (1994).
14. Lewis, S. E., Listenberger, L. L., Ory, D. S. & Schaffer, J. E. Membrane Topology of the Murine Fatty Acid Transport Protein 1. *J. Biol. Chem.* **276,** 37042–37050 (2001).
15. DiRusso, C. C. *et al.* Comparative Biochemical Studies of the Murine Fatty Acid Transport Proteins (FATP) Expressed in Yeast. *J. Biol. Chem.* **280,** 16829–16837 (2005).
16. Stahl, A., Evans, J. G., Pattel, S., Hirsch, D. & Lodish, H. F. Insulin Causes Fatty Acid Transport Protein Translocation and Enhanced Fatty Acid Uptake in Adipocytes. *Dev. Cell* **2,** 477–488 (2002).
17. Kim, J. K. *et al.* Inactivation of fatty acid transport protein 1 prevents fat-induced insulin resistance in skeletal muscle. *J. Clin. Invest.* **113,** 756–763 (2004).
18. Falcon, A. *et al.* FATP2 is a hepatic fatty acid transporter and peroxisomal very long-chain acyl-CoA synthetase. *Am. J. Physiol. Endocrinol. Metab.* **299,** E384–393 (2010).
19. Doege, H. *et al.* Silencing of Hepatic Fatty Acid Transporter Protein 5 in Vivo Reverses Diet-induced Non-alcoholic Fatty Liver Disease and Improves Hyperglycemia. *J. Biol. Chem.* **283,** 22186–22192 (2008).
20. Milger, K. *et al.* Cellular uptake of fatty acids driven by the ER-localized acyl-CoA synthetase FATP4. *J Cell Sci* **119,** 4678–4688 (2006).
21. Wu, Q. *et al.* FATP1 is an insulin-sensitive fatty acid transporter involved in diet-induced obesity. *Mol. Cell. Biol.* **26,** 3455–3467 (2006).

22. Jain, S. S. *et al.* Additive effects of insulin and muscle contraction on fatty acid transport and fatty acid transporters, FAT/CD36, FABPpm, FATP1, 4 and 6. *FEBS Lett.* **583,** 2294–2300 (2009).
23. Hui, T. Y., Frohnert, B. I., Smith, A. J., Schaffer, J. E. & Bernlohr, D. A. Characterization of the Murine Fatty Acid Transport Protein Gene and Its Insulin Response Sequence. *J. Biol. Chem.* **273,** 27420–27429 (1998).
24. Man, M. Z., Hui, T. Y., Schaffer, J. E., Lodish, H. F. & Bernlohr, D. A. Regulation of the murine adipocyte fatty acid transporter gene by insulin. *Mol. Endocrinol. Baltim. Md* **10,** 1021–1028 (1996).
25. Frohnert, B. I., Hui, T. Y. & Bernlohr, D. A. Identification of a Functional Peroxisome Proliferator-responsive Element in the Murine Fatty Acid Transport Protein Gene. *J. Biol. Chem.* **274,** 3970–3977 (1999).
26. Coe, N. R., Smith, A. J., Frohnert, B. I., Watkins, P. A. & Bernlohr, D. A. The Fatty Acid Transport Protein (FATP1) Is a Very Long Chain Acyl-CoA Synthetase. *J. Biol. Chem.* **274,** 36300–36304 (1999).
27. Black, P. N. & DiRusso, C. C. Yeast acyl-CoA synthetases at the crossroads of fatty acid metabolism and regulation. *Biochim. Biophys. Acta BBA - Mol. Cell Biol. Lipids* **1771,** 286–298 (2007).
28. DiRusso, C. C., Darwis, D., Obermeyer, T. & Black, P. N. Functional domains of the fatty acid transport proteins: studies using protein chimeras. *Biochim. Biophys. Acta* **1781,** 135–143 (2008).
29. Richards, M. R. *et al.* Oligomerization of the Murine Fatty Acid Transport Protein 1. *J. Biol. Chem.* **278,** 10477–10483 (2003).
30. Richards, M. R., Harp, J. D., Ory, D. S. & Schaffer, J. E. Fatty acid transport protein 1 and long-chain acyl coenzyme A synthetase 1 interact in adipocytes. *J. Lipid Res.* **47,** 665–672 (2006).
31. Steinberg, S. J., Wang, S. J., Kim, D. G., Mihalik, S. J. & Watkins, P. A. Human very-long-chain acyl-CoA synthetase: cloning, topography, and relevance to branched-chain fatty acid metabolism. *Biochem. Biophys. Res. Commun.* **257,** 615–621 (1999).

32. Doege, H. *et al.* Targeted deletion of FATP5 reveals multiple functions in liver metabolism: alterations in hepatic lipid homeostasis. *Gastroenterology* **130,** 1245–1258 (2006).
33. Pei, Z. *et al.* Mouse very long-chain Acyl-CoA synthetase 3/fatty acid transport protein 3 catalyzes fatty acid activation but not fatty acid transport in MA-10 cells. *J Biol Chem* **279,** 54454–62 (2004).
34. Stahl, A. *et al.* Identification of the Major Intestinal Fatty Acid Transport Protein. *Mol. Cell* **4,** 299–308 (1999).
35. Gimeno, R. E. *et al.* Characterization of a heart-specific fatty acid transport protein. *J Biol Chem* **278,** 16039–44 (2003).
36. Wu, Q. *et al.* Fatty Acid Transport Protein 1 Is Required for Nonshivering Thermogenesis in Brown Adipose Tissue. *Diabetes* **55,** 3229–3237 (2006).
37. Herrmann, T. *et al.* Mice with targeted disruption of the fatty acid transport protein 4 (Fatp 4, Slc27a4) gene show features of lethal restrictive dermopathy. *J. Cell Biol.* **161,** 1105–1115 (2003).
38. Buchanan, J. *et al.* Reduced cardiac efficiency and altered substrate metabolism precedes the onset of hyperglycemia and contractile dysfunction in two mouse models of insulin resistance and obesity. *Endocrinology* **146,** 5341–5349 (2005).
39. Bayeva, M., Sawicki, K. T. & Ardehali, H. Taking diabetes to heart--deregulation of myocardial lipid metabolism in diabetic cardiomyopathy. *J. Am. Heart Assoc.* **2,** e000433 (2013).
40. Nie, B. *et al.* Specific bile acids inhibit hepatic fatty acid uptake in mice. *Hepatology* **56,** 1300–1310 (2012).
41. Chiu, H.-C. *et al.* Transgenic Expression of Fatty Acid Transport Protein 1 in the Heart Causes Lipotoxic Cardiomyopathy. *Circ. Res.* **96,** 225–233 (2005).
42. Auinger, A. *et al.* A variant in the heart-specific fatty acid transport protein 6 is associated with lower fasting and postprandial TAG, blood pressure and left ventricular hypertrophy. *Br. J. Nutr.* **107,** 1422–1428 (2012).
43. Bing, R. J. Myocardial metabolism. *Circulation* **12,** 635–647 (1955).

44. Opie, L. H. Metabolism of the heart in health and disease. I. *Am. Heart J.* **76,** 685–698 (1968).
45. Neely, J. R., Rovetto, M. J. & Oram, J. F. Myocardial utilization of carbohydrate and lipids. *Prog. Cardiovasc. Dis.* **15,** 289–329 (1972).
46. Ashrafian, H., Frenneaux, M. P. & Opie, L. H. Metabolic mechanisms in heart failure. *Circulation* **116,** 434–448 (2007).
47. Lopaschuk, G. D., Ussher, J. R., Folmes, C. D. L., Jaswal, J. S. & Stanley, W. C. Myocardial fatty acid metabolism in health and disease. *Physiol. Rev.* **90,** 207–258 (2010).
48. Chabowski, A., Gorski, J., Glatz, J. F., JJ, P. L. & Bonen, A. Protein-mediated Fatty Acid Uptake in the Heart. *Curr Cardiol Rev* **4,** 12–21 (2008).
49. Wilson, C. R., Tran, M. K., Salazar, K. L., Young, M. E. & Taegtmeyer, H. Western diet, but not high fat diet, causes derangements of fatty acid metabolism and contractile dysfunction in the heart of Wistar rats. *Biochem. J.* **406,** 457–467 (2007).
50. Peterson, L. R. *et al.* Effect of obesity and insulin resistance on myocardial substrate metabolism and efficiency in young women. *Circulation* **109,** 2191–2196 (2004).
51. Sack, M. N. & Kelly, D. P. The energy substrate switch during development of heart failure: gene regulatory mechanisms (Review). *Int. J. Mol. Med.* **1,** 17–24 (1998).
52. Bishop, S. P. & Altschuld, R. A. Increased glycolytic metabolism in cardiac hypertrophy and congestive failure. *Am. J. Physiol.* **218,** 153–159 (1970).
53. Sanbe, A. Dilated cardiomyopathy: a disease of the myocardium. *Biol. Pharm. Bull.* **36,** 18–22 (2013).
54. van der Vusse, G. J., Glatz, J. F., Stam, H. C. & Reneman, R. S. Fatty acid homeostasis in the normoxic and ischemic heart. *Physiol. Rev.* **72,** 881–940 (1992).
55. Liedtke, A. J. Alterations of carbohydrate and lipid metabolism in the acutely ischemic heart. *Prog. Cardiovasc. Dis.* **23,** 321–336 (1981).

56. Christe, M. E. & Rodgers, R. L. Altered glucose and fatty acid oxidation in hearts of the spontaneously hypertensive rat. *J. Mol. Cell. Cardiol.* **26,** 1371–1375 (1994).
57. Taegtmeyer, H. & Overturf, M. L. Effects of moderate hypertension on cardiac function and metabolism in the rabbit. *Hypertens. Dallas Tex 1979* **11,** 416–426 (1988).
58. Wittels, B. & Spann, J. F. Defective lipid metabolism in the failing heart. *J. Clin. Invest.* **47,** 1787–1794 (1968).
59. Binas, B., Danneberg, H., McWhir, J., Mullins, L. & Clark, A. J. Requirement for the heart-type fatty acid binding protein in cardiac fatty acid utilization. *FASEB J. Off. Publ. Fed. Am. Soc. Exp. Biol.* **13,** 805–812 (1999).
60. Irie, H. *et al.* Myocardial recovery from ischemia is impaired in CD36-null mice and restored by myocyte CD36 expression or medium-chain fatty acids. *Proc. Natl. Acad. Sci. U. S. A.* **100,** 6819–6824 (2003).
61. Augustus, A. S. *et al.* Loss of lipoprotein lipase-derived fatty acids leads to increased cardiac glucose metabolism and heart dysfunction. *J. Biol. Chem.* **281,** 8716–8723 (2006).
62. Georgiadi, A. *et al.* Induction of cardiac Angptl4 by dietary fatty acids is mediated by peroxisome proliferator-activated receptor beta/delta and protects against fatty acid-induced oxidative stress. *Circ. Res.* **106,** 1712–1721 (2010).
63. Finck, B. N. *et al.* The cardiac phenotype induced by PPARalpha overexpression mimics that caused by diabetes mellitus. *J. Clin. Invest.* **109,** 121–130 (2002).
64. Yang, J. *et al.* CD36 deficiency rescues lipotoxic cardiomyopathy. *Circ. Res.* **100,** 1208–1217 (2007).
65. Chiu, H. C. *et al.* A novel mouse model of lipotoxic cardiomyopathy. *J. Clin. Invest.* **107,** 813–822 (2001).
66. Glatz, J. F. C. & Luiken, J. J. F. P. in *Cardiac Energy Metabolism in Health and Disease* (eds. Lopaschuk, G. D. & Dhalla, N. S.) 49–67 (Springer New York, 2014).
67. Stremmel, W. Fatty acid uptake by isolated rat heart myocytes represents a carrier-mediated transport process. *J. Clin. Invest.* **81,** 844–852 (1988).

68. Sorrentino, D., Robinson, R. B., Kiang, C. L. & Berk, P. D. At physiologic albumin/oleate concentrations oleate uptake by isolated hepatocytes, cardiac myocytes, and adipocytes is a saturable function of the unbound oleate concentration. Uptake kinetics are consistent with the conventional theory. *J. Clin. Invest.* **84,** 1325–1333 (1989).
69. Luiken, J. J., van Nieuwenhoven, F. A., America, G., van der Vusse, G. J. & Glatz, J. F. Uptake and metabolism of palmitate by isolated cardiac myocytes from adult rats: involvement of sarcolemmal proteins. *J. Lipid Res.* **38,** 745–758 (1997).
70. van der Vusse, G. J., van Bilsen, M. & Glatz, J. F. Cardiac fatty acid uptake and transport in health and disease. *Cardiovasc. Res.* **45,** 279–293 (2000).
71. Kuang, M., Febbraio, M., Wagg, C., Lopaschuk, G. D. & Dyck, J. R. B. Fatty acid translocase/CD36 deficiency does not energetically or functionally compromise hearts before or after ischemia. *Circulation* **109,** 1550–1557 (2004).
72. Finck, B. N. The PPAR regulatory system in cardiac physiology and disease. *Cardiovasc. Res.* **73,** 269–277 (2007).
73. Park, S.-Y. *et al.* Cardiac-specific overexpression of peroxisome proliferator-activated receptor-alpha causes insulin resistance in heart and liver. *Diabetes* **54,** 2514–2524 (2005).
74. Moran, C. M., Thomson, A. J. W., Rog-Zielinska, E. & Gray, G. A. High-resolution echocardiography in the assessment of cardiac physiology and disease in preclinical models. *Exp. Physiol.* **98,** 629–644 (2013).
75. Stypmann, J. *et al.* Echocardiographic assessment of global left ventricular function in mice. *Lab. Anim.* **43,** 127–137 (2009).
76. Ram, R., Mickelsen, D. M., Theodoropoulos, C. & Blaxall, B. C. New approaches in small animal echocardiography: imaging the sounds of silence. *Am. J. Physiol. Heart Circ. Physiol.* **301,** H1765–1780 (2011).
77. Yang, X. P. *et al.* Echocardiographic assessment of cardiac function in conscious and anesthetized mice. *Am. J. Physiol.* **277,** H1967–1974 (1999).
78. Wencker, D. *et al.* A mechanistic role for cardiac myocyte apoptosis in heart failure. *J. Clin. Invest.* **111,** 1497–1504 (2003).

79. Augustus, A. *et al.* Cardiac-specific Knock-out of Lipoprotein Lipase Alters Plasma Lipoprotein Triglyceride Metabolism and Cardiac Gene Expression. *J. Biol. Chem.* **279,** 25050–25057 (2004).
80. Fukuchi, K. *et al.* Enhanced myocardial glucose use in patients with a deficiency in long-chain fatty acid transport (CD36 deficiency). *J. Nucl. Med. Off. Publ. Soc. Nucl. Med.* **40,** 239–243 (1999).
81. Tanaka, T., Sohmiya, K. & Kawamura, K. Is CD36 Deficiency an Etiology of Hereditary Hypertrophic Cardiomyopathy? *J. Mol. Cell. Cardiol.* **29,** 121–127 (1997).
82. Nakamura, T. *et al.* CD36 deficiency has little influence on the pathophysiology of hypertrophic cardiomyopathy. *J. Mol. Cell. Cardiol.* **31,** 1253–1259 (1999).
83. Guertl, B., Noehammer, C. & Hoefler, G. Metabolic cardiomyopathies. *Int. J. Exp. Pathol.* **81,** 349–372 (2000).
84. Strauss, A. W. *et al.* Molecular basis of human mitochondrial very-long-chain acyl-CoA dehydrogenase deficiency causing cardiomyopathy and sudden death in childhood. *Proc. Natl. Acad. Sci. U. S. A.* **92,** 10496–10500 (1995).
85. Leslie, N. D., Valencia, C. A., Strauss, A. W., Connor, J. A. & Zhang, K. in *GeneReviews(®)* (eds. Pagon, R. A. et al.) (University of Washington, Seattle, 1993).
86. Wang, P., Lloyd, S. G., Zeng, H., Bonen, A. & Chatham, J. C. Impact of altered substrate utilization on cardiac function in isolated hearts from Zucker diabetic fatty rats. *Am. J. Physiol. Heart Circ. Physiol.* **288,** H2102–2110 (2005).
87. Carley, A. N. *et al.* Mechanisms responsible for enhanced fatty acid utilization by perfused hearts from type 2 diabetic db/db mice. *Arch. Physiol. Biochem.* **113,** 65–75 (2007).
88. Bonen, A. *et al.* A null mutation in skeletal muscle FAT/CD36 reveals its essential role in insulin- and AICAR-stimulated fatty acid metabolism. *Am. J. Physiol. Endocrinol. Metab.* **292,** E1740–1749 (2007).
89. Luiken, J. J. F. P. *et al.* Etomoxir-induced partial carnitine palmitoyltransferase-I (CPT-I) inhibition in vivo does not alter cardiac long-chain fatty acid uptake and oxidation rates. *Biochem. J.* **419,** 447–455 (2009).

90. Yagyu, H. *et al.* Lipoprotein lipase (LpL) on the surface of cardiomyocytes increases lipid uptake and produces a cardiomyopathy. *J. Clin. Invest.* **111,** 419–426 (2003).
91. Hagberg, C. E. *et al.* Vascular endothelial growth factor B controls endothelial fatty acid uptake. *Nature* **464,** 917–21 (2010).
92. Expression summary for Slc27a6 - Mus musculus < Expression Atlas < EMBL-EBI. Available at: http://www.ebi.ac.uk/gxa/genes/ENSMUSG00000024600?bs=%7B%22mus%20musculus%22%3A%5B%22ORGANISM_PART%22%5D%7D&ds=%7B%22kingdom%22%3A%5B%22animals%22%5D%7D#baseline. (Accessed: 4th October 2016)
93. Experiment < EMBL-EBI. Available at: http://www.ebi.ac.uk/gxa/experiments/E-MTAB-513?_specific=on&queryFactorType=ORGANISM_PART&queryFactorValues=&geneQuery=slc27a6&exactMatch=true. (Accessed: 4th October 2016)
94. Tissue expression of SLC27A6 - Summary - The Human Protein Atlas. Available at: http://www.proteinatlas.org/ENSG00000113396-SLC27A6/tissue. (Accessed: 4th October 2016)
95. Human Proteome Map. Available at: http://www.humanproteomemap.org/batch.php. (Accessed: 4th October 2016)
96. Ehler, E., Moore-Morris, T. & Lange, S. Isolation and culture of neonatal mouse cardiomyocytes. *J. Vis. Exp. JoVE* (2013). doi:10.3791/50154
97. Liao, J., Sportsman, R., Harris, J. & Stahl, A. Real-time quantification of fatty acid uptake using a novel fluorescence assay. *J. Lipid Res.* **46,** 597–602 (2005).
98. Isfort, M., Stevens, S. C. W., Schaffer, S., Jong, C. J. & Wold, L. E. Metabolic dysfunction in diabetic cardiomyopathy. *Heart Fail. Rev.* **19,** 35–48 (2014).
99. Bugger, H. & Abel, E. D. Molecular mechanisms of diabetic cardiomyopathy. *Diabetologia* **57,** 660–671 (2014).
100. Kannel, W. B., Hjortland, M. & Castelli, W. P. Role of diabetes in congestive heart failure: the Framingham study. *Am. J. Cardiol.* **34,** 29–34 (1974).

101. Dandamudi, S. *et al.* The prevalence of diabetic cardiomyopathy: a population-based study in Olmsted County, Minnesota. *J. Card. Fail.* **20,** 304–309 (2014).
102. Rubler, S. *et al.* New type of cardiomyopathy associated with diabetic glomerulosclerosis. *Am. J. Cardiol.* **30,** 595–602 (1972).
103. Bando, Y. K. & Murohara, T. Diabetes-related heart failure. *Circ. J. Off. J. Jpn. Circ. Soc.* **78,** 576–583 (2014).
104. Devereux, R. B. *et al.* Impact of diabetes on cardiac structure and function: the strong heart study. *Circulation* **101,** 2271–2276 (2000).
105. Kannel, W. B. & McGee, D. L. Diabetes and cardiovascular disease. The Framingham study. *JAMA* **241,** 2035–2038 (1979).
106. Lee, M. *et al.* Diabetes mellitus and echocardiographic left ventricular function in free-living elderly men and women: The Cardiovascular Health Study. *Am. Heart J.* **133,** 36–43 (1997).
107. Boyer, J. K., Thanigaraj, S., Schechtman, K. B. & Pérez, J. E. Prevalence of ventricular diastolic dysfunction in asymptomatic, normotensive patients with diabetes mellitus. *Am. J. Cardiol.* **93,** 870–875 (2004).
108. Shivalkar, B. *et al.* Flow mediated dilatation and cardiac function in type 1 diabetes mellitus. *Am. J. Cardiol.* **97,** 77–82 (2006).
109. Fang, Z. Y. *et al.* Screening for heart disease in diabetic subjects. *Am. Heart J.* **149,** 349–354 (2005).
110. Hällsten, K. *et al.* Enhancement of insulin-stimulated myocardial glucose uptake in patients with Type 2 diabetes treated with rosiglitazone. *Diabet. Med. J. Br. Diabet. Assoc.* **21,** 1280–1287 (2004).
111. Herrero, P. *et al.* Increased myocardial fatty acid metabolism in patients with type 1 diabetes mellitus. *J. Am. Coll. Cardiol.* **47,** 598–604 (2006).
112. Herrero, P. *et al.* PET detection of the impact of dobutamine on myocardial glucose metabolism in women with type 1 diabetes mellitus. *J. Nucl. Cardiol. Off. Publ. Am. Soc. Nucl. Cardiol.* **15,** 791–799 (2008).
113. Avogaro, A. *et al.* Myocardial metabolism in insulin-deficient diabetic humans without coronary artery disease. *Am. J. Physiol.* **258,** E606–618 (1990).

114. Gertz, E. W., Wisneski, J. A., Stanley, W. C. & Neese, R. A. Myocardial substrate utilization during exercise in humans. Dual carbon-labeled carbohydrate isotope experiments. *J. Clin. Invest.* **82,** 2017–2025 (1988).
115. Goodwin, G. W., Taylor, C. S. & Taegtmeyer, H. Regulation of energy metabolism of the heart during acute increase in heart work. *J. Biol. Chem.* **273,** 29530–29539 (1998).
116. Taegtmeyer, H., McNulty, P. & Young, M. E. Adaptation and maladaptation of the heart in diabetes: Part I: general concepts. *Circulation* **105,** 1727–1733 (2002).
117. Garvey, W. T., Hardin, D., Juhaszova, M. & Dominguez, J. H. Effects of diabetes on myocardial glucose transport system in rats: implications for diabetic cardiomyopathy. *Am. J. Physiol.* **264,** H837–844 (1993).
118. Belke, D. D., Larsen, T. S., Gibbs, E. M. & Severson, D. L. Altered metabolism causes cardiac dysfunction in perfused hearts from diabetic (db/db) mice. *Am. J. Physiol. Endocrinol. Metab.* **279,** E1104–1113 (2000).
119. Gibbs, E. M. *et al.* Glycemic improvement in diabetic db/db mice by overexpression of the human insulin-regulatable glucose transporter (GLUT4). *J. Clin. Invest.* **95,** 1512–1518 (1995).
120. Wright, J. J. *et al.* Mechanisms for increased myocardial fatty acid utilization following short-term high-fat feeding. *Cardiovasc. Res.* **82,** 351–360 (2009).
121. McGavock, J. M. *et al.* Cardiac steatosis in diabetes mellitus: a 1H-magnetic resonance spectroscopy study. *Circulation* **116,** 1170–1175 (2007).
122. Sharma, S. *et al.* Intramyocardial lipid accumulation in the failing human heart resembles the lipotoxic rat heart. *FASEB J. Off. Publ. Fed. Am. Soc. Exp. Biol.* **18,** 1692–1700 (2004).
123. Kenno, K. A. & Severson, D. L. Lipolysis in isolated myocardial cells from diabetic rat hearts. *Am. J. Physiol.* **249,** H1024–1030 (1985).
124. Paulson, D. J. & Crass, M. F. Endogenous triacylglycerol metabolism in diabetic heart. *Am. J. Physiol.* **242,** H1084–1094 (1982).
125. Zhou, Y. T. *et al.* Lipotoxic heart disease in obese rats: implications for human obesity. *Proc. Natl. Acad. Sci. U. S. A.* **97,** 1784–1789 (2000).

126. Rijzewijk, L. J. *et al.* Myocardial steatosis is an independent predictor of diastolic dysfunction in type 2 diabetes mellitus. *J. Am. Coll. Cardiol.* **52,** 1793–1799 (2008).
127. Young, M. E. *et al.* Impaired long-chain fatty acid oxidation and contractile dysfunction in the obese Zucker rat heart. *Diabetes* **51,** 2587–2595 (2002).
128. Kienesberger, P. C. *et al.* Myocardial ATGL overexpression decreases the reliance on fatty acid oxidation and protects against pressure overload-induced cardiac dysfunction. *Mol. Cell. Biol.* **32,** 740–750 (2012).
129. Nielsen, L. B., Bartels, E. D. & Bollano, E. Overexpression of apolipoprotein B in the heart impedes cardiac triglyceride accumulation and development of cardiac dysfunction in diabetic mice. *J. Biol. Chem.* **277,** 27014–27020 (2002).
130. Mazumder, P. K. *et al.* Impaired cardiac efficiency and increased fatty acid oxidation in insulin-resistant ob/ob mouse hearts. *Diabetes* **53,** 2366–2374 (2004).
131. Sambandam, N. *et al.* Metabolism of VLDL is increased in streptozotocin-induced diabetic rat hearts. *Am. J. Physiol. Heart Circ. Physiol.* **278,** H1874–1882 (2000).
132. Coort, S. L. M. *et al.* Enhanced sarcolemmal FAT/CD36 content and triacylglycerol storage in cardiac myocytes from obese zucker rats. *Diabetes* **53,** 1655–1663 (2004).
133. Luiken, J. J. F. P. *et al.* Changes in fatty acid transport and transporters are related to the severity of insulin deficiency. *Am. J. Physiol. Endocrinol. Metab.* **283,** E612–621 (2002).
134. Reed, M. J. *et al.* A new rat model of type 2 diabetes: the fat-fed, streptozotocin-treated rat. *Metabolism.* **49,** 1390–1394 (2000).
135. Ventura-Sobrevilla, J. *et al.* Effect of varying dose and administration of streptozotocin on blood sugar in male CD1 mice. *Proc. West. Pharmacol. Soc.* **54,** 5–9 (2011).
136. Bugger, H. & Abel, E. D. Rodent models of diabetic cardiomyopathy. *Dis. Model. Mech.* **2,** 454–466 (2009).

137. Chen, D. & Wang, M.-W. Development and application of rodent models for type 2 diabetes. *Diabetes Obes. Metab.* **7,** 307–317 (2005).
138. Koonen, D. P. Y. *et al.* CD36 expression contributes to age-induced cardiomyopathy in mice. *Circulation* **116,** 2139–2147 (2007).
139. Kim, J. K. *et al.* Inactivation of fatty acid transport protein 1 prevents fat-induced insulin resistance in skeletal muscle. *J. Clin. Invest.* **113,** 756–763 (2004).
140. Malaisse, W. J. & Malaisse-Lagae, F. Stimulation of insulin secretion by noncarbohydrate metabolites. *J Lab Clin Med* **72,** 438–48 (1968).
141. Zhou, Y. P. & Grill, V. E. Long-term exposure of rat pancreatic islets to fatty acids inhibits glucose-induced insulin secretion and biosynthesis through a glucose fatty acid cycle. *J Clin Invest* **93,** 870–6 (1994).
142. Shimabukuro, M., Zhou, Y. T., Levi, M. & Unger, R. H. Fatty acid-induced beta cell apoptosis: a link between obesity and diabetes. *Proc Natl Acad Sci U A* **95,** 2498–502 (1998).
143. Itoh, Y. *et al.* Free fatty acids regulate insulin secretion from pancreatic beta cells through GPR40. *Nature* **422,** 173–6 (2003).
144. El-Assaad, W. *et al.* Saturated fatty acids synergize with elevated glucose to cause pancreatic beta-cell death. *Endocrinology* **144,** 4154–63 (2003).
145. Butler, A. E. *et al.* Beta-cell deficit and increased beta-cell apoptosis in humans with type 2 diabetes. *Diabetes* **52,** 102–10 (2003).
146. Hirata, T. *et al.* Palmitic acid-rich diet suppresses glucose-stimulated insulin secretion (GSIS) and induces endoplasmic reticulum (ER) stress in pancreatic islets in mice. *Endocr. Res.* **41,** 8–15 (2016).
147. Giacca, A., Xiao, C., Oprescu, A. I., Carpentier, A. C. & Lewis, G. F. Lipid-induced pancreatic beta-cell dysfunction: focus on in vivo studies. *Am J Physiol Endocrinol Metab* **300,** E255–62 (2011).
148. Halban, P. A. *et al.* β-cell failure in type 2 diabetes: postulated mechanisms and prospects for prevention and treatment. *J. Clin. Endocrinol. Metab.* **99,** 1983–1992 (2014).

149. Cnop, M., Hannaert, J. C., Hoorens, A., Eizirik, D. L. & Pipeleers, D. G. Inverse relationship between cytotoxicity of free fatty acids in pancreatic islet cells and cellular triglyceride accumulation. *Diabetes* **50,** 1771–7 (2001).
150. Karaskov, E. *et al.* Chronic palmitate but not oleate exposure induces endoplasmic reticulum stress, which may contribute to INS-1 pancreatic beta-cell apoptosis. *Endocrinology* **147,** 3398–407 (2006).
151. Papa, F. R. Endoplasmic Reticulum Stress, Pancreatic β-Cell Degeneration, and Diabetes. *Cold Spring Harb. Perspect. Med.* **2,** a007666 (2012).
152. Biden, T. J., Boslem, E., Chu, K. Y. & Sue, N. Lipotoxic endoplasmic reticulum stress, β cell failure, and type 2 diabetes mellitus. *Trends Endocrinol. Metab.* **25,** 389–398 (2014).
153. Janikiewicz, J., Hanzelka, K., Kozinski, K., Kolczynska, K. & Dobrzyn, A. Islet β-cell failure in type 2 diabetes – Within the network of toxic lipids. *Biochem. Biophys. Res. Commun.* **460,** 491–496 (2015).
154. Maedler, K. *et al.* Distinct effects of saturated and monounsaturated fatty acids on beta-cell turnover and function. *Diabetes* **50,** 69–76 (2001).
155. Chaurasia, B. & Summers, S. A. Ceramides – Lipotoxic Inducers of Metabolic Disorders. *Trends Endocrinol. Metab.* **26,** 538–550 (2015).
156. Poitout, V. & Robertson, R. P. Glucolipotoxicity: fuel excess and beta-cell dysfunction. *Endocr Rev* **29,** 351–66 (2008).
157. El-Assaad, W. *et al.* Glucolipotoxicity alters lipid partitioning and causes mitochondrial dysfunction, cholesterol, and ceramide deposition and reactive oxygen species production in INS832/13 ss-cells. *Endocrinology* **151,** 3061–73
158. Nakashima, K. *et al.* MIN6 is not a pure beta cell line but a mixed cell line with other pancreatic endocrine hormones. *Endocr J* **56,** 45–53 (2009).
159. Anderson, C. M. & Stahl, A. SLC27 fatty acid transport proteins. *Mol. Aspects Med.* **34,** 516–528 (2013).
160. Henkin, A. H. *et al.* Real time non invasive imaging of fatty acid uptake in vivo. *ACS Chem. Biol.* **7,** 1884–1891 (2012).

161. Muller, W. A., Faloona, G. R., Aguilar-Parada, E. & Unger, R. H. Abnormal alpha-cell function in diabetes. Response to carbohydrate and protein ingestion. *N Engl J Med* **283,** 109–15 (1970).
162. Liljenquist, J. E. *et al.* Evidence for an important role of glucagon in the regulation of hepatic glucose production in normal man. *J Clin Invest* **59,** 369–74 (1977).
163. Unger, R. H. & Orci, L. The essential role of glucagon in the pathogenesis of diabetes mellitus. *Lancet* **1,** 14–6 (1975).
164. D'Alessio, D. The role of dysregulated glucagon secretion in type 2 diabetes. *Diabetes Obes Metab* **13 Suppl 1,** 126–32
165. Wang, L. *et al.* Acute stimulation of glucagon secretion by linoleic acid results from GPR40 activation and [Ca2+]i increase in pancreatic islet {alpha}-cells. *J Endocrinol* **210,** 173–9
166. Hong, J. *et al.* The short-term effect of fatty acids on glucagon secretion is influenced by their chain length, spatial configuration, and degree of unsaturation: studies in vitro. *Metabolism* **54,** 1329–36 (2005).
167. Pullen, T. J., da Silva Xavier, G., Kelsey, G. & Rutter, G. A. miR-29a and miR-29b contribute to pancreatic beta-cell-specific silencing of monocarboxylate transporter 1 (Mct1). *Mol. Cell. Biol.* **31,** 3182–3194 (2011).
168. Digel, M., Ehehalt, R., Stremmel, W. & Füllekrug, J. Acyl-CoA synthetases: fatty acid uptake and metabolic channeling. *Mol. Cell. Biochem.* **326,** 23–28 (2009).
169. Laybutt, D. R. *et al.* Endoplasmic reticulum stress contributes to beta cell apoptosis in type 2 diabetes. *Diabetologia* **50,** 752–63 (2007).
170. Akerfeldt, M. C. *et al.* Cytokine-induced beta-cell death is independent of endoplasmic reticulum stress signaling. *Diabetes* **57,** 3034–3044 (2008).
171. Cunha, D. A. *et al.* Initiation and execution of lipotoxic ER stress in pancreatic beta-cells. *J. Cell Sci.* **121,** 2308–2318 (2008).
172. Sargsyan, E. & Bergsten, P. Lipotoxicity is glucose-dependent in INS-1E cells but not in human islets and MIN6 cells. *Lipids Health Dis* **10,** 115
173. Szot, G. L., Koudria, P. & Bluestone, J. A. Murine pancreatic islet isolation. *J. Vis. Exp. JoVE* 255 (2007). doi:10.3791/255

174. Chen, J., Fontes, G., Saxena, G., Poitout, V. & Shalev, A. Lack of TXNIP Protects Against Mitochondria-Mediated Apoptosis but Not Against Fatty Acid–Induced ER Stress–Mediated β-Cell Death. *Diabetes* **59,** 440–447 (2010).
175. Stahl, A. *et al.* Identification of the Major Intestinal Fatty Acid Transport Protein. *Mol. Cell* **4,** 299–308 (1999).
176. Li, H. *et al.* High-throughput screening for fatty acid uptake inhibitors in humanized yeast identifies atypical antipsychotic drugs that cause dyslipidemias. *J. Lipid Res.* **49,** 230–244 (2008).
177. Liao, J., Sportsman, R., Harris, J. & Stahl, A. Real-time quantification of fatty acid uptake using a novel fluorescence assay. *J. Lipid Res.* **46,** 597–602 (2005).
178. Zhou, W., Madrid, P., Fluitt, A., Stahl, A. & Xie, X. (Simon). Development and Validation of a High-Throughput Screening Assay for Human Long-Chain Fatty Acid Transport Proteins 4 and 5. *J. Biomol. Screen.* **15,** 488–497 (2010).
179. Matsufuji, T. *et al.* Discovery and optimization of novel fatty acid transport protein 1 (FATP1) inhibitors. *Bioorg. Med. Chem. Lett.* **22,** 5067–5070 (2012).
180. Matsufuji, T. *et al.* Arylpiperazines as fatty acid transport protein 1 (FATP1) inhibitors with improved potency and pharmacokinetic properties. *Bioorg. Med. Chem. Lett.* **23,** 2560–2565 (2013).
181. Sandoval, A., Chokshi, A., Jesch, E. D., Black, P. N. & DiRusso, C. C. Identification and characterization of small compound inhibitors of human FATP2. *Biochem. Pharmacol.* **79,** 990–999 (2010).
182. Saini, N., Black, P. N., Montefusco, D. & DiRusso, C. C. Fatty acid transport protein-2 inhibitor Grassofermata/CB5 protects cells against lipid accumulation and toxicity. *Biochem. Biophys. Res. Commun.* **465,** 534–541 (2015).
183. Ahowesso, C. *et al.* Chemical inhibition of fatty acid absorption and cellular uptake limits lipotoxic cell death. *Biochem. Pharmacol.* **98,** 167–181 (2015).
184. Blackburn, C. *et al.* Identification and characterization of 4-aryl-3,4-dihydropyrimidin-2(1H)-ones as inhibitors of the fatty acid transporter FATP4. *Bioorg. Med. Chem. Lett.* **16,** 3504–3509 (2006).

185. Paulick, M. G., Forstner, M. B., Groves, J. T. & Bertozzi, C. R. A chemical approach to unraveling the biological function of the glycosylphosphatidylinositol anchor. *Proc. Natl. Acad. Sci. U. S. A.* **104,** 20332–20337 (2007).
186. Henkin, A. H. *et al.* Real time non invasive imaging of fatty acid uptake in vivo. *ACS Chem. Biol.* **7,** 1884–1891 (2012).
187. Weiss, W. A., Taylor, S. S. & Shokat, K. M. Recognizing and exploiting differences between RNAi and small-molecule inhibitors. *Nat. Chem. Biol.* **3,** 739–744 (2007).
188. Kazantzis, M. & Stahl, A. Fatty acid transport proteins, implications in physiology and disease. *Biochim. Biophys. Acta BBA - Mol. Cell Biol. Lipids* **1821,** 852–857 (2012).
189. Iglesias, I. *et al.* Comprehensive analysis of human pancreatic islets using flow and laser scanning cytometry. *Transpl. Proc* **40,** 351–4 (2008).
190. Stahl, A. A current review of fatty acid transport proteins (SLC27). *Pflüg. Arch.* **447,** 722–727 (2003).
191. Mihalik, S. J. *et al.* Participation of Two Members of the Very Long-chain Acyl-CoA Synthetase Family in Bile Acid Synthesis and Recycling. *J. Biol. Chem.* **277,** 24771–24779 (2002).
192. Hubbard, B. *et al.* Mice Deleted for Fatty Acid Transport Protein 5 Have Defective Bile Acid Conjugation and Are Protected From Obesity. *Gastroenterology* **130,** 1259–1269 (2006).
193. Pinkus, L. M. Separation and use of enterocytes. *Methods Enzymol.* **77,** 154–162 (1981).